On the formulation of hereditary cohesive-zone models

Marco Musto

Contents

Acknowledgments

First and foremost the author wishes to thank Dunlop Oil & Marine Ltd. in the persons of its General Managers, Mr. Mike Sloan and Dr. A.R.K. Zandiyeh, for the financial and technical support offered, without which this thesis would not have been written. The financial support of the EPSRC is also most gratefully acknowledged.

Heartfelt thanks are due to my first supervisor Dr. Giulio Alfano for both his precious scientific guidance and the untiring patience in managing the author's occasional lack of organisation.

The most sincere thanks go to my colleagues at Dunlop: only due to the impossibility of mentioning the many that contributed in some way to the present work, special thanks go to Mr. Alex Thain, Technical Draughtperson, for preparing the drawings, Mr. Chris Myshrall, Compounder, for the valuable technical advice, Mrs. Lynda Thickett and Mrs. Andrea Harris, Lab Technicians, for conducting the experimental work.

The author's gratitude goes to Dr. Joram Wiggers and Mrs. Christina Ederer as well for their careful proofreading and most objective criticism.

The author also wishes to thank Mr. Andrew 'The Landlord' Royle for his exquisite hospitality and his flatmate Mr. Roland Hammond, companion of many an inspiring philosophical discussion.

Abstract

The thesis presents novel formulations of hereditary cohesive zone models able to capture rate-dependent crack propagation along a defined interface. The formulations rely on the assumption that the measured fracture energy is the sum of an intrinsic fracture energy, related to the rupture of primary bonds at the atomic or molecular level, and an additional dissipation caused by any irreversible mechanisms present in the material and occurring simultaneously to fracture. The first contribution can be accounted for by introducing damage-type internal variables, which are to be driven by a rate-independent evolution law in order to be coherent with the definition as intrinsic energy. It is then proposed that the additional dissipation can be satisfactorily characterised by the same continuum-type material constitutive law obeyed by the interface material considered as a continuum: it is postulated that the dimensional reduction whereby a three-dimensional thin layer is idealized as a surface does not qualitatively alter the functional description of the free energy.

The specific application considered is mode-I crack propagation along a rubber interface. After focusing on viscoelasticity as a suitable candidate to reproduce rubber's behaviour, firstly the most common relaxation function, namely a single exponential term, is considerd after which the attention is turned to the use of fractional calculus and the related fractional integral kernel.

A comparison with experimental results is presented. A shortcoming of the proposed approach is then noted, in that certain features of experimentally measured responses (*i.e.* the non-monotonicity of the critical energy-release rate with respect to crack speed) will be shown to be out of reach for the described modelling paradigm. A novel micromechanical formulation is then sketched in an attempt to qualitatively understand the phenomenon. An additional interface damaging mode is introduced, physically inspired by the desire to reproduce the formation of fibrils in a neighbourhood of the crack tip. Fibril formation is then driven by a variational argument applied to the whole of the interface, yielding its non-local character. Upon the introduction of an anisotropic fracture energy, motivated by experimental considerations, it is noted how the model can predict a non-monotonic energy-release rate *vs* crack speed behaviour, at least for a simple loading mode.

Mathematical Notation

u   Displacement vector

X   Material point position in the undeformed configuration

E Elastic energy (Internal Energy in Equation (2.65))

E   Green-Lagrange strain tensor

F   Deformation Gradient

$sym(\cdot)$ Symmetrisation operator returning the symmetric part of the argument tensor

e   Linearised strain tensor

e Strain (in the one-dimensional setting)

$\Re$ Set of real numbers

$\Re^+$ Set of non-negative real numbers

$\Re^{++}$ Set of (strictly) positive real numbers

$\| \cdot \|_k$ Fading-memory norm associated to an obliviator k

$\times$ Cartesian set-product

$_{t_1}\Lambda_{t_2}$ Functional the argument of which are functions whose domain is $(t_1, t_2]$

$\mathcal{G}$ Boltzmann function

G Relaxation function, energy release rate (when no ambiguity is possible)

$\mathcal{J}$ Relaxation function

S   Stress Tensor

$\boldsymbol{\sigma}$ Traction vector (at an interface)

t   Traction vector (continuum description)

H Heaviside function

δ Displacement jump (Dirac Delta distribution in Chapter 2.1 only)

:   Application of a fourth order tensor to a second-order tensor, $\mathbf{C} : \mathbf{e} = \mathbf{C_{ijkl}e_{kl}}$

G_0 Short-term relaxation modulus

G_∞ Long-term relaxation modulus

$_aI_b^c$ Riemann-Liouville fractional operator of order c on the domain (a, b)

$\Gamma(\cdot)$ Euler's Gamma function

$\circ$ Composition operator

$_aD_t^c$	Riemann-Liouville operator of order c on the domain (a, b)
$_a^*D_t^c$	Caputo operator of order c on the domain (a, b)
$\mathcal{E}_a$	Mittag-Leffler function (single parameter) of order a
$\mathcal{L}(\cdot)$	Laplace Transform operator
A_j	j-th Grünwald coefficient
$\binom{n}{k}$	Binomial coefficients
G_c	Critical energy release rate
$\mathbf{C}$	Elastic stiffness tensor, $S = \mathbf{C} : \mathbf{e}$
$\mathcal{W}$	Elastic plus surface energy
$\mathcal{F}$	Elastic plus surface energy functional
W	Elastic energy as a function of deformation gradient
$\tilde{\Sigma}$	Traction-displacement jump cohesive law
$\otimes$	Dyadic tensor product, *i.e.* $(\mathbf{A} \otimes \mathbf{B})_{\mathbf{ij}} = \mathbf{A_i B_j}$
$\nabla(\cdot)$	Gradient
div	Divergence
u_{xy}	Partial derivative of the function u *w.r.t* to variables x and y
$W^{1,p}(\Omega)$	the space of Sobolev functions with p-summable derivatives on Ω
Dy	Distributional derivative of the function y
$\mathcal{L}^n$	n-dimensional Lebesgue measure
$\mathcal{H}^n$	n-dimensional Hausdorff measure
$\lfloor \cdot$	Operator returning the restriction to its (set-valued) argument
$[\cdot]$	"Jump" operator
$S(\cdot)$	"Jump set" operator
$D\mathcal{A}_v$	Variational derivative of the functional $\mathcal{A}$ in the direction of the test-function v
$\sharp \cdot$	Cardinality operator returning the cardinality of its set-valued argument
Ψ	Helmholtz Free Energy
$\mathbf{t}$	Traction ($\boldsymbol{\sigma} \cdot \mathbf{n}$, $\mathbf{n}$ being the unit normal vector to the boundary) vector
$\mathbf{D}$	Tensorial damage variable
$\bigcup_{n=M}^{N}$	Set-union operator over the range $(M, M+1, \ldots, N-1, N)$

$\mathcal{P}$ Set of real numbers characterising a partition

$\mathcal{F}$ Functional on the domain of piecewise-continuous functions

$d(\cdot, \cdot)$ Distance between its arguments

C^2 Space of twice-continuously differentiable functions

γ Surface energy vector

$\mathcal{N}$ Set of natural numbers

Chapter 1

Introduction

1.1 Background and Motivation

Polymeric materials rely on certain mechanisms in resisting externally applied loads which are generally different from the ones characteristic of metallic materials. Their structure is characterised by molecular constituents, *monomers*, forming an irregular, aperiodic, network. Referring specifically to elastomers, their elasticity is not in general related to internal energy stored at the level of molecular bonds, but has an entropic origin [1]. Moreover, their toughness is not a result of strong atomic/molecular bonds: it is on the other hand related to the presence of additional dissipation mechanisms which are necessarily present during any deformation process. Typically such mechanisms are rate-dependent: as an example, the typical fracture toughness of rubber measured at high temperature and low speed (conditions in which the effects of rate-dependent dissipation is conjectured to be minimized) is in the region of $\sim 50 \ J \, m^{-2}$, while values at room temperature and high crack velocity can be 10^4 times higher [2,3]. The study of such dissipative losses is of paramount importance not only theoretically but from the applications point of view as well: the exceptional (and virtually unrivalled) toughness of biological materials such as spider's silk and nacre seems to originate from additional dissipation mechanisms which would not be present in a regular, homogenous (at the atomic scale) material [4–6]. The research presented in this thesis originates from the interest manifested by the Industrial Sponsor in better understanding the fracture behaviour of certain laminated elastomeric composites not only to improve the modelling and simulation accuracy, but also to ultimately gain knowledge of how the fracture per-

formance is related to the material composition and its mechanical properties (other than obviously fracture-related ones). As a result the research presented in this thesis focuses on the formulation of material models suitable to simulate rate-dependent fracture. There is a vast range of tecniques capable of modelling crack propagation (Stress Intensity Factors, J-Integral, Virtual Crack Closure, Cohesive-Zone Models *etc.*) embedded within the most disparate numerical tecniques (Boundary Element Method, other meshless methods, Finite Volume Method, Extended Finite Element Method, *etc.*). The desire to deliver a versatile design tool to the Industrial Sponsor led to the choice of cohesive-zone models within the classical Finite Element method, but it is remarked the choice would not have been different in the lack of such constraints, for the cohesive-zone method offers, in the author's opinion, unique advantages in terms of material definition and versatility. In other words, it is believed the cohesive-zone model is the crack description more fundamentally based on the physical reality of the phenomena occurring in the crack process zone; this topic will be dealt in detail in Section 2.2.1.

1.2   Aims and Objectives

The main aim of the present work is to develop a cohesive-zone model able to accurately predict the fracture behaviour of thin layers of polymeric material subject to a realistic range of applied external loadings. To achieve this main objective, various requirements have been defined. Firstly, the need for the cohesive-zone model to be theoretically sound was acknowledged. Secondly, it was established that the formulation had to be as physically founded as possible, in a balanced compromise with computational simplicity. This requirement was motivated by the desire to make the model as robust as possible with respect to varying specimen sizes, geometries, material composition, etc. The targets of the research can be summarised as follows:

- to develop a general cohesive-zone model "template" able to reproduce history-dependence, for a vast range of inelastic material behaviours

- to specialise the cohesive-zone model to the case of an interface made of a thin elastomeric layer

- to design and execute a testing plan suitable for the validation of numerical results

Moreover, the ability to define the material parameters from routinely available lab-scale test results was deemed a highly desirable feature.

1.3   Summary of Contents

The thesis is organized as follows. Chapter 2 provides a summary of key concepts employed in subsequent sections detailing the original contribution of this work: when appropriate, a critical analysis in relation to the original subsequent elaborations is attempted as well. Three subsections deal with:

- Linear viscoelasticity (Section 2.1): after describing the mathematical formalism, some attention is given to thermodynamic requirements. The essentials of fractional calculus are also presented, in order to make the presentation of fractional viscoelasticity self-contained.

- Linear elastic fracture mechanics (Section 2.2): fundamental definitions as well as the seminal contribution of Griffith [7] are reviewed.

- Cohesive zone models (Section 2.2.2): first, the cohesive-zone model of Barenblatt [8] is introduced and reviewed from the theoretical point of view. The topic of rate-dependent cohesive-zone models is then introduced: a literature review on the topic is presented.

- The variational approach to fracture (Section 2.3): the general aspects of the theory are described in relation to the developments of Chapter 5.

Chapter 3 contains the novel formulation of a paradigm for rate-dependent cohesive-zones. The formulation is presented in some generality in the context of thermodynamics with internal variables. Later the model is specialised to a viscoelastic interface with damage in order to target the behavior of rubber interfaces. A critical comparison of the predictions to experimental results is presented, highlighting some deficiencies of the proposed approach.

In Chapter 4 the formulation is improved by resorting to a refined viscoelasticity description making use of fractional calculus. The comparison with experimental results is revisited: the prediction is now more accurate over a wider range of applied loading rates. A further limitation of the improved formulation is then evidenced, in that a

typical behaviour of rubber fracture mechanics, *i.e.* the drop in critical energy release rate above a threshold displacement rate, can not be reproduced. This is a result of the fact the presented formulation resorts to a continuum-type description for the interface's material whereby increasing the rate of applied displacements cannot result in lower stiffness, if linear viscoelasticity is employed.

A possible solution to the above problem is presented in Chapter 5. Firstly, a review of existing hypotheses aiming at explaining such behaviour is presented in Section 5.1. Then the model is introduced: the formulation is built on an admittedly extremely simplified, yet effective micromechanical non-local approach mimicking certain structural changes induced in the interface during the deformation process. Conclusions are then drawn, followed by an outlook on future work.

Chapter 2

Literature Review

2.1 Linear Viscoelasticity

Hereditary materials, or materials with memory, are characterised by the fact their mechanical response is not only a function of the actual deformation but accounts for the previous deformation history, in a sense which will be clarified later. Their study initiated in the XIX century by the hand of scientists such as L. Boltzmann and J.C. Maxwell, while a very notable contribution is due to V. Volterra in the XX century. This branch of continuum mechanics has been considered mainly of mathematical interest until technological advances such as the large scale use of polymeric materials in engineering structures led to the topic receiving more attention from applied scientists and engineers.

Geometrically linear deformations only will be considered within this thesis, henceforth the attention is focused on deformations characterised by a displacement field $\mathbf{u} = \mathbf{u}(\mathbf{X}, t)$, $\mathbf{X}$ being a point in the undeformed configuration and t standing for time, such that the condition

$$\sup_{\mathbf{X}, t} |\frac{\partial \mathbf{u}(\mathbf{X}, t)}{\partial \mathbf{X}}| \ll \mathbf{1} \tag{2.1}$$

holds, this being sufficient to satisfy the linearity assumption. Following a standard procedure [9] any finite strain measure, such as for example the Green-Lagrange strain,

$$\mathbf{E} = \frac{1}{2}(\mathbf{F}^T \mathbf{F} - 1) \tag{2.2}$$

$\mathbf{F} = 1 + \partial \mathbf{u}/\partial \mathbf{X}$ being the deformation gradient, is approximated by the linearised

strain

$$\mathbf{e} = \operatorname{sym}\frac{\partial \mathbf{u}}{\partial \mathbf{X}} \tag{2.3}$$

sym standing for the operator returning the symmetric part of a tensor. The dependence of the mechanical response at time t upon current and past deformation is mathematically modelled by the introduction of a suitable response functional $_{-\infty}\Lambda_t$, whose domain consists of strain histories up to time $t \in \Re$

$$e^t(s) = e(t - s) \quad s \in \Re^+ \tag{2.4}$$

where attention is restricted for simplicity to the one-dimensional case and $\Re^+$ stands for the set of positive reals.

The restriction of the strain history to strictly positive reals $\Re^{++}$ will be called the past history. The set of past histories can be given a Hilbert space structure through the introduction of a suitable norm. Let us consider a function k, monotonically decreasing to zero,

$$k : \Re^+ \to \Re^{++} \quad , \quad k(0) = 1 \quad , \quad \exists \alpha > 1 : \lim_{s \to \infty} s^\alpha k(s) = 0 \tag{2.5}$$

historically named *obliviator* [10]. Then let us define

$$\|e^t\|_k = \left(e(t) \cdot e(t) + \int_0^\infty |e^t(s)|^2 k(s) \mathrm{d}s \right)^{\frac{1}{2}} < \infty \tag{2.6}$$

Such norm expresses the fact that events distant in the past bear less consequences to the actual response than events closer in the past, which earned the concept the name of "fading memory".

While the main interest, as far as this thesis is concerned, is placed on the physical consequences of the fading memory principle, it is worth stressing how the definition of a suitable norm for the strain history space is a fundamental point for the investigation of the well-posedness of the initial value problem of viscoelasticity [11, 12]. If in addition the assumption is made that the functional $_{-\infty}\Lambda_t$ is

1) bounded, *i.e.* $|_{-\infty}\Lambda_t(e^t)| \leq C\|e^t\|_k$, $C \in \Re^+$ a constant

2) linear,*i.e.* $_{-\infty}\Lambda_t(c_1 e_1^t + c_2 e_2^t) = c_{1-\infty}\Lambda_t(e_1^t) + c_{2-\infty}\Lambda_t(e_2^t)$

then Riesz's Representation Theorem indicates that the functional can be expressed in a unique way as [11, 13]

$$\sigma(t) =_{-\infty} \Lambda_t(e^t) = g(0)e^t(0) + \int_0^\infty g(s)e^t(s)k(s)\mathrm{d}s \tag{2.7}$$

This conclusion is justified as follows. Riesz's Representation Theorem states that given a Hilbert space H and its dual H^*, *i.e.* the space of all continuous linear functionals from H into $\Re$, any functional $_{-\infty}\Lambda_t(e^t) \in H^*$ can be written uniquely as $_{-\infty}\Lambda_t(e^t) =< g, e^t >$, where $g \in H$ and $< \bullet, \bullet >$ stands for the inner product (related in this specific instance to the norm expressed by equation (2.6)). The *Boltzmann function* $\mathcal{G}$ is then defined as $\mathcal{G} = g(s)k(s)$. In the engineering literature another formulation equivalent to equation 2.7 seems to be preferred, obtained by defining the *relaxation function G* by the conditions $G(0) = \mathcal{G}(0)$ and $G'(s) = \mathcal{G}(s)$, equation 2.7 can be written as [14]

$$\sigma(t) = G(0)e^t(0) + \int_0^\infty G'(s)e(t - s)\mathrm{d}s \tag{2.8}$$

which can be integrated by parts and yields, assuming $\lim_{t \to -\infty} e(t) = 0$

$$\sigma(t) = \int_0^\infty G(s)\,\dot{e}(t - s)\mathrm{d}s \tag{2.9}$$

For later reference it is stressed that $G'(0)$ is not necessarily finite, which indeed is the case for certain relaxation functions obtained exploiting fractional calculus. For completeness it is also noted that the case of $G(0)$ being not finite can be covered by the theory but is generally physically inappropriate.

It can be verified that the response functional described in equation (4.1) is continuous with respect to the fading memory norm, as it is bounded and linear. While referring to [11, 15] for a detailed exposition, it is noted that the continuity of the response functional with respect to the "fading memory" norm is named as the *weak principle of fading memory* [11]. The linearity (and continuity) of the response functional were assumed *a priori* by Boltzmann himself who arrived at the same integral representation of equation (4.1) by the following argument, [16]. He characterised the response to an imposed step strain $e(t) = \Delta\,\mathrm{H}(t)$, H standing for the Heaviside function and Δ being a constant, using the function $G(t) = \sigma(t)/\Delta$. Then, the stress at time following an imposed strain $e_1(t) = \Delta_1\mathrm{H}(t - \zeta_1)$, $\Delta_i \in \Re^+$ is

$$\sigma_1(t) = G(t - \zeta_1)\Delta_1 \tag{2.10}$$

If at a successive instant ζ_2 another strain step increment of magnitude Δ_2 is imposed, the stress due to this input only would equal

$$\sigma_2(t) = G(t - \zeta_2)\Delta_2 \tag{2.11}$$

11

Hence, assuming an imposed strain $e_1(t) = \Delta_1 \mathrm{H}(t - \zeta_1) + \Delta_2 \mathrm{H}(t - \zeta_2)$, linearity allows us to write

$$\sigma(t) = \sigma_1(t) + \sigma_2(t) = G(t - \zeta_1)\Delta_1 + G(t - \zeta_2)\Delta_2 \qquad (2.12)$$

If it is assumed the applied strain $e(t)$ is smooth enough to be approximated with desired accuracy by a piecewise constant function, then equation (2.12) in the general case will reduce to equation (4.1) as $\Delta_i \rightarrow 0$. This procedure underlines the direct physical importance of the continuity assumption. It is to be noted that in an entirely similar way the strain can be expressed as a function of the stress history, the integral kernel in this case being referred to as *creep function* [14].

2.1.1 Rheological Models

An alternative approach to model viscoelastic behaviour is based on the so-called rheological models of viscoelasticity, *i.e.* mechanical analogues of viscoelastic behaviour constructed by joining, in series and/or in parallel, springs and dashpots (the latter being material elements obeying a Newtonian viscosity law). Their importance, apart from their essential role during the development of the theory, lies in their ease of visualisation which allows very effective physical reasoning. For example, the use of springs and dashpots with positive material constants naturally prevents the formulation of material constituive laws not complying with the Second Law of Thermodynamics, and allows for a clear definition of free energy by identifying the latter with the elastic energy stored in the springs. This is not possible in the general case as will be briefly recalled later. In spite of these advantages, modern treatments of viscoelasticity attempt to achieve full generality, in which case rheological models could prove restrictive. Indeed the complete equivalence between Volterra-Boltzmann type integral representations and rheological mechanical models has been proven in [17] under certain conditions on the properties of the fading memory, answering an observation made in [18]. Under such conditions the equivalence between integral and rheological representations is complete: still the possibility of the fading memory principle being interpreted in a different, *integral* sense exists [19] and is possibly relevant for application on composites and in general heterogenous materials [20]. A model characterised by an integral fading memory principle then does not need to exhibit a monotonic response in a relaxation test (this being a striking difference from the class of models considered by Beris and Edwards

in the previously cited work [17]), while complying with the Second Law of Thermo-dynamics: the topic will be expanded upon in the next Section 2.1.2.

It is also mentioned, for later reference, that rheological models naturally lead to the viscoelastic constitutive law being described through a differential equation of the type

$$s_0\sigma(t) + s_1\frac{\mathrm{d}}{\mathrm{d}t}\sigma(t) + \dots s_n\frac{\mathrm{d}^n}{\mathrm{d}t^n}\sigma(t) = c_0 e(t) + c_1\frac{\mathrm{d}}{\mathrm{d}t}e(t) + \dots c_n\frac{\mathrm{d}^n}{\mathrm{d}t^n}e(t) \qquad (2.13)$$

$s_0, s_1, \dots s_n$ and $c_0, c_1, \dots c_n$ being material constants, which is often compactly expressed as

$$S(D)\,\sigma(t) = C(D)\,e(t) \qquad (2.14)$$

upon setting

$$S(D) = \sum_{k=0}^{n} s_k D^k \qquad C(D) = \sum_{k=0}^{n} c_k D^k \qquad (2.15)$$

where D^k stands for the operator $\mathrm{d}^k/\mathrm{d}t^k$. Finally mention is given to a particular set of viscoelastic material constitutive laws, named "differential" in [21], and characterised by the constitutive functional depending on the current strain and its time derivatives only:

$$\sigma(t) =_{-\infty} \Lambda_t(e^t) = \hat{\Lambda}(e(t), e^{(1)}(t), e^{(2)}(t) \dots e^{(k)}(t)) \qquad (2.16)$$

where $e^{(k)}(t)$ denotes the $k-th$ time derivative of $e(t)$. Such models are characterised by an "abruptly fading memory" [21] in that due to the local nature of the derivation operation only a neighbourhood of the history around the current time is considered. A functional dependence of such type is often invoked in fracture mechanics studies of polymers [22], to which a later section is devoted. It is relevant to note that under appropriate mathematical conditions [23] the differential representation (2.16) arises as a first-order approximation for slow processes of the general functional representation, equation (2.7).

An additional note concerns the concept of deformation history and state. It has been noted that the stress at current time will depend in general on the whole past deformation experienced by the material point under consideration. In general, all the past history has to be known to characterise the actual state of the material. Consequently, in [24] the

state is defined as a "pair whose entries are an equivalence class of histories and a deformation" (it can be appreciated this definition considers separately the past history and the current strain value). This fact does not exclude the possibility to express the state more compactly. A notable example is given by materials whose relaxation function is a linear combination of exponential functions. For such materials the state reduces to a vector of suitably defined *internal variables*, in the framework of thermodynamics with internal variables, whose knowledge completely characterises and "condenses" the past history. Such approach will be used within Chapter 3.

The Section is closed by presenting the concept of complex modulus, which is useful when characterising the mechanical response in terms of frequency rather than loading rate. It is the complex function $\mu : \omega \mapsto \mathcal{C}$ such that the steady-state stress response $\sigma(t)$ to a sinusoidal strain history $Re[\epsilon_0 e^{i\omega t}]$ can be computed as $\sigma(t) = Re[\mu(i\omega)\epsilon_0^{i\omega t}]$, $Re[\bullet]$ standing for operator returning the real part of its argument. The ratio between real and imaginary part of the complex modulus is often referred to as *loss tangent* and has a clear physical interpretation, for it is equal to the tangent of the phase lag angle between stress and strain response during the harmonic excitation.

2.1.2 Thermodynamic Restrictions

So far the general form of the response functional has been characterised. It remains to consider what limitations on the relaxation function G, if any, are imposed by thermodynamic consistency. A brief exposition of some essential results, whose knowledge is essential to guarantee the formulation of physically realistic materials, is to be presented. The interested reader is referred to [11, 21, 25, 26] for an extensive treatment of the subject. Attention will be given to the one-dimensional case, relevant to the work presented later. Firstly, let us focus on the scalars $G_0 = G(0)$, named the *istantaneous elastic modulus* and $G_\infty = \lim_{s \to \infty} G(s)$, named the *equilibrium elastic modulus*, required to be bounded away from zero for a solid [10, 14].

It can be proved [11] that compliance with the Second Law of thermodynamics requires

$$G_0 > G_\infty \qquad (2.17)$$

It is important to note that a relaxation function need not to be monotonically decreasing to comply with the Second Law of Thermodynamics, as demonstrated through a

counter-example in [25]. On the other hand, it is shown in [26] that a sufficient condition for positive dissipation is the monotonicity and convexity of the relaxation function. Interestingly the fact that there are no direct empirical examples of non-monotonic relaxation functions even pushed some authors [21] to question if the Second Law of Thermodynamics is properly described in the current mathematical formalism.

A striking feature of materials with memory is that in general the free energy potential turns out to be non-unique [15, 21, 24, 27]. As a consequence of great physical importance it is noted then that the knowledge of the stress-strain behaviour of a material does not allow its full energetic characterisation, *i.e.* the free energy and the dissipation can not be uniquely determined. This observation bears relevance to the formulation of the cohesive-zone presented in Chapter 3, where a cohesive-zone model will be formulated making use of energetic arguments. In the case presented no ambiguity will arise because the free-energy can be shown to be unique for a single-exponential relaxation function [28], but in general (should for example the material description be improved by adding one or more Maxwell arms) the exact definition of free energy and dissipated power is required as an additional assumption that has to be made with a certain degree of independency from the material constitutive law.

2.1.3 Fractional Calculus Viscoelasticity

Fractional Calculus is a branch of analysis dealing with the meaning and implications of defining differential operators of real order, for example $D_x^\nu = \frac{\mathrm{d}^\nu}{\mathrm{d}x^\nu}$ when $\nu \notin \mathcal{N}$, $\mathcal{N}$ standing for the set of natural numbers. The subject, whose historic origins are traced back to a letter to G. L' Hôpital from W. Leibniz in the year 1695 [29], has attracted some attention in recent years from the viscoelasticity community as a result of some significant advantages entailed by the use of fractional derivatives in the development of viscoelastic models. The essential concepts only will be herein referred to, referring the reader to [30, 31] for further details.

Firstly, the fractional integral is considered. Restricting the attention to scalar functions f such that $f(t) = 0 \quad \forall t < a$, the following notation is introduced

$$_aI_t^n f = f_n(t) = \int_a^t \int_a^{\xi_1} \ldots \int_a^{\xi_{n-1}} f(\xi_n)\,\mathrm{d}\xi_n \ldots \mathrm{d}\xi_1 \qquad (2.18)$$

The R.H.S of equation (2.18) can be shown to satisfy

15

$$\int_a^t \int_a^{\xi_1} \cdots \int_a^{\xi_{n-1}} f(\xi_n)\,\mathrm{d}\xi_n \ldots \mathrm{d}\xi_1 = \frac{1}{(n-1)!}\int_a^t (t-\tau)^{n-1} f(\tau)\mathrm{d}\tau \quad , \quad n \in \mathrm{N} \tag{2.19}$$

a result known as Cauchy's formula for repeated integration. The meaning of equation (2.19) is extended from the case $n \in \mathrm{N}$ to $\nu \in \Re^+$ by using the Gamma function Γ, which can be defined as

$$\Gamma(x) = \int_0^\infty s^{x-1} e^{-s}\mathrm{d}s \tag{2.20}$$

The above definition is restricted to positive reals in order for the integral to be convergent, but can be extended in the whole complex plane by analytical continuation. In fact, integration by parts of equation (2.20) yields the relationship

$$\Gamma(x+1) = x\Gamma(x) \tag{2.21}$$

from which it can be appreciated how the Γ function interpolates the factorial on the real line. This explains its ubiquitous presence (it appears for example in the formula for the volume of a sphere in n-dimensions). The *Riemann-Liouville fractional integral* of order $\nu > 0$ is then:

$$_aI_t^\nu f(t) = \frac{1}{\Gamma(\nu-1)}\int_a^t (t-\tau)^{\nu-1} f(\tau)\mathrm{d}\tau \quad , \quad t > a \quad , \quad \nu \in \Re^{++} \tag{2.22}$$

The fractional derivative definition is based on computing the result of left- and right-composition of the classical derivative and integral operator just defined,

$$D_t^n \circ {}_aI_t^n f(t) = f(t) \quad , \quad t > a \tag{2.23}$$

while

$$_aI_t^n \circ D_t^n f(t) = f(t) - \sum_{k=0}^{n-1} f^{(k)}(a^+)\frac{(t-a)^k}{k!} \tag{2.24}$$

where the notation f^k denotes the k-th derivative and $f^k(a^+)$ indicates the right limit of f^k at a, allowing hence for jump-discontinuities. Then the fractional derivative $_0D_t^\nu$ is defined, upon setting $a = 0$, as the left-inverse to $_0I_t^n$. In detail, after selecting an integer $m \in \mathcal{N}$ such that $m - 1 < \nu < m$ the *Riemann-Liouville fractional derivative* of order $\nu > 0$ is defined as [31]:

$$_0D_t^\nu = D_t^m \circ {}_0I_t^{m-\nu} f(t) \quad , \quad m - 1 < \nu < m \tag{2.25}$$

or explicitly

$$
{}_0D_t^\nu = \begin{cases} \frac{1}{\Gamma(m-\nu)} \frac{\mathrm{d}^m}{\mathrm{d}t^m} \int_0^t \frac{f(\tau)\mathrm{d}\tau}{(t-\tau)^{\nu+1-m}} & m-1 < \nu < m \\[2ex] \frac{\mathrm{d}^\nu}{\mathrm{d}t^\nu} f(t) & \nu = m \end{cases} \tag{2.26}
$$

An alternative definition leading to the so-called *Caputo fractional derivative* of order ν can be obtained by considering the right inverse, as in equation (2.24). This yields

$$
{}_0^*D_t^\nu = {}_0I_t^{m-\nu} \circ D_t^\nu f(t) \quad , \quad m-1 < \nu < m \tag{2.27}
$$

or explicitly

$$
{}_0^*D_t^\nu = \begin{cases} \frac{1}{\Gamma(m-\nu)} \int_0^t \frac{f^{(m)}(\tau)\mathrm{d}\tau}{(t-\tau)^{\nu+1-m}} & m-1 < \nu < m \\[2ex] \frac{\mathrm{d}^\nu}{\mathrm{d}t^\nu} f(t) & \nu = m \end{cases} \tag{2.28}
$$

The problem of initial conditions in fractional differential formulations is avoided in the present work by the physically plausible assumption of zero strain (and stress) for negative times. In some cases such condition can be overly restrictive: the Caputo definition has the advantage that integer-order initial conditions are needed only [31], while initial conditions of fractional type have to be considered for the Riemann-Liouville formulation, whose physical interpretation is provided in [32] (see also [31, p.40] for compatibility conditions for stress and strain in the most general case). Under such initial conditions (which are hardly restrictive for the intended application) the total equivalence of the Riemann-Liouville and Caputo definitions can be proved [31, 33].

Physical Meaning of Fractional Models

It is far from trivial to assign a physical meaning to the fractional operators just introduced, a suggestive attempt being made in [34]. Much clearer are the specific benefits that can be obtained applying this approach in viscoelasticity. For this purpose let us consider the problem of determining the relaxation function G (3.17) for a specific material of interest. It can be appreciated from equation (2.8) (with the aid of a formal calculation or, more rigorously, using tools of distribution theory) that the function G describes the stress reponse following the imposition of a step strain history, discontinuous at the origin. Experimentally such a response could be approximately determined by a *relaxation test*, in which a strain jump is applied as quickly as possible, and then kept constant. The author is not aware of any engineering viscoelastic material exhibiting a

response that could be reasonabably reproduced, over a realistic time horizon, by any exponential function. Typically, at short time durations the stress will decrease more rapidly than an exponential function, to switch to the opposite behaviour for longer time durations. This phenomenon is a result of the presence of numerous dissipative mechanism with very different (and continuously distributed) characteristic relaxation times. This observation goes back to the work of Nutting [35] in the early 1920s, when it was noted that stress relaxation is naturally described by a power law-type function, whereby the general response can be given by

$$\sigma(t) = A \int_0^t (t-s)^{-\nu} \dot{e}(s)\, ds \tag{2.29}$$

Setting the constant $A = \frac{c}{\Gamma(1-\nu)}$ yields

$$\sigma(t) = c \cdot {}_0D_t{}^\nu \epsilon = \int_0^t \frac{c}{\Gamma(1-\nu))} (t-s)^{-\nu} \dot{\epsilon}(s)\, \mathrm{d}s \tag{2.30}$$

c being a positive scalar, which coincides with the Riemann-Liouville definition of fractional derivative. Incidentally equation (2.30) is the first historic archetype of fractional viscoelasticity, the *Scott-Blair* model from the English researcher who first introduced it [36]. This model represents a mechanical behaviour which interpolates between a fluid (for $\nu = 1$) and a Hookean solid (for $\nu = 0$). Interestingly the line of thought just exposed seems to have been used in the monography by Rabotnov [30] to justify the use of a specific type of kernel (given by the so-called *Abelian* functions), without explicitly mentioning fractional derivatives.

The ability of fractional formulations to replicate real-world behaviours can be also appreciated by considering the differential equation

$$\,{}_0^*D_t^\nu u(t) + u(t) = 0 \quad t \geq 0 \quad , \quad u(0^+) = 1 \tag{2.31}$$

For $\nu = 1$ the solution of equation (2.31) is the exponential function, $u(t) = e^{-t}$. For $\nu \in (0,1)$ the solution can be shown to be $u(z) = \mathcal{E}_\nu(-z^\nu)$, where $\mathcal{E}_\nu$ is the *Mittag-Leffler* function of order ν, whose representation in series reads

$$\mathcal{E}_\alpha(z) = \sum_{n=0}^\infty \frac{z^n}{\Gamma(\alpha n + 1)} \quad \alpha > 0 \quad , \quad z \in \mathrm{C} \tag{2.32}$$

Evidently, $\mathcal{E}_1(z) = e^z$. The advantage of using fractional calculus models can then be once more appreciated by observing the behaviour of Mittag-Leffler functions of order

$\alpha, 0 < \alpha < 1$, see Fig.2.1:
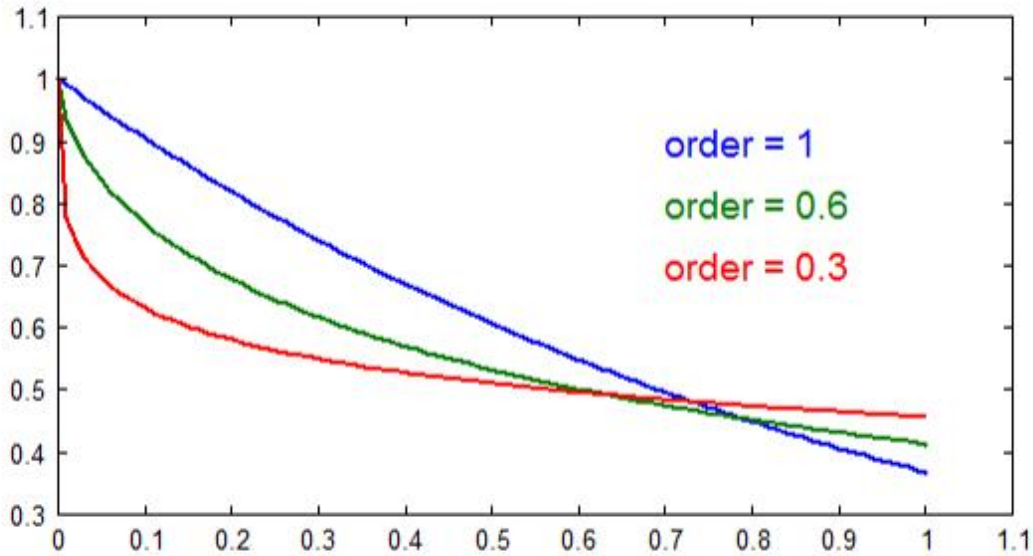
Figure 2.1: Various-order solutions to the relaxation fractional ODE.

It can be noted that at short times the relaxation is steeper than the exponential function, the opposite being true for longer times. This echoes the behaviour of real materials [37, 38]. Of course the material characterisation achieved using relaxation functions made by summing exponential functions can be improved by adding more terms. Exploiting the rheological analogy, this equals to adding dashpots with different relaxation times, remembering that this approximation process is mathematically well-defined, in the sense that the exponentials form a complete basis for continuous, monotonic functions. However, such a procedure adds complexity to the problem of determining the material constants, and is furthermore ill-posed in general [39], see also the discussion in [33], Section 6.4. This makes intuitive sense, as a result of the fact the relaxation kernel has "smoothing" properties (for the purposes of the actual discussion the term will be assigned its intuitive meaning renouncing to a rigorous mathematical definition which is anyhow available [39]). Given a "sharp" (not-differentiable in the classical sense) impulse input (such a Heaviside or Dirac distributions) the output becomes more "regular" as time progresses: calculating the relaxation function from the measured output then tries to go against the "smoothing" direction and causes ill-conditioning (in analogy with the difficulties in computing the gradient flow of a non-convex potential [40],

a topic which will be touched upon in Section 2.3, or the problems incurred in trying to solve the Heat Equation with a negative conductivity constant). For such reasons the possibility of improving the description by adding more exponential terms is covered in difficulties.

An alternative but equivalent way of appreciating the difference between fractional and exponential kernels is given by the computation of the resulting spectrum of relaxation times $\mathcal{R}$, which can be defined for the present purpose, given a relaxation function G, as the function such that

$$G(t) = G_\infty + \int_0^\infty \mathcal{R}(\xi) e^{-\frac{t}{\xi}} \mathrm{d}\xi \tag{2.33}$$

The relaxation spectrum is hence a function $\mathcal{R}$ needed for the representation of the relaxation function G as in equation (2.33). In words, the relaxation spectrum describes the distribution of relaxation times (physically describing how much weight is to be given at a specific dissipation mechanism to which a range of relaxation times is assigned). For a classical rheological model $\mathcal{R}$ can be expressed as a discrete sum of suitably shifted Dirac-delta generalised functions, one for every relaxation time, while it can be shown [31] that in general the same is not valid for the spectrum $\mathcal{R}$ related to a fractional calculus-based model, which in a sense encompasses an infinity of smoothly varying relaxation times and is therefore represented by a continuous function.

There is an interesting remark to be made here with regards to the relaxation spectrum. Let us assume a material of interest is characterised by a discrete spectrum with n components $\tau_1, \tau_2, ... \tau_{n-1}, \tau_n$. Then, $G(t) = \sum_{j=1}^{j=N} e^{\frac{-t}{\tau_j}}$. The long-term asymptotic behaviour of the material submitted to a relaxation test will be exponential,

$$G(t) \sim e^{\frac{-t}{\min_j \tau_j}}, t \to \infty \tag{2.34}$$

Fractional relaxation functions instead tend to exhibit algebraic instead of exponential decay (in loose language often referred to as a "fat tail" in technical literature), for example the kernel employed in Chapter 4 behaves asymptotically as

$$\mathcal{E}_\nu(-t^\nu) \sim \frac{t^{-\nu}}{\Gamma(1-\nu)}, t \to \infty \tag{2.35}$$

The algebraic decay characteristic of many engineering materials (and often essential in the modelling of engineering problems for which the long-term behaviour is of paramount importance) can not be captured then by summing exponential kernels (physically, Maxwell arms) regardless of their number. It is only in the limit of an "infinite"

number of Maxwell arms that the algebraic decay is recovered. As neatly expressed in [41], fractional calculus-based models incorporate complexity in themselves, while radically simpler classical models are forced to resort to numerous material constants to attempt the same achievement.

So far only a phenomenological justification for the use of fractional calculus has been given. The question then arises about the existence of a deeper physical connection. Apart from its academic interest, such a question is often essential for the practising engineer as well. Indeed, regardless of the degree of success of the numerical fitting procedures oten employed to determine the required material costants, purely phenomenological models should not be extended, in principle, outside the range of test loading conditions over the results of which the mentioned fitting procedures had been applied. Only a theoretical, physical basis can enhance the confidence with which such extrapolations are made.

A fundamental contribution in this sense was provided by Bagley and Torvik [42]. They provided an explict link between Rouse's theory [43], able to predict macroscopic viscoelastic behaviour of a dilute solution of non-cross linked polymers in a Newtonian fluid starting from molecular physics, and fractional calculus. This is achieved by noting, in essence, that Rouse's results can be concisely and naturally expressed using fractional calculus formalism. It is interesting in this connection to underline that fractional calculus formalism can arise in the description of classical phenomena, without any need to invoke "fractality" (see incoming discussion) or otherwise equally "exotic" properties of the continuum: as an example of historic relevance, please note the celebrated *Tautochrone* problem, solved in 1659, can be expressed as an integral equation in the unknown s of the form

$$\frac{1}{\sqrt{2g}} \int_0^y \frac{1}{\sqrt{y - \eta}} s(\eta) \mathrm{d}\eta = t(y) \tag{2.36}$$

g standing for the gravitational constant, or can be written using fractional formalism by using directly the fractional derivative definition as

$$\mathcal{C}_0 D_t^{\frac{1}{2}} s(y) = t(y) \tag{2.37}$$

$\mathcal{C}$ standing for a constant. Other examples from applications can be found in [33].

A micro-mechanically motivated model characterised by a power-law kernel was proposed in [44]. The model assumes relaxation is a random-walk driven process and

it is the conceptually most simple physically-based model the author is aware of, which makes it very instructive.

Another connection between fractional calculus and physical reality deserves mention. The question indeed can be posed of what would the rheological equivalent of a fractional calculus-based model be. The answer was provided in [41] for the fractional Maxwell model. This is obtained from the differential representation of the classical Maxwell model (spring and dashpot in series)

$$\sigma(t) + \lambda \frac{\mathrm{d}\sigma(t)}{\mathrm{d}t} = \eta \frac{\mathrm{d}e(t)}{\mathrm{d}t} \tag{2.38}$$

λ being the relaxation time, η being the Newtonian viscosity coefficient, by generalizing the differential to the fractional case

$$\sigma(t) + \hat{\lambda}\,_0D_t{}^\alpha \sigma(t) = \hat{\eta}\,_0D_t{}^\beta e(t) \tag{2.39}$$

Thermodynamic consistency was addressed in [45] and results in the condition $0 < \alpha \le \beta \le 1$. Interestingly, the model "interpolates" between hookean ($\alpha = \beta = 0$) and classical Maxwell-model ($\alpha = \beta = 1$) behaviour. The rheological analogue of the generalized Maxwell model was found to be the hierarchical, self-similar (fractal), model depicted in Fig.2.2.

The relation between fractional derivative and "fractal" rheological models is surprisingly simple and can be appreciated readily in [46], see also [47], the key mathematical step being an equation relating a *continued fraction* to a polynomial

$$x(x+1)^{\gamma-1} = \frac{x}{1+}\,\frac{(1-\gamma)x}{1+}\,\frac{\frac{1\cdot(0-\gamma)}{1\cdot2}}{1+}\,\frac{\frac{1\cdot(2-\gamma)x}{2\cdot3}}{1+}\,\frac{\frac{2\cdot(3-\gamma)x}{3\cdot4}}{1+}\,\dots \tag{2.40}$$

where a commonly used notation for continued fractions is employed [48], as exemplified by the following:

$$a_0 + \frac{1}{a_1 + \frac{1}{a_2 + \frac{a_3}{a_4}}} = a_0 + \frac{1}{a_1+}\,\frac{1}{a_2+}\,\frac{a_3}{a_4} \tag{2.41}$$

Equation (2.40) shows how a continued fraction (physically originating from a fractal rheological struture) leads to a power-law behaviour.

This rheological analogy also provides a direct visualization of the relaxation spectrum of the fractional model and justifies the fact the spectrum is continuous. It is very fascinating in that it explains in a fully deterministic way how the microscopic structure
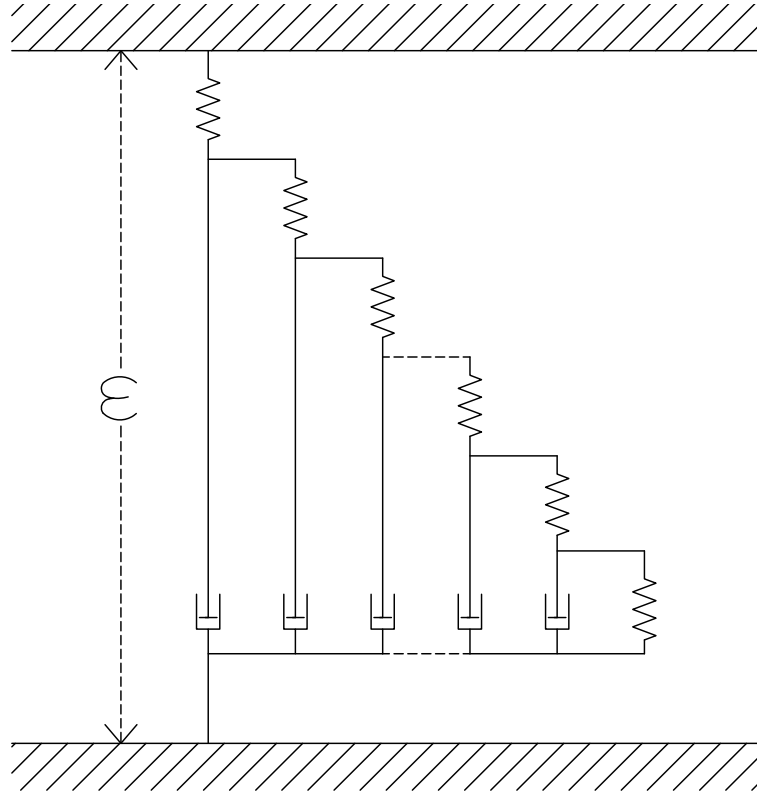
Figure 2.2: Fractal-type rheological analogue.

yields the macroscopic, power-law type relaxation behaviour. This is in contrast with statistical theories [49], possibly based on self-similarity, with various degrees of rigorousness. It is very interesting to note that it has been recently proven rigorously [50] that a logarithmic distribution arises as the statistical limit of sampling random samples from randomly selected distributions (in a sense made rigourous in the given reference). In this sense it is interesting to mention the possible connection, so far completely unexplored, to Self-Organized Criticality (*SOC*), a physical theory explaining the origins of universally present scale-free behaviours [51] in certain complex systems [52,53]).

Another application of fractional calculus from which physical understanding can be gained is presented in [54], where a mass balance equation for a heterogeneous medium infringing the continuum-hypothesis is established. The fascinating relationship between fractional calculus and fractal structure can be appreciated also in other contexts. For example, the paper [55] considers the differentiability of Cantor's function [56], also referred to as the *Devil's staircase* in reference to the puzzling fact it grows continuously yet its derivative is zero almost everywhere. It is there shown that Cantor's

function admits a fractional derivative of order α if and only if $\alpha \leq \mathcal{H}$, $\mathcal{H} = \frac{log2}{log3}$ being the Hausdorff dimension of the set over which the derivative of $\mathcal{C}$ is defined and null. The proof is disarmingly straighforward and provides a certain insight in the fractional derivative's meaning, whose full understanding remains however elusive. The literature on fractals and fractional calculus in various fields of Physics is rapidly growing: a "fractal" treatment of elasticity is sketched for example in [57] and references there reported.

2.2   Fracture Mechanics

Fracture Mechanics is a relatively young discipline whose exceptional importance in applications motivated a large interest and led to very significant improvements in the last century. One of the major contributions is due to Griffith [7]. His attention was attracted by the well known fact that estimates of the cohesive atomic force in a crystal are up to four times [58] higher than measured fracture strengths. Fracture necessarily involving the opening of an interatomic plane, the observed difference gained the status of paradox. Numerous experiments on glass whiskers of different sizes allowed Griffith to observe and quantify the dependence of the fracture strength upon a specimen's characteristic size (interestingly, similar observations have been made by Leonardo da Vinci centuries before in the Codex Atlanticus, and Galileo too was very familiar with size-effects in mechanics [59]). Griffith's first groundbreaking intuition was to invoke the presence of flaws in the material, hence justifying the discrepancy between estimated cohesive force and measured fracture strength by evoking the stress concentration induced by the flaws. Considering the flaws as elliptical holes in an unbounded plate, the elastic solution of this problem due to Inglis [60] could be exploited, if a failure criterion were introduced. The second fundamental idea then consisted in establishing a thermodynamical balance between the decrease in potential energy due to crack advancement, and the increase in surface energy [61]. Assuming the surface energy depends only on the crack surface (hereafter such energy will be referred to as *Griffith-type* energy) he established the celebrated, eponymous crack propagation criterion.

Consider a cracked body occupying a domain Ω in $\Re^2$, made of a homogenous hyperelastic material whose energy density is characterised by a function W of the gradient of the displacement field u, which we assume belongs to a space $\mathcal{M}$ sufficiently regular

to justify the following developments. For simplicity, we consider only displacement boundary conditions, *i.e.* time-dependent displacements are prescribed on the boundary $\partial\Omega$ of Ω, named $\partial_d\Omega$, such that $u|\partial_d\Omega = u_0(t)$: the inclusion of mixed boundary conditions is straightforward. Without loss of generality one single rectilinear crack is considered, described in a suitable reference system by the set $\Gamma = \{(x,0) : 0 \leq x \leq l\}$.

The elastic energy, dependent on the crack length is computed as:

$$E(u;l) = \int_{\Omega\setminus\Gamma} W(\nabla u)\,\mathrm{d}\Omega \tag{2.42}$$

The equilibrium energy $\hat{E}$ is then solution of the variational problem

$$\hat{E}(t,l) = \inf_{u\in\mathcal{M},\,u|\partial_D\Omega=u_0(t)} E(u;l) \tag{2.43}$$

Upon defining the *energy release rate* $G(t,l)$

$$G(t,l) = -\frac{\partial}{\partial l}\,\mathcal{E}(t,l) \tag{2.44}$$

Griffith's criterion can be stated as follows. Upon introducing a material property, the *fracture energy*, denoted by G_c, the following holds:

1) A crack is in equilibrium at time t if

$$G(t,l) \leq G_c \tag{2.45}$$

2) A crack can advance if and only if

$$G(t,l) \geq G_c \tag{2.46}$$

It can be noted that, if the free energy $\mathcal{W}$ of the elastic body is defined as

$$\mathcal{W}(t,l) = \hat{E}(t,l) + G_c l \tag{2.47}$$

Griffith's criterion then reduces to the condition

$$\frac{\partial}{\partial l}\mathcal{W}(t,l) \geq 0 \tag{2.48}$$

25

from which it is apparent how Griffith's criterion entails meta-stability, for more details see [62]. An alternative criterion for crack propagation based on global stability [63] will be briefly considered in Section 2.3.

The case $G \geq G_c$ is not considered in the quasistatic framework as the energy balance could not hold without introducing dynamic terms [58].

Griffith's contribution appears even more profound when compared to the use of local stress/strain criteria, *i.e.* attempts to predict crack propagation based solely on the local knowledge of the stress/strain fields. These criteria are not applicable in the general case due to the appearance of stress/strain singularities in the presence of a crack. The first fully general results in this respect were provided by Williams [64], who demonstrated, using methods of complex analysis [65,66], the presence of a singularity of order $\sim \frac{1}{\sqrt{r}}$ at the tip of a sharp crack in an elastic material, r being the radial coordinate in a polar coordinate system centered at the crack tip. In fact, the stress field for a 2D problem can be shown to satisfy the expression [58]:

$$\sigma_{ij} = \left(\frac{k}{\sqrt{r}} \right) f_{ij}(\theta) + A(r, \theta) \tag{2.49}$$

where k is a constant (the *stress intensity factor*), r and θ stand for the radial and angular coordinates in a polar coordinate system centered at the crack tip, f is a dimensionless function of θ in the leading term, and A is a function characterised by

$$\lim_{r \to 0} A(r, \theta) = c \quad , \quad c \in \Re^+ \tag{2.50}$$

and hence inconsequential for the asymptotic behaviour of the stress field as $r \to 0$. The fact that the stress (hence the strain) diverges at the crack tip defines limitations for the use of local criteria based on stress, strain or energy density [67,68]. Griffith's approach is immune from such issues, for the presence of this singularity does not prevent the total energy from being bounded (mathematically this is equivalent to the fact the energy density is integrable).

Griffith's criterion on the other hand suffers in general from the inability to predict cracking in an initially sound and undamaged body, for which the energy release rate is null (for a counter-example see *e.g.* [69]). This can be verified by computing, for a specific crack geometry, the energy release rate G_ϵ considering the initial crack size ϵ as a parameter , and then noting that

$$\lim_{\epsilon \to 0} G_\epsilon = 0 \tag{2.51}$$

according to which cracks will never appear in a sound, flawless body, see [70,71]. This is hardly a paradox in that the engineer will advocate that no such thing as a flawless body exists in practice, yet it forces, at least in principle, the designer to assess the sizes of flaws present in the material of interest. In Chapter 2.3 this issue will be re-visited in more detail in relation to the so-called variational approach to fracture mechanics: essentially by relaxing the smoothness requirements on the function describing the crack length over time $l(t)$ so-called "brutal" cracks can appear even from the uncracked initial configuration [62,72].

A remark on the size-effect deserves to be noted. As described above the fact that the fracture strength is not a constant with respect to variations in the specimen characteristic size has been known for long time. Griffith's approach introduces a size-effect, *i.e.* a typical scaling between the, say, maximum stress and a characteristic length of the specimen, which can be shown to obey a power law relationship [73]. Griffith's approach seems to introduce a length-scale in the physical description (noting that the stress at fracture σ_f, Young's modulus E and surface energy G_c can be combined in the parameter EG_c/σ_f [73]): hence it might appear surprising that such theory scales with a power -law, as power-law scaling relationships are expected for self-similar, scale-free theories. While the reader is referred to [74] for a proof of the fact a theory will exhibit a power law scaling for the size-effect if and only if there are no characteristic dimensions in its description, it is noted that the explanation of the apparent contradiction lies in the fact the internal length-scale in Griffith's approach is "hidden", *i.e.* the process zone is thought as collapsed to a point and in Bažant's words "there is no change in failure mechanism associated with the (*characteristic*) length" [73]. A different size-effect can be exhibited by the variational theory of fracture where it originates from the competition between bulk-energy terms (related to volume) and surface energy terms (related to area): more attention to this aspect will be given in Section 2.3.

Only a brief mention will be given to viscoelastic extensions of Griffith's criterion: in this case the energy balance has to be modified to introduce a term accounting for dissipation. In general also the history-dependence of the surface energy might need to be accounted for: assuming the surface energy per created crack unit area is constant with respect to crack speed, one could write the energy balance for a self-similar crack

moving through a body over which external forces do not perform work as in [75]

$$\dot{l}G_c + \int_\Omega \Lambda \mathrm{d}\Omega + \dot{W} = 0 \tag{2.52}$$

where $\dot{l}$ is the crack speed, Λ is the specific dissipation (integrated over the body volume Ω) and $\dot{W}$ is the time derivative of the elastic energy. It was highlighted in Section 2.1.2 that in general the free energy for a viscoelastic material is not unique, in that different free energies could correspond to the same mechanical material behaviour: it will be then assumed the choice of the energy W is made on the basis of an improved knowledge of the material, whether such knowledge can or cannot be obtained through the experimental characterisation of the material. Interesting theoretical manipulations could originate from balance (2.52) [75], but in general a number of difficulties arise in computational applications. For example, if the stress field around the crack is modelled via linear elasticity, it turns out the strain rate at the crack tip is infinite for any crack speed! The problem was circumvented in [76, 77] by the introduction of an additional material parameter lacking, in the author's opinion, physical meaning: formulations based on cohesive zone models [78], introduced in the next section, avoid this problem but seem still unmanageable, as far as analytical computations are concerned, with the exception of few simple geometries. A final note on the energy balance in viscoelastic fracture mechanics: if the local form of energy balance is looked at instead of the integral form (2.52), a heat supply term has to be introduced if the deformation is supposed isothermal. Neglecting this term is tantamount to neglecting dissipation [14] and leads to fallacious paradoxes [79].

2.2.1 Equilibrium Cracks and the Contribution of G. I. Barenblatt

In the seminal work [8] Barenblatt starts by reviewing the state of art of the discipline at his time. He notes that, as presented above, if "we assume the surface of the crack to be free of stress $< \ldots >$ we obtain a paradoxical result; however we select the contour of a crack, the tensile stress at its edge is always infinitely large. Consequently, there are no equilibrium cracks: at as small a fraction stress as you please, a body having a crack breaks in two!"

Barenblatt was of course perfectly aquainted with the work of Griffith, according to which the singularity of tensile stresses is not sufficient for a crack to propagate. Indeed in his review the deficiencies of the approach based on elasticity theory only,

which had been overcome by Griffith's contribution, are pointed at (for example the fact that an elastic solution could be found for any crack length, given the same boundary conditions), yet evidently the presence of infinite stresses is still deemed as physically unacceptable ("It is clear that solutions in which infintely great stresses are obtained at the edge of the crack are unsuitable for any physically tenable model of brittle fracture").

He claims the inconsistency stems from not accounting fully, in the linear elastic solution considering traction-free crack surfaces, for all the forces acting on the body. It is then necessary in his view to consider the molecular cohesive forces acting in the vicinity of the crack tip where "the distance between the opposing faces is small and they attract one another powerfully". Interestingly, Griffith is credited for first bringing cohesive forces into consideration, stating that Griffith considers cohesive forces as forces of surface tension which act only on the interior of the body, and not on the crack faces. Moreover, Barenblatt notes how Griffith tried to improve the description of tensile forces near the crack tip by considering the crack as an ellipse. However, the fact that such procedure resulted in estimating the radius of curvature at the crack tip being in the order of atomic distances is viewed by Barenblatt as a clear admission of failure.

Instead, Barenblatt considers a slit-shaped crack, on whose lips a given traction is applied. Imposing the vanishing of the stress singularity a condition is determined, according to which in an equilibrium crack the crack faces "unite smoothly", in typical cusp-shaped geometry, see Fig.2.3. Following Barenblatt, credit must be given to [80] for first suggesting such a possibility.

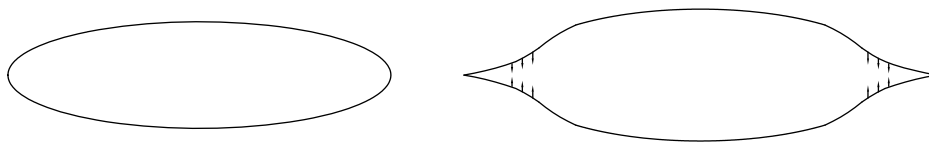Figure 2.3: Left: deformed shape of the contour of a slit crack according to the linear elastic solution without cohesive forces. Right: effect on the deformed shape of the cohesive forces (indicated by the small arrows) acting in a neighbourhood of the crack tips.

The dependence of the intensity of cohesive forces upon the distance between crack faces is in general quantitatively unknown. From the qualitative point of view, Baren-

blatt describes the cohesive forces in a crystal by stating that the maximum will be reached for atomic distances in the order of one and a half the average interatomic distance, before dropping quickly. In relation to amorphous solids the same qualitative behaviour is expected. These observations are justified by referring to experimental results regarding the strength of filaments and whiskers, which was known, as discussed above, to exceed the strength of larger specimens of the same material and in some cases even reach values very close to the theroretical value. As the latter is linked to cohesive forces only and not, in the idealised limit, to the presence of structural defects or instabilities, measurements on whiskers do provide an estimate of the magnitude of cohesive forces. Direct measurements for quartz and glass were available too, but are not sufficient to determine the relationship $\varrho = \Sigma(\delta)$ between displacement jump across the crack lips δ and cohesive forces ϱ.

While in principle the knowledge of Σ would provide a well posed problem for an equilibrium crack in a body acted upon by given forces, Barenblatt claims that the analytical solution of the resulting equation would be out of reach, and avoids the problem by the introduction of suitable hypotheses. According to the first hypothesis the size of the surface on which cohesive forces act is considered negligible compared to the crack size. The second hypothesis assumes that in a small neighbourhood of the tip of a crack at which cohesive forces reach their maximum the shape of the crack does not depend upon the applied loads. Both assumptions are physically justified, for "large" enough cracks *i.e.* sufficiently longer than the process zone, the latter being defined in this context as the region over which the crack lips exchange mutual attraction forces), by noting, as stated above, that the intensity of cohesive forces very steeply reaches a maximum as the distance between crack faces increases, after which their intensity drops quickly. The introduction of such hypotheses allows rigorous analytical solutions to be derived.

Of course if a numerical solution is sought then there is no need for such assumptions, and the cohesive forces can be introduced in the problem formulation once the *traction-displacement jump relationship* $\varrho = \Sigma(\delta)$ (which can be thought of as a constitutive relationship for the interface along which the crack propagates) is known.

2.2.2 Cohesive-Zone Models

Having in mind the application of finite-element computations using interface elements, it will be assumed for the rest of the section that the crack path is known *a priori* by explicitly describing the curve (in $\Re^2$) or surface (in $\Re^3$), later referred to as *interface*. In general the interfacial traction might not depend only on the displacement jump δ across the interface, whereby the traction might be for example described by a relationship as $\varrho = \Sigma(\delta, \boldsymbol{\alpha})$, with $\boldsymbol{\alpha}$ a vector of internal variables.

A cohesive-zone model (CZM) for the interface along which the crack is expected to propagate is fully described by the knowledge of the function Σ. CZMs can be classified as rate-independent and rate-dependent according to whether the crack propagation is affected by varying the imposed loading rate. In mathematical terms rate-independence entails invariance under an arbitrary time-rescaling of the external loading process. In the framework of thermodynamics with internal variables rate-independence can be shown to be necessarily related to the dissipation potential being positive and homogenous of order one (a function $f : x \to \Re$ is defined homogenous of degree n if $f(\alpha x) = \alpha^n f(x)$).

In the variational approach to fracture, see Section 2.3, the assumption of known crack path can be relaxed but as a result in this case Σ has to be assumed monotone decreasing in a neighbourhood of the origin, an explanation of the underlying reasons being postponed until Section 2.3. This is not the case for the majority of constitutive laws Σ proposed in the literature for use in finite-element schemes, *e.g.* bilinear, exponential, trapezoidal, *etc.*, which present a maximum for a certain $\delta = \bar{\delta}$; such formulations are still fully rigorous at the cost of imposing the crack path in advance. The aforementioned cohesive-zone constitutive laws also possess the property of being increasing in a right-neighbourhood of the origin, which greatly simplifies convergence of the numerical solver in finite-element schemes where the interface is modelled *via* interface elements.

The presence of a softening branch of Σ might suggest the explicit use of damage mechanics to reproduce the interface behaviour, although it is not in general necessary to introduce a damage process to justify the presence of a softening branch, for example see [81, 82] for attempts to found the cohesive-zone formulation on inter-atomic potentials of the Lennhard-Jones type.

The accurate determination of Σ for an engineering material is a daunting task. Generally the relationship is assumed *a priori* to obey a certain functional law, and the specific parameters are then numerically fitted based on experimental evidence. The determination of the cohesive traction-displacement jump law is a complex matter even relying on an extensive database of experimental results from fracture-mechanics specimens. This is a direct consequence of the fact that, in general, material parameters pertaining to a cohesive zone can be only indirectly evaluated from the overall specimen behaviour, in contrast for example with the ease with which the stress-strain properties can be measured. The possibility of estimating the cohesive law from classical tests such as uniaxial tension, shear, etc would have a conspicuous practical impact, in that such tests are generally easier, quicker and less expensive to perform. However, it seems at the moment prohibitely complex, although for example in [83] Chaboche states that "starting with the elastic, plastic and damage constitutive equations for an interphase, written in terms of a bulk stress, strain, and damage, it is easy to formulate the corresponding "interface" constitutive equations". The statement is of course absolutely correct from a theoretical point of view, but a close inspection of the proposed procedure, originally presented in [84], in the author's opinion reveals though that the results have very little practical relevance. The first assumption made is that bulk strains are uniform through the interface thickness, so that the following euqation characterises the (infinitesimal) strain tensor $\mathbf{e}$:

$$\mathbf{e} = \mathrm{sym}\frac{\mathbf{1}}{\mathbf{h}}(\boldsymbol{\delta} \otimes \mathbf{n}) \tag{2.53}$$

$\mathbf{n}$ standing for the unitary vector normal to the interface, $\mathbf{e}$ for the linearised strain tensor, $\boldsymbol{\delta}$ for the displacement jump and h for the interface thickness. The question arises if this is a reasonable assumption in practice, in other words if the complexity of the damaging phenomena occuring at the interface allows the definition itself of a bulk strain: the question whether it is acceptable or not to neglect surface stress effects [85–88], once the behaviour of the interface is sought in the limit of vanishing thickness, might be relevant. The reader is referred to the above mentioned sources and references therein for a detailed exposition, of which here the conclusion only is presented. If the stress-strain response of the finite-thickness interface material is described as $\boldsymbol{\sigma} = F(D)\mathbf{C}^0 :$ $\mathbf{e}$, where $\mathbf{C}^0$ is a material-dependent tensor and $F(D)$ is a scalar function depending on the damage state of the interphase, then the following expression for the elastic modulus

Y can be shown to hold:

$$Y = \frac{\delta_{max}}{h} \mathbf{C^0} \tag{2.54}$$

where δ_{max} is the maximum discontinuity jump for which cohesive forces do not vanish. The conclusion is that in order to achive a finite stiffness in the limit $h \to 0$, the tensor $\mathbf{C^0}$ has to be singular with linear dependence on the thickness ($\mathbf{C}^0 = \tilde{\mathbf{C}}h$, $\tilde{\mathbf{C}}$ being a constant tensor), which "does not seem to be realistic for the continuum properties of the material" (see also [89,90] for similar conclusions obtained by asymptotic analysis). As a result, Chaboche proposes two alternatives:

1) The interface is to be viewed as a finite thickness layer, and the interface model could be found by integrating through the thickness, obtaining then a (thickness-depending) constitutive law.

2) The interface is simply to be seen as a spatial regularisation of a classical fracture mechanics model

Option 2 seems to preclude the option of estimating cohesive zone parameters by "bulk" tests, while option 1 is reasonable, and will be our general choice for the interface model presented in Chapters 3 and 4, although the "through the thickness" integration operation again does not seem trivial at all.

For finite-element analyses using interface elements and interface constitutive laws characterised by a maximum it can be shown [91] that generally the problem solution is rather insensitive to the shape of the curve given that σ_{max}, G_c and K are unvaried

$$K = \Sigma'(0) \qquad G_c = \int_0^\infty \Sigma(\delta) \, \mathrm{d}\delta \tag{2.55}$$

where K represents the interface initial stiffness, G_c is the specific work needed to achieve complete separation, *i.e.* the critical energy release rate and σ_{max} is the maximum interfacial traction. This conclusion is challenged though by very stiff specimens (for which the ratio of their stiffness over the interfacial stiffness is very high). Restricting the discussion to pure Mode-I, let us underline that while in the theory of Barenblatt the case $\delta < 0$ is not physically significant as it implies interpenetration, in most numerical implementations this case has to be dealt with. The matter will be addressed in Chapter 3: it is though noted that should Σ not be continuosly differentiable at the origin then the derivative in equation $(2.55)_1$ is to be understood as a right-derivative [56].

It is of interest to note that in analyses based on the finite-element method and interface elements the initial stiffness K does introduce some spurious compliance in the model, an issue which is especially delicate for dynamic analyses [92]. The magnitude of K is in general critical in order to achieve numerical convergence [93, 94].

This section is ended by a brief exposition of the thermodynamics of the cohesive zone, mainly following [95] but restricting the analysis to the isothermal case. For this purpose, let us consider a two-dimensional body occupying the region Ω in $\Re^2$, with boundary $\partial\Omega$, in the undeformed configuration. Without loss of generality the body is assumed to contain a single crack originating from the boundary and generally varying with time. Let the crack be parametrised by its arc-length l, $0 \leq l \leq \beta(t)$, $l = 0$ corresponding to the body boundary. The crack is characterised by two regions:

1) a *free zone* along which no cohesive forces are exchanged between the crack lips, described by the condition $0 \leq l \leq \alpha(t)$

2) a *cohesive zone* along which cohesive forces are present, described by the condition $\alpha(t) \leq l \leq \beta(t)$

Then the power $\mathcal{P}$ exerted on the body by the outer world in the case of vanishing body forces equals

$$\mathcal{P} = \int_{\partial\Omega} \mathbf{S}\mathbf{n} \cdot \dot{\mathbf{u}} \, \mathrm{d}s - \int_0^{\alpha(t)} [\mathbf{S^T} \cdot \dot{\mathbf{u}}] \cdot \mathbf{m} \, \mathrm{d}\mathbf{s} \tag{2.56}$$

where $\mathbf{S}$ stands for a suitable stress tensor, $\mathbf{u}$ for the displacement field, $\mathbf{n}$ and $\mathbf{m}$ for the normal vector to the boundary and the free zone respectively. The term

$$-[\mathbf{S^T} \cdot \dot{\mathbf{u}}] = -\mathbf{S^+}\mathbf{m} \cdot \dot{\mathbf{u}}^+ + \mathbf{S^-}\mathbf{m} \cdot \dot{\mathbf{u}}^- \tag{2.57}$$

quantifies the power expended on the free zone. Along the cohesive zone stress is defined as

$$\boldsymbol{\sigma} = \mathbf{S^+}\mathbf{m} = \mathbf{S^-}\mathbf{m} \tag{2.58}$$

as a result of forces' balance. Setting $\boldsymbol{\delta} = [\mathbf{u}] = \mathbf{u}^+ - \mathbf{u}^-$, equations (2.56) and (2.57) yield

$$\mathbf{S^+}\mathbf{m} \cdot \dot{\mathbf{u}}^+ - \mathbf{S^-}\mathbf{m} \cdot \dot{\mathbf{u}}^- = \boldsymbol{\sigma} \cdot \dot{\boldsymbol{\delta}} \tag{2.59}$$

Consequently an application of the divergence theorem yields, keeping present Cauchy's equilibrium equation $\nabla \cdot \mathbf{S} = \mathbf{0}$

$$\int_\Omega \mathbf{S} \cdot \nabla\dot{\mathbf{u}} \, \mathrm{d}\Omega = \int_{\partial\Omega} \mathbf{S}\mathbf{n} \cdot \dot{\mathbf{u}} \, \mathrm{d}s - \int_\alpha^\beta [\mathbf{S}^T\dot{\mathbf{u}}] \cdot \mathbf{m} \, \mathrm{d}l \tag{2.60}$$

Equations (2.56, 2.59) allow to re-write the last result as

$$\int_\Omega \mathbf{S} \cdot \nabla \dot{\mathbf{u}} \, \mathrm{d}\Omega + \int_\alpha^\beta \boldsymbol{\sigma} \cdot \dot{\boldsymbol{\delta}} \, \mathrm{d}l = \mathcal{P} \tag{2.61}$$

which very neatly expresses how the power exterted by the rest of the world on the body is spent to deform the bulk and to perform work of separation along the cohesive zone. Coleman-Noll's procedure suggests that (please also refer to Section 3.2)

$$\mathbf{S} = \frac{\partial \boldsymbol{\Psi}}{\partial \nabla \mathbf{u}} \tag{2.62}$$

where Ψ is the free energy of the elastic material. Then equation (2.61) can be seen to be equivalent to

$$\frac{\mathrm{d}}{\mathrm{d}t} \int_\Omega \Psi(\nabla \mathbf{u}) \, \mathrm{d}\Omega + \int_\alpha^\beta \boldsymbol{\sigma} \cdot \dot{\boldsymbol{\delta}} \, \mathrm{d}l = \mathcal{P} \tag{2.63}$$

If the strain energy is the free energy of the elastic body, then equation (2.63) is a weak form of Griffith's criterion (written in rate form). It is worth noting that the balance equation is only a necessary condition for crack propagation, hence it is not to be considered as a criterion for crack propagation (although it "might very well be", in Gurtin's own words [95]). With similar arguments and algebraic manipulations the following forms of the First and Second Laws of Thermodynamics can be obtained:

$$\dot{E} = \mathcal{P} - \int_\alpha^\beta \boldsymbol{\sigma} \cdot \dot{\boldsymbol{\delta}} \, \mathrm{d}l \tag{2.64}$$

$$\boldsymbol{\sigma} \cdot \dot{\boldsymbol{\delta}} - \dot{\Psi} \geq 0 \tag{2.65}$$

E standing for the internal energy.

To conclude this Section it is remarked that the cohesive-zone modelling approach can be used in a wide range of numerical approaches, which might or might not require *a priori* knowledge of the crack path. Classical finite element methods using interface elements along the crack path belong to the first category, while extended finite-element methods and methods based on discretisation and regularisation of non-convex functionals incorporating the surface energy in the energy definition [96] belong to the second. The cohesive-zone approach can also be enriched allowing the rate-dependent case to be considered. This step requires the formulation of a rate-dependent traction-displacement jump law.

2.2.3 Rate-dependent Cohesive-Zone Models

The rate dependence of the mechanical response leading to crack initiation and/or growth cannot be neglected for a wide class of engineering applications. The complexity of the problem and the presence of numerous competing factors is evident from the fact the fracture thoughness may not show a monotonic trend with respect to crack speed, even when the latter is small enough not to consider inertial effects. Furthermore, even when such trend is monotonic, fracture toughness can increase with crack speed for some materials and decrease for others [97–99]. The importance of the problem has justified numerous experimental investigations. For example, results for a DCB test on a rubber modified epoxy show a decrease in fracture thoughness with increasing rate of applied displacement [100], whilst for a DCB made of Al 6061-T6 adherends and polyethylene as the adhesive the opposite trend has been reported [101].

Ancillary issues such as the possible sudden transition in some cases from stable to unstable propagation, also known as "*stick-slip*" behaviour ([102–104]), have been suggested to depend on the rate dependence of the fracture mechanism in the process zone [105–107].

In general, the overall rate dependence can arise as a consequence of rate dependence of the bulk material's behaviour, of the interface response itself, or of both. A number of cohesive zone models and modelling strategies have been presented covering these different assumptions.

Among the first group the work of Geers *et al.* [108] is mentioned, who analysed peel testing of PET. They were able to capture the rate sensitivity of the test results by only modelling the rate dependence of the bulk material. A similar approach is followed in a study by Nguyen and Govindjee [109], who studied the propagation of a crack in an infinitely long strip of visco-elastic material. To demonstrate how the total fracture energy dissipated during crack propagation increases with the crack speed they use a cohesive-zone model with an intrinsic fracture energy so that the rate-dependence originates from the bulk material only. As examples of the second approach a reference is made to Xu *et al.* [101,110] who similarly constructed a rate-dependent model by adding the contributions from a rate-independent and a rate-dependent element, the latter given by a Maxwell element. This quite satisfactorily replicates a class of experimental results but suffers from some inconsistencies in the formulation such as the fact that the

traction discontinuously goes to zero after reaching a threshold displacement given by a critical separation. Corigliano *et al.* [111] also focus on the rate-dependence of the interface to model a DCB carbon fibre-Poly-Ether-Imide (PEI) specimen. The interface deterioration is reproduced using two alternative phenomenological approaches, one of them based on softening plasticity and a second one in which a rate-dependent damage evolution law is adopted. Another example of this type of approach is the model proposed by Allen and Searcy [112], in which the interface element is conceived through a homogenisation procedure conducted at the micromechanical scale.

Liechti *et al.* [113] introduced rate-dependent behaviour in both the bulk material and the interface, motivating their decision by observing significant differences in crack surface depending on test speed, which convinced them of the necessity of modelling the viscous losses at the interface. They also assumed the interface strength could be assimilated to a non-linear elastic response summed to a viscous contribution, given by a non-Newtonian dashpot. Damage evolution is implicit in their formulation as the elastic response is given by a bilinear elastic traction-separation law. Furthermore, the authors suggest that the use of a non-Newtonian dashpot could possibly reproduce the rate-dependent nature of void formation. The model proposed by Hutchinson *et al.* [114] follows the same approach of introducing the rate-dependence in both the bulk and the interface. They are able to investigate the competing effects and present an explanation for the possible non-monotonic relationship between crack speed and toughness. The rate dependence of the cohesive zone is taken to obey a functional form similar to the elasto-viscoplastic formulation used to model the bulk material.

To the author's knowledge a rigorous discussion on the merit and fallacies of each of the above mentioned general approaches has not been tackled. It is evident that the dissipation occurring in the bulk material has to be accounted for in any realistic modelling attempt, so the problem eventually condenses to whether it is possible to neglect the dissipation occurring at the interface, capturing the overall behaviour by simply focusing on the bulk material (as for example attempted with analytical tools by Xu *et al.* [115], Persson and Brener [3]) or Christensen [116]). In the author's opinion the answer is negative. In the cohesive-zone approach the zero-thickness interface is assigned a mechanical behaviour which indeed originates from the interaction of the crack with a process zone which is possibly very thin, yet of finite thickness. This region of finite measure is "lumped" into a line (or a surface in 3D) and hence it seems

37

to be necessary to account for its own time-dependence. It is interesting to compare this observation with the experimental work of Hauch and Marder [117]. They observed how the increase in fracture energy with crack speed was matched by the development of a microstructure of branching transversal cracks whose length and density was increasing too. They also noted though that below a certain speed the fracture energy was still not constant in spite of the lack of any observable transversal crack pattern. Upon dissection of the specimens it was found that the additional dissipation was likely to be connected with some "subsurface activity", in their terminology. It is postulated that these occurences can only be accounted for by introducing the rate-dependence at the interface level. Also it is worth noting that this approach has a very significant advantage for the practising engineer. In many structures elastic materials are bonded using polymers, and the analysis could avoid modelling the polymeric layer altogether, under certain restrictions, replacing it with interface elements.

As for the use of plasticity [111], it might be deemed not physically justified as it can hardly be evoked to explain that tractions decrease to zero at incipient fracture. It is possibly an effective numeric tool to reproduce softening but, as crack formation and/or propagation ultimately involves breaking bonds at the molecular or atomic scale, it seems to be better described by damage mechanics from the physical point of view.

The above presented considerations represent a point of departure for the development of novel cohesive-zone models presented in Chapters 3 and 4 which aim at capturing the history-dependence of the crack growth.

2.3   Variational Approach to Fracture

It has been already noted in Chapter 2.2 that Griffith's criterion clarifies and disciplines the competition between two energetic contributions: the bulk energy released by a crack advance is to balance the amount of energy needed to create the new crack surface (regardless of how this is accounted for, by a Griffith-type or a Barenblatt-type energy). This is a cornerstone of Fracture Mechanics which was recently re-visited in a series of papers [24, 63, 72, 118], originating the so-called *variational approach to fracture*. A limitation of Griffith's criterion is represented by the regularity required by the potential energy, as this has to be differentiable for the energy release rate to be defined. Recalling the discussion in Chapter 2.2, it was shown how Griffith's criterion, equations (2.45),

(2.46), derives from considering the stationarity of the potential energy, equation (2.48), assuming there is sufficient regularity in $\mathcal{W}$ to allow the definition of the derivatives involved. In the variational approach to fracture instead the starting point is directly a potential energy functional $\mathcal{W}$ which in the case of a Griffith-type energy reads as:

$$\mathcal{W}(t; u, l) = \int_{\Omega \setminus \Gamma(l)} W(\nabla u(t, l)) \, \mathrm{d}x - \mathcal{A}(t, u(t, l)) + G_c l \qquad (2.66)$$

with

$$\mathcal{A}(t, y) = \int_{\Omega} f_b(t) \cdot u \, \mathrm{d}x + \int_{\partial \Omega_s} f_s(t) \cdot u \, \mathrm{d}s \qquad (2.67)$$

where f_b and f_s stand for body and surface forces respectively, while $\partial_s \Omega$ is the portion of the boundary of Ω, $\partial \Omega$, on which surface forces f_s are applied, whereas on the portion $\partial_d \Omega$ an imposed displacement $g(t)$ is considered.

A stationary point for the functional $\mathcal{W}$ can be sought under more general conditions than required by the application of Griffith's criterion in the form of equations (2.45) and (2.46). As a result the variational formulation allows dealing with much "wilder" crack geometries and evolutions, for example allowing for discontinuous crack growth, a case clearly out of reach for the classical formulation, not to mention the fact that the requirement for an *a priori* knowledge of the crack path can be relaxed.

The foundation of the variational approach to fracture consists in proving that the energy $\mathcal{W}$ provides a variational principle [119] for a fractured elastic body. In the presence of smooth fields the proof that a functional yields a variational principle usually involves showing that the Euler-Lagrange equations coincide with the strong form of the governing equations. In the present case some extra steps are required, after which (the reader is referred to Proposition 2.1 of [72] for further details) it is shown that a stationary point $(l(t), u(t))$ of the functional $\mathcal{W}$ in the class of admissible competitors $\bar{l} \geq l(t)$ (necessary condition to ensure irreversibility of the cracking process) satisfies the equilibrium equation, the displacement boundary condition, the traction boundary condition and the traction-free condition at the crack lips respectively.

Different definition for the crack energy are available: should a cohesive-zone energy be preferred to the Griffith-type energy $G_c l$, in [72] it was proposed to replace the latter with a term as

$$\int_{\Gamma} \Sigma(|[\![u(\zeta)]\!]|) \, \mathrm{d}\zeta \qquad (2.68)$$

or, after defining the cumulated jump as $\chi(t) = \sup_{\tau \leq t} [u(\tau)]$ (for a pure Mode-I case),

by

$$\int_{\Gamma} \Sigma(\,|\min([\,y(\zeta)\,],\chi(t)|)\,\mathrm{d}\zeta \qquad (2.69)$$

The latter definition [120] is based on the physical consideration that once a discontinuity jump is reached, further dissipation can occur only for increasing discontinuity jump (the same physical reasoning will be employed in the formulation of the cohesive-zone model presented in Chapter 3).

So far only stationarity has been considered, in the spirit of Griffith's formulation. The introduction of a minimality principle can be done in two ways. A local minimality setting, pending the definition of a suitable topology, *i.e.* a well-defined definition of neighbourhood of a solution, leads to seeking a local minimizer of $W(t:u,l)$ among all $l \geq l(t)$ and $u = u_0(t)$ on $\partial_d \Omega \setminus \Gamma(l)$. Alternatively a global minimizer could be sought. Certain differences of the two approaches will be pinpointed in a later Section, the reader is referred again to [72] for a more detailed discussion, as well as considerations on the status of postulates of the aforementioned minimality criteria. The crack set $\Gamma(t)$ will be considered in more detail now. In the seminal paper [121] it was proposed to set the minimization problem for the *free discontinuity functional* in a functional space allowing for discontinuities, in such a way that the crack set is automatically defined as the jump set $S(u)$ of the argument function u, *i.e.* the set of points at which u is discontinuous, and such set replaces Γ in previous definitions. The space first used by De Giorgi was the SBV space of *special functions of bounded variations*. Denoting with $\mathcal{L}^n$ the n-dimensional Lebesgue measure, a function $z \in L^1(\Omega)$ belongs to the space SBV of special functions of bounded variations if its distributional derivative can be expressed as

$$Dz = \nabla z(x)\mathcal{L}_n + (z^+ - z^-)\nu \mathcal{H}^{n-1} \lfloor S(z) \qquad (2.70)$$

where ν indicates the normal vector to the jump set $S(z)$ and the operator $\lfloor \cdot$ indicates the restriction to its set-valued argument.

The term $(z^+ - z^-)\nu \mathcal{H}^{n-1} \lfloor S(z)$ is the *jump part* of the distributional derivative. The definition could be appreciated operationally by calculating the distributional derivative of a one-dimensional piecewise smooth function, verifying that on the jump set (in the one-dimensional case, a set of points) the distributional derivative is given by the Dirac measure multiplied by the magnitude of the jump.

Attention is restricted from now to the one-dimensional case, which contains all the physical richness needed in the sequel without the burden of significantly increased mathematical complexity. In dimensions higher than one the method requires the ability to deal with possibly complicated sets and the associated topologies might be highly non-trivial. In addition, any functional space must not only enjoy properties (such as compactness, lower semicontinuity) necessary for the theory of Calculus of Variations to be employed, but must also satisfy the requirements of mechanics such as quasiconvexity [122, 123], injectivity, *etc.* leading to additional complications. For example, a vector-valued function whose components belong to SBV would not be acceptable in the three-dimensional case [124]. In the one-dimensional setting the crack set is a countable collection of points, and considering piecewise-continuous functions as the space for candidate minimizers is more than adequate for the purposes of this thesis. As far as the numerical implementation of the above presented scheme for realistic applications, it is worth mentioning the possibility of approximating the functional $\mathcal{W}$, see equation (2.66), by the introduction of suitable internal variables in order to smoothen possible discontinuities, [82, 96]. Such approach is tightly related to the so-called *phase-field* models [125, 126]. The chapter ends by presenting and discussing two examples which are relevant for later developments.

2.3.1   A Cohesive Bar

Consider a constant cross-section bar of length L loaded in a displacement-controlled test machine (the reader interested in the traction control case can refer to [72], [127]). The displacement field of the bar is described by the map $u : [0, L] \to \Re$. The function u is assumed to be C^1 with the exception of a countable set $S(u)$ of jump points. For simplicity the extremities of the bar are not allowed to belong to $S(u)$. The admissible space so defined will be denoted by $\mathcal{Y}(0, L)$. The bulk energy of the bar depends only on the local gradient of u through the convex function $\omega = \omega(u')$, with the usual conditions

$$\omega(0) = \omega'(0) = 0 \tag{2.71}$$

The energy associated to a displacement jump is given by the function $\theta = \theta([u])$. θ is assumed lower semicontinuous and monotonic non-decreasing over the real positive line. Please note these assumptions do not exclude from consideration a Griffith type

energy

$$\theta([u]) = \begin{cases} 0 & \text{if} \quad [u] = 0 \\ G_c & \text{if} \quad [u] > 0 \\ \infty & \text{if} \quad [u] < 0 \end{cases} \tag{2.72}$$

It is easy in fact to see, at least heuristically, that the cohesive-zone approach converges (in the sense of Γ-convergence, [82]) to Griffith's crack model as the process zone length tends to zero (a claim that has been rigorously proved by Giacomini [128], see also equation 2.63 for an intuitive insight).

The total energy of the bar is then given by the functional

$$\mathcal{W} = \int_0^L \omega(u'(x))\mathrm{d}x + \sum_{S(u)} \theta([u](x)) \tag{2.73}$$

subject to the boundary conditions

$$u(0) = 0 \quad , \quad u(L) = \bar{L} - L \tag{2.74}$$

where $\bar{L}$ is the imposed elongation. The same symbol $\mathcal{W}$ as before but it is made clear that the functional $\mathcal{W}$ is now argument of the displacement field u only, following the discussion in the previous section on how the crack is automatically defined as the jump set of u. Boundary conditions can also be expressed in integral form (to within a rigid translation) as

$$\int_o^L u'(x)\,\mathrm{d}x + \sum_{S(u)} [u](x) = \bar{L} \tag{2.75}$$

The non-convexity of the functional (2.73) is noted. Consider for example a Griffith type energy. Let us take

$$u_1 = \mathcal{I}_{[0,a]} \quad , \quad u_2 = \mathcal{I}_{[0,b]} \tag{2.76}$$

where $\mathcal{I}_\Omega$ stands for the indicator function over the set Ω, i.e the function

$$\mathcal{I}_\Omega(x) = \begin{cases} 0 & \text{if} \quad x \notin \Omega \\ 1 & \text{if} \quad x \in \Omega \end{cases} \tag{2.77}$$

For such displacement fields the elastic energy contribution vanishes and it can be observed that

$$\mathcal{W}(\frac{u_1 + u_2}{2}) = 2G_c > \frac{1}{2}[\mathcal{W}(u_1) + \mathcal{W}(u_2)] = G_c \tag{2.78}$$

contradicting the definition of convexity of a functional.

Define now $\mathcal{W}_\eta$, the first variation of $\mathcal{W}$ in direction η as

$$DW_\eta = lim_{\epsilon \to 0+} \frac{\mathcal{W}(u + \epsilon\eta) - \mathcal{W}(u)}{\epsilon} \tag{2.79}$$

Define an equilibrium configuration $u \in \mathcal{Y}$ at imposed elongation $\bar{L}$ as a configuration satisfying the inequality

$$DW_\eta \geq 0 \tag{2.80}$$

for all perturbations η such that $\eta(0) = \eta(L) = 0$. The limit is understood to take the value of $+\infty$ for perturbations with newly created fracture points [127].

Please note as the functional is in general non-smooth it is not possible to follow the classical derivation of the stationarity condition for a functional as this usually implies a Taylor series development centered in u. As a result and as noted in the introductory section, no classical Euler-Lagrange differential equations can be derived.

A local equilibrium configuration will require the definition of a norm, which can be used to characterise a neighbourhood. The norm of the total variation

$$\|u\| = \int_0^L |u'(x)|\mathrm{d}x + \sum_{S(u)} |[u](x)| \tag{2.81}$$

is chosen in [118] based on physical grounds (a translation of a jump point is "felt" by this norm as two configurations with same jumps but different jump sets), while the sup-norm is chosen in [118]. The choice of a norm is inconsequential though in the case the minimization is carried out in a finite-dimensional space, as for such spaces all norms are equivalent. A local minimizer of $\mathcal{W}$ will then be defined as a function $u \in \mathcal{Y}$ if there exists a $\beta > 0$ for which

$$\mathcal{W}(u + \eta) \geq \mathcal{W}(u) \quad \forall\eta : \eta(0) = \eta(L) = 0, \|\eta\| < \beta \tag{2.82}$$

Appealing only to the stationarity condition, equation (2.80), the following statements can be proven

$$u'(x) = c \quad c \in \Re \quad \forall x \in (0, L) \setminus S(u) \tag{2.83}$$

$$\theta'([u](x)) = \omega'(c) \quad \forall x \in S(u) \tag{2.84}$$

$$0 \leq \omega'(c) \leq \theta'(0^+) \tag{2.85}$$

The proof relies on inserting suitable test perturbations in equation (2.80) and can be found in [118]. Equations (2.83), (2.84), (2.85) have a direct physical meaning. Equation (2.85) bounds the stress in the bar, giving hence a condition for the apperance of cracks. Equation (2.84) expresses the fact the strain has to be constant along the bar, while equation (2.83) expresses the stress continuity condition on the jump set.

An essential role is played by the value $\theta'(0^+)$, which dictates when initiation (apperance of a cracked configuration) will occur. $\theta'(0^+) = \infty$ for a Griffith-type energy as one described by equation (2.77). Hence, stationarity is satisfied for any homogeneous deformation. This fact echoes equivalent statements in classical fracture mechanics, please compare the discussion of Section 2.2. A similar result can be proven, within the variational theory of fracture, in a two-dimensional context as well [129]. Under certain assumptions on the bulk energy and using local minimality instead of stationarity, it was proved that no crack can initiate from an uncracked configuration. Essentially, the thereom proves that the bulk energy released by removing a ball of material of arbitrary radius is more than the associated surface energy created by appearance of the circular contour.

The case of a Griffith-type energy is considered now, which is solved using conditions (2.83, 2.84, 2.85). As just noted, the use of stationarity alone does not allow much progress, as the uncracked configuration satisfies such condition regardless of the loading parameter $\bar{L}$. The matter would not change if local minimality is employed [72]. Only global minimality brings some novel behaviour.

It is useful to write equation (2.73) as

$$\mathcal{W} = \int_0^L \omega(u'(x))\mathrm{d}x + \sharp S(u)G_c \tag{2.86}$$

where $\sharp(\cdot)$ is an operator returning the cardinality of its set-valued argument. The global minimality setting is considered. If $S(u) = \emptyset$ then

$$\mathcal{W} = \int_0^L \omega(u'(x))\mathrm{d}x \tag{2.87}$$

and as a result of the assumed convexity of ω the unique minimizer will be the linear function $u = \frac{\bar{L}}{L}x$.

Incidentally, given any displacement field $u \in \mathcal{Y}(0, L)$, the displacement field $\tilde{u}$

$$\tilde{u} : S(u) = S(\tilde{u}), \tilde{u} \text{ is linear on } [0, L] \setminus S(u) \tag{2.88}$$

can be seen to satisfy

$$\mathcal{W}(u) \geq \mathcal{W}(\tilde{u}) \tag{2.89}$$

If on the other hand $\sharp S(u) = N \neq 0$, as no cohesive forces are exchanged between two fractured parts of the bar if a Griffith energy is employed then

$$\mathcal{W} = NG_c \tag{2.90}$$

As a result, any configuration with more than one crack is energetically disadvantageous. Given that the only admissible cracking process consists in the apperance of a single crack from the pristine state, the condition

$$\int_0^L \omega(u'(x))\mathrm{d}x = G_c \tag{2.91}$$

allows the computation of the value of the loading parameter $\bar{L}$ at which the crack appears.

The analysis of a cohesive energy proper depends heavily on its convexity properties. While referring to [118] for a detailed analysis covering concave, convex-concave and "bi-modal" energies, the presentation is limited here to some facts which will be referred to in Chapter 5. From equations (2.83), (2.84), (2.85) it can be inferred that the homogenous configuration satisfies stationarity as long as $\omega'(u') \leq \theta'(0^+)$, after which the elastic stress ω' can not increase any more and cracks have to appear. Incidentally, note that if $\theta'(0^+) = 0$ the bar can sustain no elongation. Noting that $\theta' = \Sigma$, Σ having been defined in section 2.2, it can be seen that the variational approach rejects the possibility of a Σ such that $\Sigma(0) = 0$, *e.g.* the bilinear traction-discontinuity jump, law, if the crack path is assumed not known *a priori*. Having understood that at least a crack has to appear once $\omega'(u') > \theta'(0^+)$, the question arises of how many cracks will do so. The answer depends on the convexity properties of θ. First consider the case of θ concave. Concavity implies *sub-additivity*, a property according to which

$$\theta(w + v) \leq \theta(w) + \theta(v) \tag{2.92}$$

Such property has a direct physical consequence, in that it will always be convenient to replace two cracks with one crack whose opening is the sum of the two original openings. As this can be done without altering the state in the elastic portion of the bar, one can conclude that there can be at most one crack. If the cohesive energy

θ is not sub-additive (over a set of its definition domain), then this line of reasoning fails and the analysis must account for the possibility of multiple cracking. It is noted that sub-additivity does not imply concavity, *e.g.* any function $\varrho : \Re \rightarrow \Re$ such that $k < \varrho(x) < 2k \quad \forall x$, k being a constant, is sub-additive. A convex function though is not sub-additive. By reversing the argument above, if θ is convex then, given a cracked configuration, a lower energy configuration could be found by "splitting" the cracks in two, without altering the state in the elastic portion of the bar. Configurations characterised by the appearance of multiple cracks with infinitesimal jumps occur, which do not converge in the space SBV. As a result, no minimizer can be found (mathematically, this is related to the fact the functional ceases to be compact). An attempt to define a generalised solution and give it a physical meaning in terms of diffuse cracking (and plasticity) can be found in [127].

Chapter 3

A Novel Rate-Dependent CZM

3.1   Description of the Mathematical Problem

The two-dimensional setting will be considered only for simplicity's sake. Let Ω be the reference configuration of a two-dimensional body $\mathcal{B}$ with boundary $\Gamma = \partial\Omega$. The body is characterised by the presence of an interface Γ^C, dividing the body in two subregions Ω^A and Ω^B with boundaries Γ^A and Γ^B respectively, so that $\Gamma^C = \Gamma^A \cap \Gamma^B$, as Fig. 3.1 illustrates. Boundaries Γ^j, $j = A, B$, are assumed regular so that normal unit vector fields $\mathbf{n^j}$ can be defined.
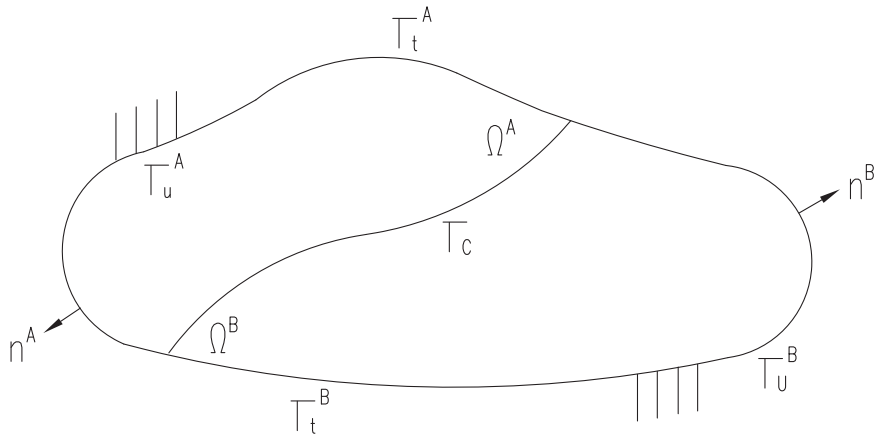

Figure 3.1: The body $\mathcal{B}$, the two subregions Ω^A and Ω^B and the interface Γ^C.

Time-varying displacements $\mathbf{u}$ are prescribed, $\mathbf{u} = \bar{\mathbf{u}}$ over parts of the outer boundary (which are labeled as Γ_u^ξ depending on whether they belong to Γ^A or Γ^B) in order

to model loading by a hard device. Time-varying tractions $\mathbf{t}$ are prescribed, $\mathbf{t} = \bar{\mathbf{t}}$ over parts Γ_t^j, the same naming conventions applying. By necessity $\Gamma_t^j \cap \Gamma_u^j = \emptyset$.

The material behaviour of the subregions Ω^j is modelled by an appropriately chosen continuum material constituive law. The main interest of the present work being focused on the interface response, upon restricting the analysis to a kinematically linear setting, elastic behaviour is assumed for the domains Ω^A nd Ω^B, characterised then by a material law $\mathbf{S} = \mathbf{C} : \mathbf{e}$, where $\mathbf{C}$ is the fourth-order stiffness tensor. The interface, along which the two subregions Ω^j can debond, is on the other hand to be assigned a point-wise traction-separation law $_{-\infty}\Lambda_t$, depending (not necessarily linearly, in contrast to the "bulk" constituive laws presented in Section 2.1) on the history of displacement jumps at the interface, see Sections 2.2.2 and 3. Attention is restricted to the case where debonding occurs in Mode I exclusively, *i.e.* the relative displacement at the interface contains only a normal (to the interface) component. This condition entails a restriction on the body geometry and its loading. In the numerical examples discussed in Sections 3.4 and 4.2 compliance to this conditions is guaranteed by appropriate symmetry conditions.

The process is assumed isothermal and quasi-static.The mathematical problem is then defined as follows:

Given:

1) Displacement boundary conditions $\mathbf{u}(t) = \bar{\mathbf{u}}(\mathbf{X}, t)$ on Γ_u^A and Γ_u^B

2) Traction boundary conditions $\mathbf{t}(\mathbf{X}, t) = \bar{\mathbf{t}}(\mathbf{X}, t)$ on Γ_t^A and Γ_t^B

3) The stiffness tensor $\mathbf{C}$

4) The traction separation law $\boldsymbol{\sigma} = _{-\infty}\Lambda_t(\boldsymbol{\delta})$

Find the time varying displacement field $\mathbf{u}$ (not necessarily continuous along Γ^C), satisfying Cauchy's equilibrium equation and boundary conditions. This is in essence the problem described in Section 2.2.1, solved analytically by Barenblatt upon establishing a number of assumptions which are not necessary if a numerical solution is sought. The main difference between the presented problem and Barenblatt's problem described in Section 2.2.1 lies in that in the latter the bonded, undamaged part of the interface is not equipped with a traction-separation law and the continuum description applies. On the other hand, in the problem just presented all the interface, even the bonded portion,

48

is governed by the assigned traction-separation law. This difference clarifies the issue of spurious compliance possibly caused by the implementation of a cohesive-zone *via* interface elements, hinted at in Section 2.2.2.

It is noted that, as stress is not defined on the interface, the equilibrium equations can be written separately for the two domains, paying attention to the fact that additional boundary conditions (accounting for the interface response) are now to be imposed on the bonded part of the interface, for each subregion, in order to correctly model the interaction (given by interface tractions) of the two subregions. The following tasks are now in order:

1) Identify a physically sound traction-separation law capable of simulating rate-dependent debonding as experimentally observed (while special attention will be given to elastomeric interfaces, but a formulation with the potential of being generalised to other rate-dependent materials will be sought)

2) Formulate and implement a suitable algorithmic scheme for the numerical solution of the presented problem

3) Validate the model against experimental data

The objectives will be achieved in two steps: in the rest of the Chapter a general framework will be presented, later to be specialised in Chapter 4. The functional-based description used for viscoelastic materials (see Section 2.1) is to be enriched introducing an (irreversible) damage variable, effectively yielding a non-linear functional representation.

3.2   Formulation of the Interface Model

Based on the considerations expressed at the end of Chapter 2.2, the aim is to capture the rate dependence within the process zone of the interface itself regardless of the behaviour of the surrounding material, resorting to first principles. It is clear that assumptions will be necessary to model such a complex phenomenon as fracture, yet the intention is to develop a general, physically well based cohesive model, without resorting to any phenomenological law other than basic physical and engineering understanding.

As a cornerstone of our modelling approach the existence of an intrinsic,*i.e.* rate-independent, fracture energy is acknowledged. This is related to an elastic energy threshold needed to break bonds at the micro or possibly the atomistic scale [2]. A damage-mechanics approach is employed following which a suitably defined damage variable is introduced, whose evolution is related to the difference between the energy threshold and the elastic energy. The rate-dependence of the overall dissipated energy during crack propagation is a natural by-product of the visco-elastic dissipation lumped on the zero-thickness interface. It is postulated that a reasonable characterisation of the interface rate-dependence can be achieved by assuming that the interfaces behaves, in a suitably defined way, as its constituent material considered as a continuum. The cohesive model formulation is then enclosed in the general framework of thermodynamics.

To validate the concept (i) the formulation is specialised to the case of a rubber interface, (ii) the simplest possible assumption is made by assuming a quadratic form for the elastic energy and by choosing a linear viscoelastic law with exponential kernel and one relaxation time only and (iii) a comparative analysis of numerical and experimental results is presented.

It is postulated that the interface response can be described by resorting to the free energy potential of the material considered as a continuum. Such decision stems from the review of numerous experimental results, [22, 76, 130–137]. The functional dependence of the free energy upon its arguments is then kept the same as in the continuum case while the variables themselves are suitably adapted. This is a result of the dimension reduction implied by the use of a cohesive-zone model, whereby a thin layer is modelled as a surface in 3D and a two dimensional slender region is "shrunk" into a line in 2D. Accordingly, displacement discontinuity jumps at the interface replace continuum strains as new deformation measures. Progressive degradation of the interface and its ultimate failure is then reproduced naturally through a damage variable, see Fig.3.2.

No *ad hoc* phenomenon is invoked to explain the additional dissipation other than the dissipative mechanisms inherent to the material. More specifically, the damage law is assumed to be rate-independent and to be driven by the specific elastic energy. In the following presentation lower-case letters will be employed for vectors while capital bold letters stand for tensors, to underline the generality of the approach. This notational convention will become redundant after the formulation is specialised to the pure Mode-I case in a subsequent section. In general, the traction σ at time t at a point of an

(a) Micromechanical model

material 2

σ

$\bot$ thickness > 0

σ

material 1

damaged interface

microcracks

(b) Mesomechanical model
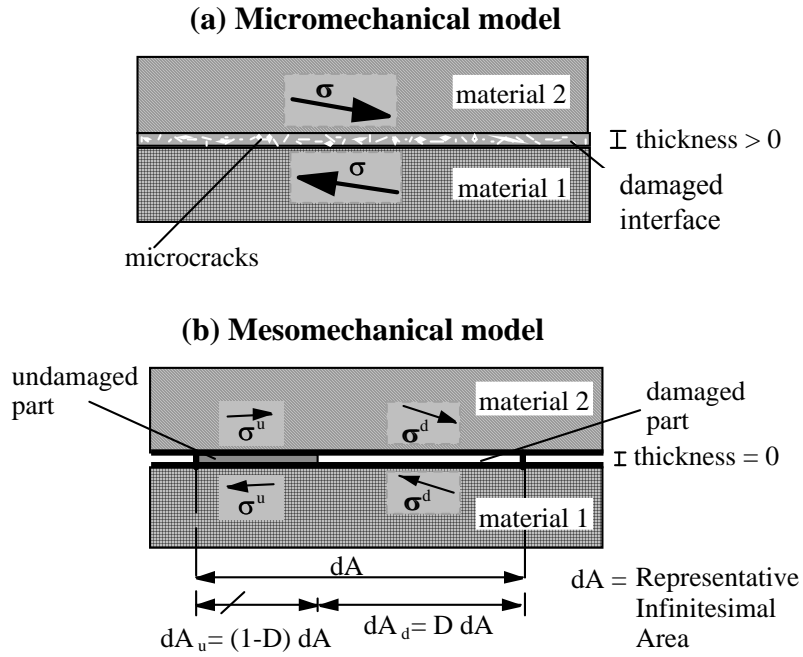
undamaged

Representative
Infinitesimal
Area

Figure 3.2: Schematic explanation of the implicit "homogenisation" process implied by the introduction of the damage variable: a) "micromechanical" view of an infinitesimal portion of the finite-thickness damaged interface b) "mesomechanical" view of the same, the detailed information on micro-cracks being exchanged for an "averaged" description based on damage variables.

interface with memory is characterised by a functional $_{-\infty}\Sigma_t$ defined on a suitable set of displacement jump histories $\boldsymbol{\delta}:]-\infty, t] \to \Re^n$:

$$\boldsymbol{\sigma}(t) =_{-\infty} \Sigma_t(\boldsymbol{\delta}) \tag{3.1}$$

where n denotes the number of components of $\boldsymbol{\delta}$ (and $\boldsymbol{\sigma}$). In the framework of thermodynamics with internal variables, we consider all the past history as "condensed" in suitably defined internal variables, which together with the so-called observable variables [106] fully define the state of the material.

The free energy Ψ is chosen as

$$\Psi = \Psi(\boldsymbol{\delta}, \boldsymbol{\alpha}, \mathbf{D}) \tag{3.2}$$

where $\boldsymbol{\delta}$ represents the displacement discontinuity jump, $\boldsymbol{\alpha}$ denotes internal variables

associated with the rate-dependence of the mechanical response and $\mathbf{D}$ represents an internal variable too, which is grouped separately as it exclusively describes the damaging process. In a general case, $\boldsymbol{\delta}$, $\boldsymbol{\alpha}$ and $\mathbf{D}$ are vectors and therefore they have been denoted with boldface characters.

Following the classic definition of damage due to Kachanov [138] it is suggested that Ψ will depend linearly on $\mathbf{D}$, which is assumed to be m-dimensional:

$$\Psi(\boldsymbol{\delta}, \boldsymbol{\alpha}, \mathbf{D}) = (\mathbf{1} - \mathbf{D}) \cdot \tilde{\boldsymbol{\Psi}}(\boldsymbol{\delta}, \boldsymbol{\alpha}) \tag{3.3}$$

where $\tilde{\boldsymbol{\Psi}}$ denotes a suitably defined vector of free-energy, whose components are denoted $\tilde{\Psi}_i$, $i = 0, 1 \ldots m$, '$\cdot$' indicates the scalar product and $\mathbf{1}$ is the m-dimensional vector $\mathbf{1} = \begin{bmatrix} 1 & 1 & \ldots & 1 \end{bmatrix}$.

The choice of the number and type of the internal variables depends of course on the phenomenon being addressed. The great flexibility and power of the procedure lies in that these variables can be chosen to represent a vast range of physical phenomena occurring within the material.

In this thesis attention is devoted to mode-I crack propagation and therefore the displacement jump specialises to a scalar δ. Next, the rheological model represented in Figure 3.3 is introduced, commonly denominated as the Standard Linear Model (SLS) or alternatively Zener model, from the first scientist to propose it based on a thermomechanical argument [139]. A single scalar α is used as internal variable, which denotes the inelastic displacement jump in the viscous unit.
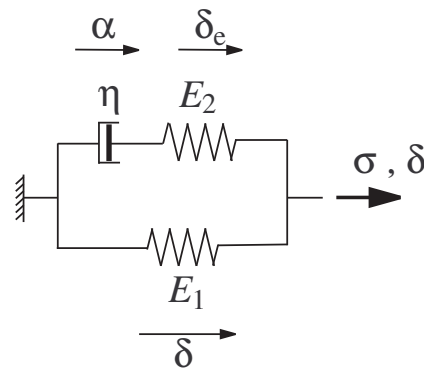

Figure 3.3: Rheological representation of the model.

The following relation between total (observable) displacement jump δ and the in-

ternal variable α is stated

$$\delta = \delta_e + \alpha \tag{3.4}$$

where δ_e represents the internal elastic displacement jump within the inelastic arm.

The following expression for the free energy is chosen, upon introducing a (formally) two-component damage vector $\mathbf{D} = \begin{bmatrix} D_1 & D_2 \end{bmatrix}$ (*i.e.* $m = 2$):

$$\Psi = \Psi(\delta, \alpha, \mathbf{D}) = (\mathbf{1} - \mathbf{D}) \cdot \begin{bmatrix} \frac{1}{2} E_1 < \delta >_+^2 \\[2ex] \frac{1}{2} E_2 < \delta - \alpha >_+^2 \end{bmatrix} + K_c \mathbf{1} \cdot \begin{bmatrix} \frac{1}{2} E_1 < \delta >_-^2 \\[2ex] \frac{1}{2} E_2 < \delta >_-^2 \end{bmatrix} \tag{3.5}$$

where symbols $< \bullet >_+$ and $< \bullet >_-$ represent the positive and negative parts of the argument, respectively, while E_1 and E_2 are the elastic stiffness values in the elastic and the inelastic arm of the rheological model in tension. The second term at the RHS in the above equation reflects the further assumptions that damage does not influence the response in compression due to crack closure, rate-dependence is negligible and the interface stiffness is amplified by a scalar K_c. Notice that the last two assumptions are physically justified by the typical behaviour of rubber under confined compression [140].

3.3   Thermodynamical Consistency

The definition of evolution laws for the internal variables cannot be established without ensuring such laws do not violate the Second Law of thermodynamics for any arbitrary process; this can be achieved by following the rational mechanics approach introduced by Coleman and Noll [10, 141, 142].

As the process is assumed to be isothermal the Second Law specialises [142] to the following:

$$\sigma \dot{\delta} - \dot{\Psi} \geq 0 \tag{3.6}$$

neatly expressing the fact that dissipation has to be positive (as the rate at which energy is supplied can at the most equal the rate of increase of the free energy). For the free energy of our choice, given by equation (3.5), an application of the chain rule yields:

$$
\dot{\Psi} = \left[(\mathbf{1} - \mathbf{D}) \cdot \left[\begin{array}{c} E_1 <\delta>_+ \\ \\ E_2 <\delta - \alpha>_+ \end{array} \right] + K_c \mathbf{1} \cdot \left[\begin{array}{c} E_1 <\delta>_- \\ \\ E_2 <\delta>_- \end{array} \right] \right] \dot{\delta}
$$

$$
+ \left[(\mathbf{1} - \mathbf{D}) \cdot \left[\begin{array}{c} 0 \\ \\ -E_2 <\delta - \alpha>_+ \end{array} \right] \right] \dot{\alpha} \qquad (3.7)
$$

$$
- \left[\begin{array}{c} \frac{1}{2} E_1 <\delta>_+^2 \\ \\ \frac{1}{2} E_2 <\delta - \alpha>_+^2 \end{array} \right] \cdot \dot{\mathbf{D}}
$$

Upon inserting in Equation (3.6) and factorising $\dot{\delta}$

$$
\left\{ \sigma - \left[(\mathbf{1} - \mathbf{D}) \cdot \left[\begin{array}{c} E_1 <\delta>_+ \\ \\ E_2 <\delta - \alpha>_+ \end{array} \right] + K_c \mathbf{1} \cdot \left[\begin{array}{c} E_1 <\delta>_- \\ \\ E_2 <\delta>_- \end{array} \right] \right] \right\} \dot{\delta} +
$$

$$
+ \left\{ (\mathbf{1} - \mathbf{D}) \cdot \left[\begin{array}{c} 0 \\ \\ E_2 <\delta - \alpha>_+ \end{array} \right] \right\} \dot{\alpha} + \qquad (3.8)
$$

$$
+ \left[\begin{array}{c} \frac{1}{2} E_1 <\delta>_+^2 \\ \\ \frac{1}{2} E_2 <\delta - \alpha>_+^2 \end{array} \right] \cdot \dot{\mathbf{D}} \geq 0
$$

Sufficient conditions for the above inequality to hold are as follows:

$$
\begin{cases}
\sigma = (\mathbf{1} - \mathbf{D}) \cdot \left[\begin{array}{c} E_1 <\delta>_+ \\ \\ E_2 <\delta - \alpha>_+ \end{array} \right] + K_c \mathbf{1} \cdot \left[\begin{array}{c} E_1 <\delta>_- \\ \\ E_2 <\delta>_- \end{array} \right] \\
\\
\dfrac{\partial \tilde{\Psi}_2}{\partial \alpha} \dot{\alpha} = E_2 \dot{\alpha} <\delta - \alpha>_+ \geq 0 \\
\\
\dot{D}_1, \dot{D}_2 \geq 0 \\
\\
D_1, D_2 \leq 1
\end{cases} \qquad (3.9)
$$

It is more difficult to prove that such conditions are necessary, if they are so at all. Indeed, compared to the continuum case [141], the degree of independence with which

the fields δ and $\dot{\alpha}$ can be varied is less clear, see [95] for a similar discussion in the case of a rate-independent cohesive-zone with heat conduction. Conditions 3.9 will have to be considered and complied to during the selection of the relevant internal variables evolution laws, task to which the next Section is devoted.

3.3.1 Internal Variables Evolution Law

Having established thermodynamical constraints for the internal variables, complying evolution laws can be chosen. With regards to the internal variable α, a simple candidate equation capable of fulfilling Equations (3.9) is then found in:

$$\dot{\alpha} = \frac{\sigma - \sigma_1}{\eta} \tag{3.10}$$

where σ_1 denotes the stress in the elastic arm of the rheological model and η is a positive constant. With this choice linear visco-elasticity with an exponential kernel is recovered. This law is considered sufficiently accurate to model the process zone in order to capture the essential aspects of the time-dependent response within an expected range of validity.

As far as $\mathbf{D}$ is concerned, it has be noted that a characterisation of its evolution should rely on the availability of a micromechanical argument. In more detail, once attention is directed towards a specific material, micromechanics might suggest different evolution laws to be tailored for the components of $\mathbf{D}$. For the purposes of the algorithm presentation it is assumed without loss of generality that $D_1 = D_2$, reducing hence $\mathbf{D}$ to a scalar variable D.

For the evolution of $D = D_1 = D_2$ the law proposed in [143] is chosen, as a result of the fact it reflects our assumption that damage is driven solely by local elastic energy: such evolution law was derived *via* a thermodynamic argument. An energy threshold for damage growth $Y_c = Y_c(D)$ is introduced and the following Kuhn-Tucker constraints [144] are then obtained (analogous to equations (2.45) and (2.46) expressing Griffith's criterion)

$$Y \leq Y_c \qquad \dot{D} \geq 0 \qquad (Y - Y_c)\dot{D} = 0 \tag{3.11}$$

where

$$Y = \frac{\partial \Psi_1}{\partial \delta} \tag{3.12}$$

It is important to underline the choice made on the damage-driving function Y, which does depend on the elastic energy stored in the elastic arm only, not the total stored elastic energy. This decision is crucial for the model behaviour and is motivated by rubber's microstructure. In more detail, the attempt of using linear viscoelasticity to model rubber could rely on assuming that its free energy is the sum of elastic (equilibrium) and viscous (non-equilibrium) contributions. The former is thought to be related to the stretch and distorsion of the load-bearing network, while the latter originates from entanglements and motions of parts of the network that are deforming with the main load-bearing network as a result of topological constraints (sulphur bonds as a first example), more details can be found in [145]. Incidentally, it is acknowledged that rubber elasticity is entropic in nature [1], *i.e.* the free energy of a volume of rubber is largely dependent on the chains' configuration: in other words the amount of elastic energy stored in the load-bearing network is negligible when compared to the contribution given by configurational entropy. It is on the other hand clear that appealing to micromechanical energetical arguments such as the ones sketched above is not in contradictory terms with the entropic origin of free energy in rubber.

Within this conceptual scheme it is remarked that the damage variable has to be driven by its related energy exclusively, as fracture is caused by failure in the load-bearing network, The following relationship between Y_c and D is then assumed:

$$Y_c = \begin{cases} G_0 & \text{if} \quad D = 0 \\ \dfrac{G_0}{\left(1 - \dfrac{G_c - G_0}{G_c} D\right)^2} & \text{if} \quad 0 \leq D \leq 1 \\ \overline{Y}_c & \text{if} \quad D = 1 \end{cases} \tag{3.13}$$

where G_c is the intrinsic fracture energy, G_0 the elastic energy threshold below which there cannot be damage growth and $\overline{Y}_c = \max_{\tau \leq t} Y$ is the maximum of Y over the previous history. Notice that equation $(3.13)_3$ is introduced for completeness, so that equation $(3.11)_1$ continues to be satisfied, but it only has a formal importance, because when $D = 1$ cohesion is lost and no more energy is dissipated. It was shown in [143] that this relationship, when used in conjunction with a free energy of the form $\Psi(\delta, D) = \frac{1}{2}(1 - D)E\delta^2$, results in the widely used bilinear traction-discontinuity jump law. Also, it was shown in [143] how the proposed relationship between Y_c and D is equivalent to stating that

$$D = \begin{cases} 0 & \text{if } \delta_{max} \leq \delta_0 \\ \min\left\{1, \left(\dfrac{G_c}{G_c - G_0}\right)\left(1 - \dfrac{\delta_0}{\delta_{max}}\right)\right\} & \text{if } \delta_{max} \geq \delta_0 \end{cases} \qquad (3.14)$$

where δ_{max} is defined as follows:

$$\delta_{max} = \delta_{max}(t) = \max_{\tau \leq t} \delta(\tau) \qquad (3.15)$$

and $\delta_0 = \sqrt{2\,G_0/E_1}$ is the value of the displacement jump at which damage starts growing in the elastic arm.

Notice that the damage-driving function Y is path independent because it only depends on the current value of the relative displacement, whereby the energy eventually dissipated in the elastic arm of the rheological model, after complete decohesion, is always equal to G_c. Instead, the total energy dissipated does depend on the whole displacement history $\delta :]-\infty, t] \to \Re$, because it is the sum of G_c and of the the energies dissipated in the inelastic arm. This introduces rate-dependence in the simulated dissipative process within the process zone at the interface.

The proposed model reproduces a bilinear traction-separation law only in the extreme cases of instantaneous and infinitely slow loading, in total analogy with how linear viscoelasticity reduces to linear elasticity in the fast and slow rate limit [14].

The time-integration algorithm required to solve the obtained governing equations is described in the next section.

3.4 Algorithmic Implementation

This section describes how the constitutive equations of the interface are solved during an incremental step, in the context of a general displacement-based finite element method.

Limiting the discussion for the sake of simplicity to a specific integration point, the problem essentially consists of determining the traction $\sigma(t)$ corresponding to a given displacement-jump history $\delta :]-\infty, t] \to \Re$. Without loss of generality it is assumed that $\lim_{t \to -\infty} \delta(t) = 0$, whereby the problem consists in solving the following system of differential equations in the unknown functions $\sigma(t), D(\delta_{max})$:

$$
\begin{cases}
\sigma(t) = [1 - D(\delta_{max}(t))] < \displaystyle\int_{-\infty}^{t} \mathcal{J}(t - \tau)\,\dot{\delta}(\tau)\,d\tau >_+ + [1 - D(\delta_{max}(t))]\,E_1 < \delta >_+ \\
\qquad\qquad\qquad\qquad\qquad\qquad\qquad\qquad\qquad\qquad\qquad + K_c\,(E_1 + E_2) < \delta >_- \\[2mm]
D(\delta_{max}) = \begin{cases}
0 & \text{if } \delta_{max} \leq \delta_0 \\
\min\left\{1, \left(\dfrac{G_c}{G_c - G_0}\right)\left(1 - \dfrac{\delta_0}{\delta_{max}}\right)\right\} & \text{if } \delta_{max} \geq \delta_0
\end{cases} \\[4mm]
\delta_{max} = \max_{\tau \leq t}\ \delta(\tau)
\end{cases}
\tag{3.16}
$$

where $\mathcal{J}$ is the relaxation function, defined by

$$
\mathcal{J}(s) = E_2\,e^{-\frac{s}{\lambda}}
\tag{3.17}
$$

and λ is the relaxation time $\lambda = \eta/E_2$. The first term in equation 3.16 refers to the Maxwell arm, the second to the elastic arm.

Equations (3.16) cannot be solved by analytical means in the general case and a numerical integration scheme has to be employed. Evidently all the difficulty arises from equation $(3.16)_1$, as equation $(3.16)_2$ is an algebraic equation and equation $(3.16)_3$ can be easily implemented.

Equation $(3.16)_1$ is approximated by adapting a widely used recursive algorithm [146, 147]. Assuming (again without loss of generality) that the displacement-jump history is null before $t = 0$ the time interval over which the computation is to be carried out, $[0, T]$, is discretized into a partition of N time increments:

$$
[0, T] = \bigcup_{n=1}^{N} [t_n, t_{n+1}] \qquad\qquad t_{n+1} = t_n + \varDelta t_n
\tag{3.18}
$$

In the n-th time step, the times at the start and the end of the increment are t_n and t_{n+1}, respectively, the proposed algorithm yields the result

$$
\frac{1}{E_2}\int_{-\infty}^{t_{n+1}} \mathcal{J}(t_{n+1} - \tau)\,\dot{\delta}(\tau)\,d\tau \approx
$$

$$
\cong e^{-\frac{\varDelta t_n}{\lambda}}\int_{-\infty}^{t_n} e^{-\frac{t_n - \tau}{\lambda}}\,d\tau + \frac{\delta(t_{n+1}) - \delta(t_n)}{\varDelta t_n}\int_{t_n}^{t_{n+1}} e^{-\frac{t_{n+1} - \tau}{\lambda}}\,d\tau
\tag{3.19}
$$

$$
= e^{-\frac{\varDelta t_n}{\lambda}}\,\delta_e(t_n) + [\delta(t_{n+1}) - \delta(t_n)]\frac{1 - e^{-\frac{\varDelta t_n}{\lambda}}}{\frac{\varDelta t_n}{\lambda}}
$$

The solution scheme proceeds iteratively, so it suffices to describe one iteration step. At the beginning of a generic time step n the following quantities are known: $\delta_n = \delta(t_n)$, $\delta_{e,n} = \delta_e(t_n)$, $\delta_{max,n} = \delta_{max}(t_n)$ and $D_n = D(t_n)$. Their knowledge completely defines the state of the interface. Given a tentative relative displacement $\delta_{n+1} = \delta(t_{n+1})$ all the pertinent quantities are then updated as follows

$$
\begin{cases}
\delta_{max,n+1} = \max(\delta_{max,n}, \delta_{n+1}) \\[2mm]
D_{n+1} = \max\left\{ D_n, \min\left\{ 1, \left(\dfrac{G_c}{G_c - G_0}\right)\left(1 - \dfrac{\delta_0}{\delta_{max,n+1}}\right) \right\} \right\} \\[3mm]
\sigma_{n+1} = (1 - D_{n+1})\, E_2 < \left[e^{-\frac{\Delta t_n}{\lambda}}\, \delta_{e,n} + \dfrac{1 - e^{\frac{-\Delta t_n}{\lambda}}}{\frac{\Delta t_n}{\lambda}}\,(\delta_{n+1} - \delta_n) \right] >_+ + \\[3mm]
\qquad\qquad + (1 - D_{n+1})\, E_1 < \delta_{n+1} >_+ + K_c\,(E_1 + E_2) < \delta_{n+1} >_-
\end{cases}
\tag{3.20}
$$

The consistent tangent stiffness is computed through routine algebraic manipulations as follows:

$$
\frac{\partial \sigma}{\partial \delta} = \begin{cases}
0 & \text{if} \quad D = 1\, \forall \delta \\[2mm]
(1 - D)[E_1 + E_2 \dfrac{\lambda}{\Delta t}(1 - e^{\frac{-\Delta t}{\lambda}})] - \dfrac{\partial D}{\partial \delta}\, \sigma & \text{if} \quad D \neq 0 \,\text{and}\, \delta \geq 0 \\[2mm]
K_c & \text{if} \quad D \neq 0 \,\text{and}\, \delta \leq 0
\end{cases}
\tag{3.21}
$$

3.5   Analysis of Experimental and Numerical Results

The general geometry described in Section 3.1 is specialised to a common fracture mechanics test specimen, whose geometry is sketched in Fig.3.5. A 25mm wide double-cantilever-beam (DCB) specimen made of 8mm thick steel arms separated by a 1mm thick interface of filled SBR / NR blend rubber has been tested under displacement control at nine different rates of the monotonically increasing prescribed cross-head displacement, equal to 0.01, 0.1, 1, 10, 100, 500, 1000, 10000, 100000 mm min^{-1}. A summary of all test results is presented in Fig.3.4. A close-up of the delamination front is presented in Fig.3.6.

The DCB specimen has been chosen as the most suitable test geometry because it offers a unique advantage when compared to other possible Mode-I specimen geometries such as the peel test, the pure-shear test or the notched tensile dumbell specimen.

Indeed, sandwiching the interface of interest between two metallic arms guarantees that no rate-dependent losses other than the ones occurring within the interface are present: the modelling of the T-peel test geometry on the other hand would be dependent upon a satisfactory description of the rate-dependent behaviour of the arms. This test geometry is also interesting in that the energy release rate is not constant with respect to crack length (as is the case for the peel test or the pure shear test piece, [75]): this generally will lead to a non-constant crack speed, making the experimental validation more challenging. Another desirable feature of the test geometry is the fact it does adress both crack inititiation (no sharp crack tip is introduced in the specimen prior to testing) and crack propagation.

The cohesive-model has been implemented into a user subroutine (UMAT) for the finite-element code ABAQUS$^{\text{TM}}$, version 6.12.2, as a constitutive law of interface elements, also called 'cohesive elements' in the ABAQUS manual. The UMAT code is included in the Appendix. The numerical model employs fully integrated 4-noded (linear) plane-strain elements with incompatible modes (CPE4I by Abaqus naming conventions) for the steel arms, while 4-noded (linear) 2D interface elements (COH2D4) are used for the rubber interface. Three uniform structured meshes have been used:

1) 4 x 100 solid elements (60 interface elements)

2) 6 x 133 solid elements (80 interface elements)

3) 8 x 200 solid elements (120 interface elements)

For the numerical analysis a Young's modulus of 210 GPa and a Poisson's ratio of 0.3 have been used for the steel arms. For the interface the constants reported in Table 3.1 have been used. The first three parameters in the table have been calibrated based on the test speed of 100 min mm^{-1}. For the relaxation time and the ratio between E_2 and E_1 the additional test speed of 10 min mm^{-1} has been used.

Due to symmetry with respect to the crack plane only the top half of the specimen was modelled. The 2D approximation cannot of course capture the fact that the crack front is not a straight line, but it was shown in [148] that in general this leads to reasonably accurate results for wide enough specimen, such as the one tested in our case.

Fig.3.7 shows the experimental and the numerical load-displacement curves for the case of test speed of 100 min mm^{-1} and shows that the numerical model can correctly
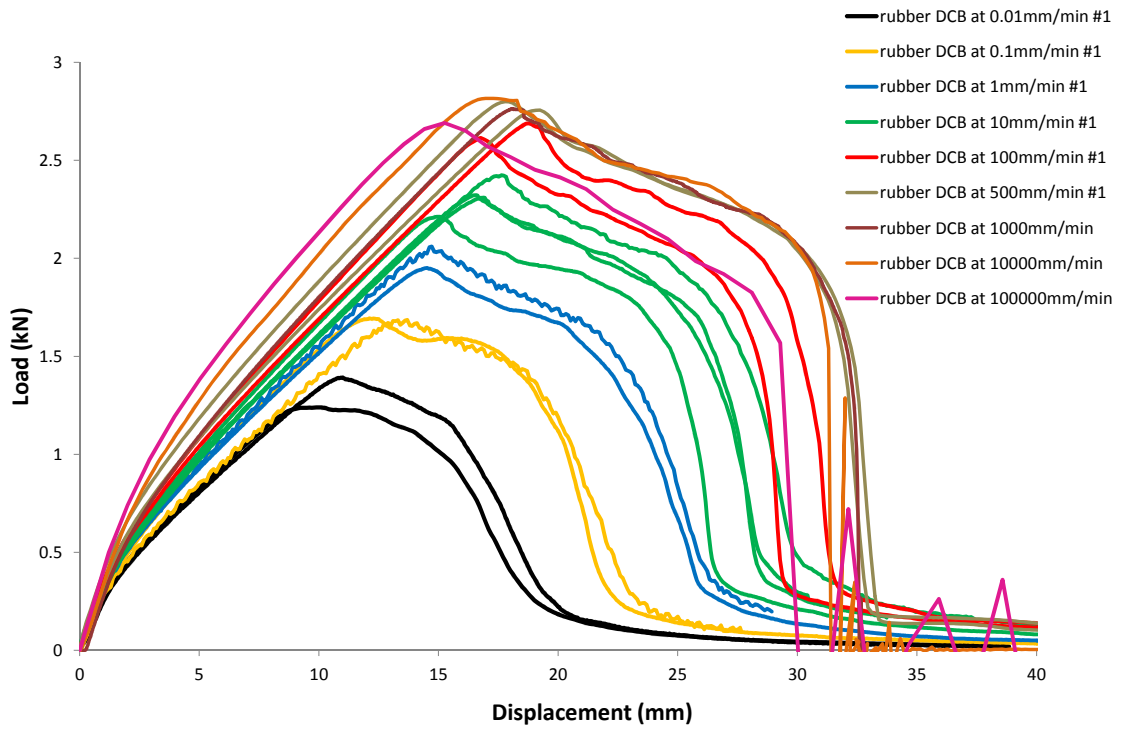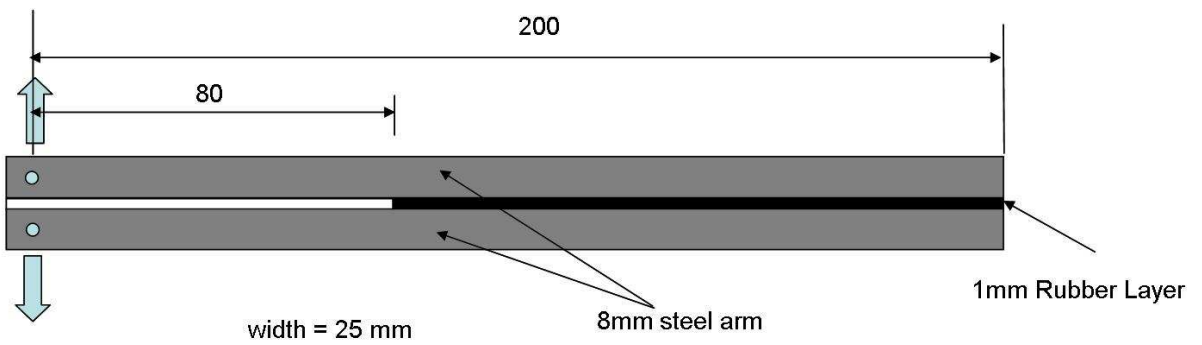
Figure 3.4: Summary of all test results.

Figure 3.5: Geometry and loading of the tested DCB specimen.

capture all aspects of the experimental behaviour, with good agreement both qualitatively and quantitatively. In this figure five points of the debonding process have been
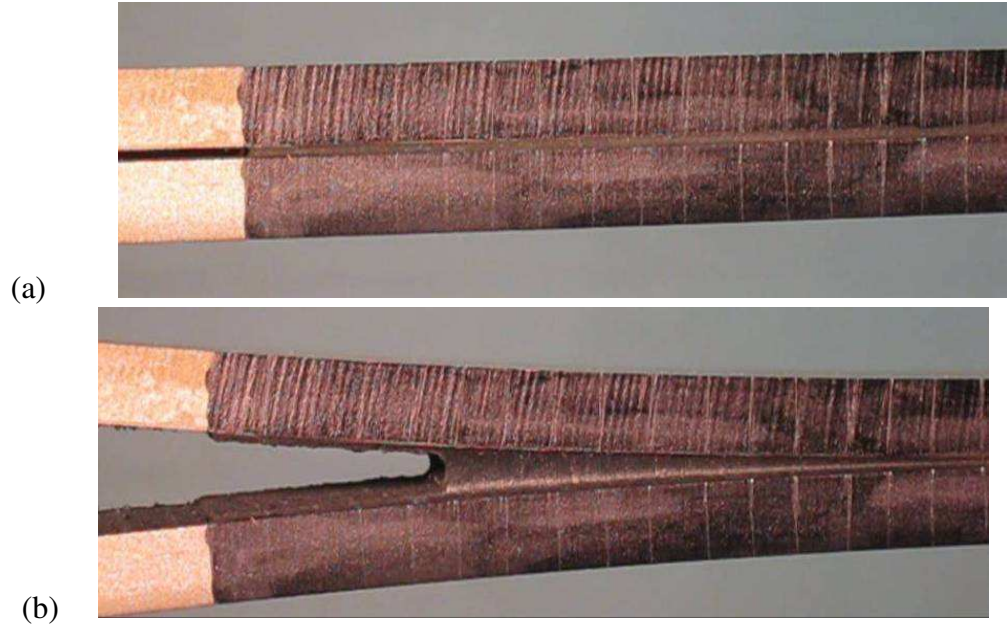
61

(a)

(b)

Figure 3.6: Experimental test: particular of the (a) undeformed and (b) deformed specimen.

G_c (N mm^{-1})	δ_c (mm)	E_1 (N mm^{-3})	E_2 (N mm^{-3})	λ (s)
9.5	1.1875	18.5	15.1	148

Table 3.1: Input parameters used for the rubber interface.

marked with the letters a, b, c, d and e, to identify the following five essential parts or moments of the debonding process: (a) elastic loading, (b) onset of fracture, (c) (approximately) self-similar crack propagation, (d) disruption of approximate self-similarity due to the crack-tip field reaching the specimen boundary and (e) almost-rigid rotation following the almost complete propagation of the crack.

The direct stress in the vertical direction across the steel arm (σ_{yy} in the model reference system) has been chosen as a reasonable indicator of the process-zone activity and Figs.3.8.a-e show the contour plots of S_{yy} (**S** standing for the stress tensor) at the points of the debonding process indicated in Fig.3.7. At point a (elastic loading), a stress concentration is forming at the crack tip: the interface discontinuity-jump, albeit non zero, is 'small', and the stress profile resembles the singularity field characteristic of classical continuum elements. At point b, the crack has just started propagating, causing the stress distribution to be more spread. At point c the crack is now moving
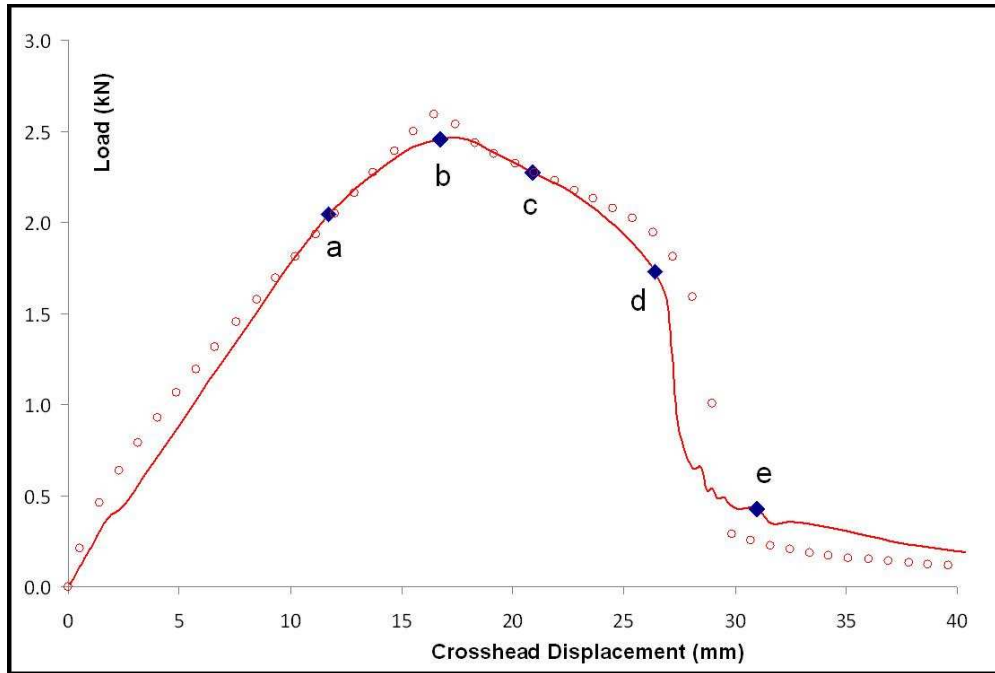
62

Figure 3.7: Numerically and experimentally obtained load-displacement curves for the test speed of 100 min mm^{-1}, showing the points of the debonding process referred to in Figure 3.8.

in an approximately self-similar way. This is happening on a rather limited length due to the relatively large size of the process zone in relation to the sample. At point d the compression distribution at the far left side is changing, as the lack of available space and the need of maintaining the overall resultant bending moment lead to a narrower and more intense stress distribution. Finally, at point e debonding is almost complete, the arm can only sustain negligible bending and the total force has now reduced to almost zero.

Fig.3.9 shows a comparison of the numerical and experimental load-displacement curves for all the considered test speeds. Therefore, their analysis allows validating the capability of the model to capture rate-dependence. The model prediction is satisfactory only on a range of applied displacement rates. More in detail, it can be seen that the model does not capture the change of the response when the applied rate is increased from 100 min mm^{-1} to 500 min mm^{-1}, in fact the numerical curve obtained at 500 min mm^{-1} practically overlaps with the one obtained at 100 min mm^{-1}. The same happens at the low range of speed, indeed the computed response at 0.1 min mm^{-1} is rather close
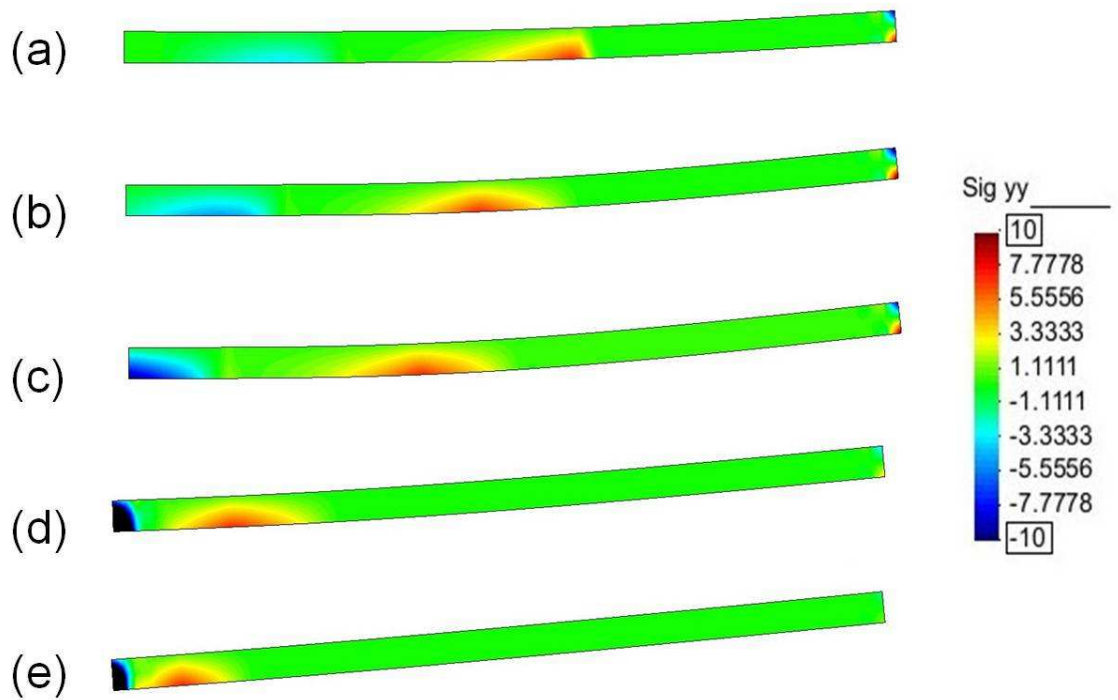
63

Figure 3.8: Contours plots of the direct stress in the vertical direction at the points of the debonding process indicated in Figure 3.7.

to the computed response at 0.01 mm/min, while the experimental response is characterized by lower global loads. This lack of ability to predict the rate dependence over 5 logarithmic decades of applied displacement rate is not surprising at all. The same qualitative behaviour can be seen in similar viscoelastic analyses if the relaxation spectrum employed in the costituive model is too narrow with respect to the real material. This is certainly our case, as a discrete spectrum with a single relaxation time is being employed to model rubber behaviour, whose spectrum is not only continuous but rather wide too, spanning certainly more than 5 logarithmic decades. Incidentally, it is also interesting to note how the quality prediction degrades as the crack progresses towards the end of the approximatedly self-similar propagation region: this might be a result of the fact the crack is by then travelling at a speed for which dynamic effects on the energy release rate might not be negligible [149, 150].

On the other hand, a viscoelastic model with one relaxation time is expected to capture relatively well the rate dependence roughly over three/four logarithmic decades.

64

This is indeed what happens in the presented model;this is a promising result as it indicates that the use of a wider relaxation spectrum or of a more complex, possibly nonlinear, viscoelastic law will be likely to improve the predictive capacity without substantially altering the conceptual framework herein presented.
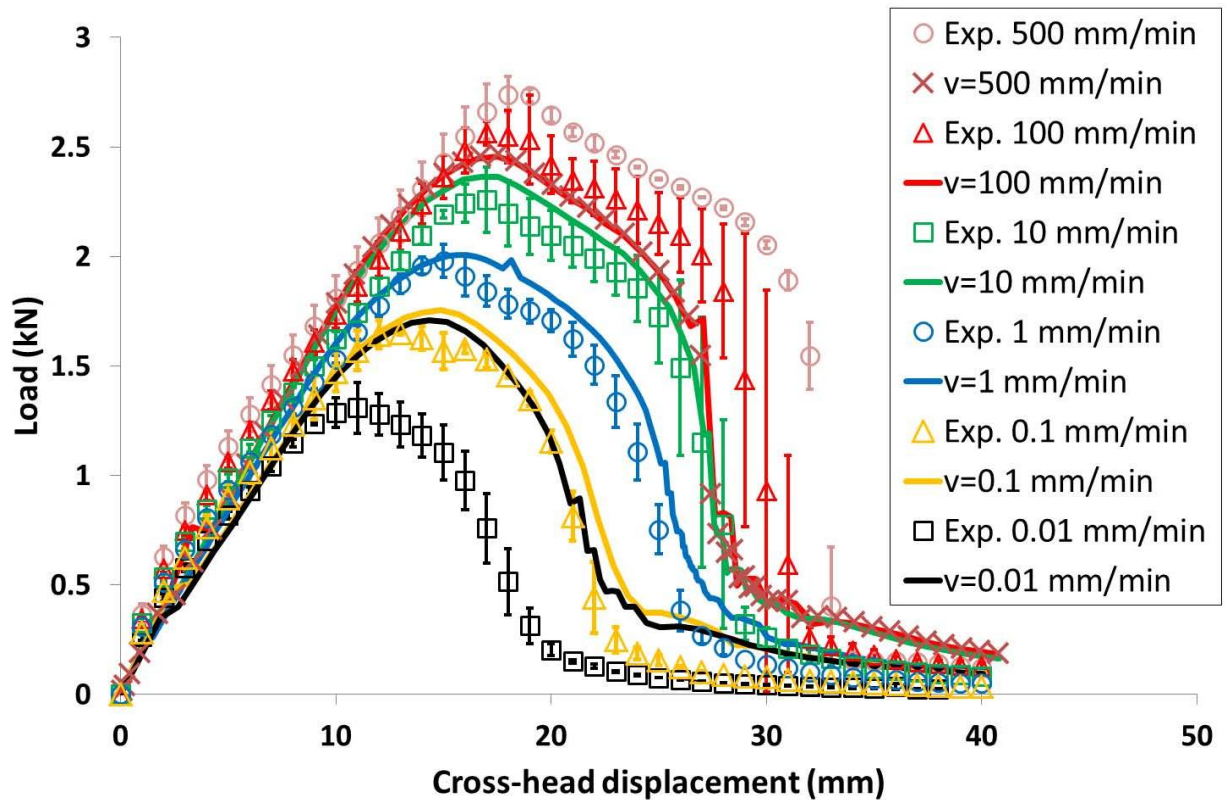
Figure 3.9: Experimental *vs* numerical load-deflection curves for the six considered test speeds.

The section is closed by presenting some convergence tests, the results of which are collated in Fig.3.10. Analyses related to one test rate only are presented, but analogous convergence performance has been achieved at all rates employed during testing. The convergence with respect to the mesh density was checked by comparing entire load-deflection curves, as well as focusing on the response of one material point, in the present case the tip of the initially present crack. Both approaches confirm mesh-convergence. The convergence with respect to the algorithmic step Δt was checked as well and found satisfactory.
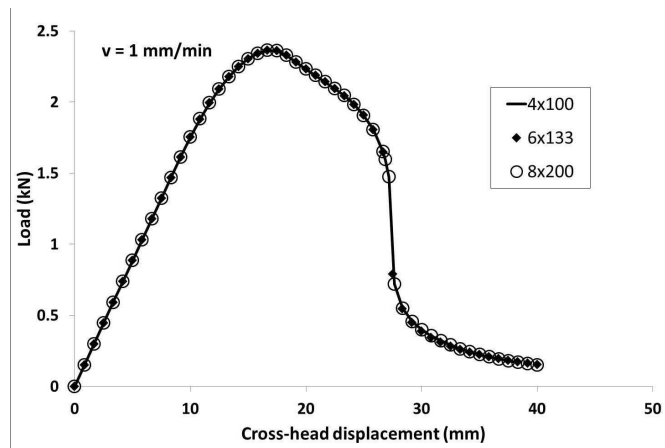
(a)
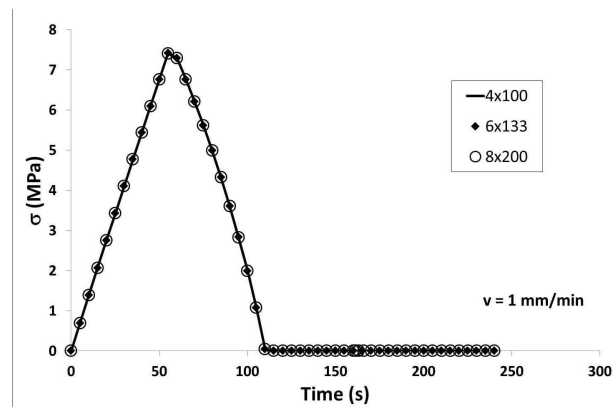
(b)
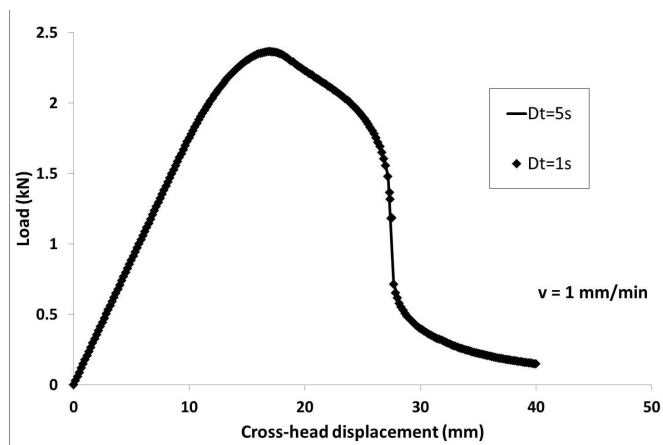
(c)

Figure 3.10: Convergence analysis, test speed of 1 mm/min: (a) Load-deflection curves and (b) traction at the initial crack tip, for increasing mesh density (c) Convergence of the numerical response with respect to time step Δt.

Chapter 4

Fractional Calculus Formulation of a Rate-Dependent CZM

The cohesive-zone model formulated in the previous Chapter will now be modified to improve its predictive ability. Following the discussion in Section 2.1.3 it seems natural to attempt to modify the presented model by exploiting certain features of fractional calculus: to make the comparison more effective the rheologic structure of the model presented in the previous Chapter is left unaltered, by considering a fractional Standard Linear Model instead of the classical, integer-order derivative, version.

The stress response of the classical Standard Linear Solid (SLS) model is governed by the following response functional

$$\sigma(t) = \int_0^t \left(E_1 + E_2 \, e^{-\frac{t-\zeta}{\lambda}} \right) \dot{e}(\zeta) \, \mathrm{d}\zeta \tag{4.1}$$

where λ stands for the relaxation time, E_∞ denotes the long-term (fully relaxed) elastic constant and E_0 is the short-term elastic constant, $E_1 = E_\infty$ and $E_2 = E_0 - E_\infty$. In the rheological representation of the SLS, depicted in Fig.4.1.a, E_1 and E_2 are the stiffnesses of the two springs in the elastic arm and in the Maxwell arm, respectively, while $\lambda = \eta/E_2$, η being the viscosity constant of the Newtonian damper.

The representation provided by equation (4.1) is equivalent to the following ODE (to which homogenous initial boundary conditions are appended)

$$\sigma + \lambda \dot{\sigma} = E_1 \, e + \gamma \, \dot{e} \tag{4.2}$$

where $\gamma = \lambda \, (E_1 + E_2)$. The fractional SLS model is obtained by altering the order of
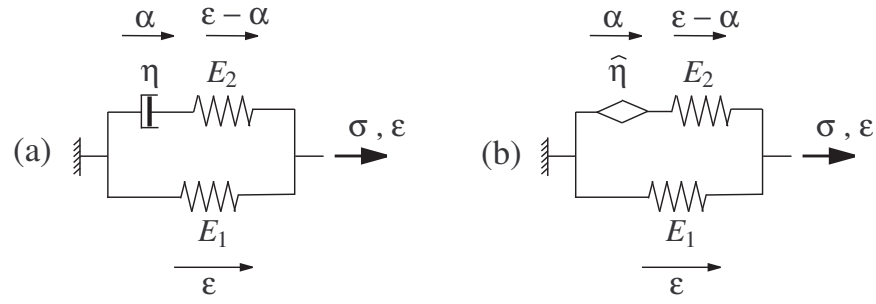
67

Figure 4.1: Rheological representation of the (a) classic and (b) fractional Standard Linear Solid model.

derivation, as follows

$$\sigma + \hat{\lambda} \, _0D_t^\nu \, \sigma = E_1 \, e + \hat{\gamma} \, _0D_t^\nu e \tag{4.3}$$

with $\nu \in (0,1)$, whereby $\hat{\lambda} = \hat{\eta}/E_2$ and $\hat{\gamma} = \hat{\lambda}(E_1 + E_2)$ have a physical meaning similar to the classical case but are dimensionally different. The rheological representation of the fractional SLS model is depicted in Fig.4.1.b by replacing the Newtonian damper with a springpot element with constant $\hat{\eta}$.

There is no reason *a priori* not to consider different fractional exponents for the stress and strain time derivatives [45], the present choice being motivated by the physical interpretation through the rheological model of Fig.4.1.b: a more refined choice would ideally derive from a deeper understanding of the related physical behaviour of the material under scrutiny (generic numerical examples can be found in [151]).

Remark 4.0.1 It can be shown that the solution to equation (4.3) can be expressed as [33],

$$\sigma(t) = \int_0^t \left(\frac{\hat{\gamma}}{\alpha}\right) \mathcal{E}_\nu \left(-\frac{t-\tau}{\hat{\lambda}}\right)^\nu \dot{e} \, \mathrm{d}\tau \tag{4.4}$$

where $\mathcal{E}_\nu$ stands for the Mittag-Leffler function (see Section 2.1.3) of order ν. It is remarked that $\mathcal{E}_1(z) = e^z$. Mittag-Leffler functions for three values of ν have been plotted in Fig.2.1, where the qualitative difference with an exponential function is made tangible. Interestingly, the model "interpolates" between hookean ($\nu = 0$) and classical SLS model ($\nu = 1$) behaviour. ∎

Thermodynamic consistency for $0 \le \nu \le 1$ is proved immediately by considering a Theorem in [26] stating that if the relaxation function is monotonic, decreasing, con-

cave and tends to a non-negative asymptotic value, then the work done on any strain path starting from equilibrium is non-negative, which is an alternative statement of the Second Law [21]. The same result was proved by appealing to the rheological analogy in [45].

Before considering the fractional formulation of the cohesive-zone model, it seems appropriate to investigate the behaviour of the fractional SLS model in order to achieve the basic understanding of its characteristics needed to later rationally calibrate the material parameters. One property of the classical Standard Linear Solid SLS is of particular interest: it approaches the behaviour of an elastic material in the limit of infinite or zero strain rate [14]. This can be seen analytically by considering suitable transformations of the time variable. In complete analogy the fractional counterpart exhibits the same property: also, the ratio of the elastic moduli in the "fast" and "slow" limits does not vary with respect to its classical counterpart. The difference between classical and fractional case consists in that the transition from "soft" to "hard" elastic solid behaviour occurs at a different pace: this is exemplified by Fig.4.2, which displays the analytical solutions of ODEs (4.2) and (4.3) for constant strain-rate imposed histories, in a case for which $E_1 = 0$, hence recovering a Maxwell's model, $E_2 = 1$ and $\lambda = 1$. The surfaces depicted are the envelope of the stress response as a function of time, at varying the imposed strain rate.

The difference between the two surfaces is plotted in Fig.4.2.c: the plot is in line with the discussion in Section 2.1.3 on the differences between fractional and exponential behaviour (steeper relaxation at short times, but algebraic rather than exponential decay for longer times).

4.1   Formulation of the Interface Model

Focusing on a mode-I problem, and making again the assumption that relative-displacements at the interface are zero for negative times, the interface traction σ at time t at a point of an interface with memory is characterised by a (generally non-linear) functional defined on a suitable set of displacement jump histories $\delta : [0, t] \rightarrow \Re$.

The fractional SLS model is chosen as a reasonable representation of rubber viscoelasticity, and the rheological representation of its specialisation to a cohesive-zone model is simply obtained by replacing the strain e with the relative displacement δ.

69

The stress response at time t of the SLS model (*i.e.* without considering the damage variable) due to a displacement jump history δ (without loss of generality assumed to be null for non-positive times) will be denoted as $\Sigma_t(\delta)$ and, for what explained above, is the solution of the following ODE, which is the CZM equivalent of ODE (4.3):

$$\sigma + \hat{\lambda} \; _0D_t^\nu \sigma = E_1 \delta + \hat{\gamma} \; _0D_t^\nu \delta \qquad (4.5)$$

The damaging process is instead described as before through an internal damage variable D, whereby the overall response is given as a product of a damage term and a linear functional:

$$\sigma(t) = [1 - D(t)] \, \Sigma_t(\delta) \qquad (4.6)$$

As far as the evolution of the damage variable is concerned the same evolution equations presented in Section 3.3.1 is employed, as the physical assumptions on which it has been based, see Section 3.2, are completely unrelated the specific choice of the viscoelastic relaxation function.The same argument is valid with regards to the modeling of compression, see Section 3.2.

4.1.1 Algorithmic Solution of Fractional Models - Grünwaldian Formalism

Numerical computations in the case of fractional models are more complicated than in the case of an exponential relaxation function or, more generally, viscoelastic material models formulated within the framework of thermodynamics with internal variables [106]. In the first case a recursive algorithm can be formulated using properties of exponentials functions, as presented in the previous Chapter. In the second case incremental variational schemes are available [152, 153]: such schemes do not apply in general to fractional viscoelastic formulations (which are characterised, loosely speaking, by an infinite number of internal variables, see Section 2.1.3).

Numerical fractional differentiation/integration algorithms can be classified into three categories [154]. The first category comprises algorithms whose starting point is the Riemann-Liouville definition, in Equation (2.22): the integral expression can be numerically evaluated using various tecniques from numerical integration. The second category relies instead on an alternative definition of fractional derivative/integral [155], which was later shown to be equivalent to the Riemann-Liouville definition [156]. The

third type of approach is based on exploiting the linearity of the viscoelastic functionals by approximating the strain history as a piecewise constant function and superimposing the responses due to each increment: this is the approach historically introduced by Boltzmann [16] and described in Section 2.1.

In this work the second of these strategies has been followed, based on the the Grünwald-Letnikov definition of fractional derivative. Such a numerical approximation strategy has been used in [157, 158], among others. To the best of the author's knowledge, this is the first application of a fractional calculus-based model in a non-linear finite-element computation.

Grünwald-Letnikov fractional derivative

The Grünwald-Letnikov expression of the fractional derivative is derived from the observation that the usual, first integer order derivative can be approximated *via* a backward difference scheme

$$\frac{\mathrm{d}f(t)}{\mathrm{d}t} = \lim_{\Delta t \to 0} \frac{1}{\Delta t}[f(t) - f(t - \Delta t)] \tag{4.7}$$

and iterated applications yield

$$\frac{\mathrm{d}^2 f(t)}{\mathrm{d}t^2} = \lim_{\Delta t \to 0} \frac{1}{\Delta t^2}[f(t) - 2f(t - \Delta t) + f(t - 2\Delta t)] \tag{4.8}$$

$$\frac{\mathrm{d}^3 f(t)}{\mathrm{d}t^3} = \lim_{\Delta t \to 0} \frac{1}{\Delta t^3}[f(t) - 3f(t - \Delta t) + 3f(t - 2\Delta t) - f(t - 3\Delta t)] \tag{4.9}$$

which can be generalised using induction to

$$\frac{\mathrm{d}^n f(t)}{\mathrm{d}t^n} = \lim_{\Delta t \to 0} \left[\frac{1}{\Delta t^n} \sum_{j=0}^{n} (-1)^j \binom{n}{j} f(t - j\Delta t) \right] \tag{4.10}$$

After setting $\Delta t = t/N$, Equation (4.10) can be written

$$\frac{\mathrm{d}^n f(t)}{\mathrm{d}t^n} = \lim_{N \to \infty} \left[\left(\frac{t}{N} \right)^{-n} \sum_{j=0}^{N-1} (-1)^j \binom{n}{j} f\left(t - j\frac{t}{N} \right) \right] \tag{4.11}$$

In order to allow the applicability of Equation (4.11) outside integer order derivation, the binomial coefficient definition is extended, for $\nu \in \Re$ and $j \in \mathcal{N}$ as

$$\binom{\nu}{j} = \begin{cases} \frac{\nu(\nu-1)(\nu-2)\ldots(\nu-j+1)}{j!} & \text{for} \quad j > 0 \\ \\ 1 & \text{for} \quad j = 0 \end{cases} \tag{4.12}$$

Then $(-1)^j \binom{\nu}{j}$ can be expressed as

$$(-1)^j \binom{\nu}{j} = (-1)^j \frac{\nu(\nu-1)(\nu-2)\ldots(\nu-j+2)(\nu-j+1)}{j!} \tag{4.13}$$

which leads to

$$(-1)^j \binom{\nu}{j} = \binom{j-\nu-1}{j} = \frac{\Gamma(j-\nu)}{\Gamma(-\nu)\Gamma(j+1)} \tag{4.14}$$

where Γ stands for the Γ function. Replacing expression (4.14) in Equation (4.11) provides the following formula, in which ν is required only to belong to $\Re$ (an extension to the complex field $\mathcal{C}$ is possible too, [31])

$$\frac{\mathrm{d}^\nu f(t)}{\mathrm{d}t^\nu} = \lim_{N\to\infty} \left[\left(\frac{t}{N}\right)^{-\nu} \sum_{j=0}^{N-1} \frac{\Gamma(j-\nu)}{\Gamma(-\nu)\Gamma(j+1)} f\left(t - j\frac{t}{N}\right) \right] \tag{4.15}$$

It can be recognised how the given definition agrees with the usual integer-order derivation definition for $\nu = n, n \in \mathcal{N}$, in that only the first $n+1$ of the so-called Grünwald-Letnikov coefficients A_j

$$A_{j+1} = \frac{\Gamma(j-\nu)}{\Gamma(-\nu)\Gamma(j+1)} \tag{4.16}$$

are nonzero due to properties of the inverse Γ function, which vanishes for negative integers (the Γ function itself has simple poles for negative integers). If $\nu \notin \mathcal{N}$ then all the A_j are different from 0, which underlines how in general the fractional derivative is a non-local operator.

The Grünwald-Letnikov coefficients obey the useful recursive formula

$$A_{j+1} = \frac{\Gamma(j-\nu)}{\Gamma(-\nu)\Gamma(j+1)} = \frac{j-1-\nu}{j} \frac{\Gamma(j-1-\nu)}{\Gamma(-\nu)\Gamma(j)} = \frac{j-1-\nu}{j} A_j \,, A_0 = 1 \tag{4.17}$$

which is very useful in that definition (4.16) could lead to numerical problems if ν is close to an integer or for large iteration index.

Numerical approximation of the Grünwald-Letnikov derivative

In general the Grünwald-Letnikov definition requires handling an infinite series expansion, the time step t/N tending to zero. To overcome the impracticality it is natural to consider a truncation, *i.e.* to approximate

$$\frac{\mathrm{d}^\nu f(t)}{\mathrm{d}t^\nu} = \lim_{N\to\infty} \left[\left(\frac{t}{N}\right)^{-\nu} \sum_{j=0}^{N-1} A_{j+1} f\left(t - j\frac{t}{N}\right) \right] \tag{4.18}$$

by

$$\frac{\mathrm{d}^\nu f(t)}{\mathrm{d}t^\nu} \cong \left[\left(\frac{t}{\mathring{N}}\right)^{-\nu} \sum_{j=0}^{\mathring{N}-1} A_{j+1} f\left(t - j\frac{t}{\mathring{N}}\right) \right] \tag{4.19}$$

The value of $\mathring{N}$ fixes the time step used for sampling the function in the Grünwald-Letnikov and is to be chosen as a compromise between accuracy and computational time. Its choice impacts the size of the integration time step (as well as the number of addends in the series). The computability of the Grünwald-Letnikov at fixed $\mathring{N}$ can further be improved by remembering the Grünwald-Letnikov coefficients are in absolute value decreasing for fractional coefficients $0 < \nu < 1$, a manifestation of the fading-memory principle, see Fig.4.3. The truncated sum (4.19) at fixed $\mathring{N}$ can be written as

$$\left(\frac{t}{\mathring{N}}\right)^{-\nu} \sum_{j=0}^{\mathring{N}-L-1} A_{j+1} f\left(t - j\frac{t}{\mathring{N}}\right) + R(\mathring{N}, L) \tag{4.20}$$

where the truncation error term R is given by

$$R(\mathring{N}, L) = \left(\frac{t}{\mathring{N}}\right)^{-\nu} \sum_{j=\mathring{N}-L}^{\mathring{N}-1} A_{j+1} f\left(t - j\frac{t}{\mathring{N}}\right) \tag{4.21}$$

An upper bound for R is obtained as follows

$$|R(\mathring{N}, L)| = \left| \left(\frac{t}{\mathring{N}}\right)^{-\nu} \sum_{j=\mathring{N}-L}^{\mathring{N}-1} A_{j+1} f\left(t - j\frac{t}{\mathring{N}}\right) \right| \leq$$

$$\leq \left(\frac{t}{\mathring{N}}\right)^{-\nu} \sum_{j=\mathring{N}-L}^{\mathring{N}-1} |A_{j+1}| \left| f\left(t - j\frac{t}{\mathring{N}}\right) \right| \leq$$

$$\leq \left(\frac{t}{\mathring{N}}\right)^{-\nu} \sum_{j=\mathring{N}-L}^{\mathring{N}-1} \max_{j\in[\mathring{N}-L,\mathring{N}-1]} |A_{j+1}| \max_{j\in[\mathring{N}-L,\mathring{N}-1]} \left| f\left(t - j\frac{t}{\mathring{N}}\right) \right| =$$

$$= \left(\frac{t}{\mathring{N}}\right)^{-\nu} L \left| A_{\mathring{N}-L} \right| \max_{j\in[\mathring{N}-L,\mathring{N}-1]} \left| f\left(t - j\frac{t}{\mathring{N}}\right) \right| \tag{4.22}$$

It appears then that truncation error generally increases with decreasing ν, as a result of the fact the Grünwald-Letnikov coefficients decrease more slowly. The entity of the numerical error is graphically illustrated for a simple case in Fig.4.4 by displaying the analytical and numerical derivatives for a power-law function, together with the two different approximation tecniques described above.

Numerical solution of the fractional SLS cohesive model

By using equation (4.19) to obtain a numerical approximation of the two fractional derivatives of σ and ε and observing that $A_1 = 1$ one has:

$$_0D_t^\nu \sigma \cong \left(\frac{t}{\mathring{N}}\right)^{-\nu} [\sigma(t) + S_\sigma] \qquad _0D_t^\nu \delta \cong \left(\frac{t}{\mathring{N}}\right)^{-\nu} [\delta(t) + S_\delta] \tag{4.23}$$

where:

$$S_\sigma = \sum_{j=1}^{\mathring{N}-1} A_{j+1} \, \sigma\left(t - j\frac{t}{\mathring{N}}\right) \qquad S_\delta = \sum_{j=1}^{\mathring{N}-1} A_{j+1} \, \delta\left(t - j\frac{t}{\mathring{N}}\right) \tag{4.24}$$

Replacing the above expressions into equation (4.5), and making the dependence on t explicit, the following expression is obtained:

$$\sigma(t) + \hat{\lambda} \left(\frac{t}{\mathring{N}}\right)^{-\nu} [\sigma(t) + S_\sigma] = E_1 \, \delta(t) + \hat{\gamma} \left(\frac{t}{\mathring{N}}\right)^{-\nu} [\delta(t) + S_\delta] \tag{4.25}$$

Solving for $\sigma(t)$ provides the following numerical (approximate) solution of the response Σ of the cohesive SLS model in absence of damage:

$$\Sigma(\delta, t) = \left[1 + \hat{\lambda} \left(\frac{t}{\mathring{N}}\right)^{-\nu}\right]^{-1} \left\{ \left[E_1 + \hat{\gamma} \left(\frac{t}{\mathring{N}}\right)^{-\nu}\right] \delta(t) + \left(\frac{t}{\mathring{N}}\right)^{-\nu} \left(\hat{\gamma} \, S_\delta - \hat{\lambda} \, S_\sigma\right) \right\} \tag{4.26}$$

Finite-step solution of the cohesive-zone model

Having described the numerical approximation for the solution of the SLS cohesive model in Section 4.1.1, this can be combined with the damage evolution law, see Section 3.3.1 to obtain the constitutive law (4.6). The time-integration algorithm to determine the response of the CZM is now described.

Recalling that it has ben assumed the displacement-jump history to be nihil before $t = 0$ the time interval over which the computation is to be carried out, $[0, T]$, is discretized into a partition of N_{inc} time increments:

$$[0, T] = \bigcup_{n=1}^{N_{inc}} [t_n, t_{n+1}] \qquad t_{n+1} = t_n + \Delta t_n \qquad (4.27)$$

In the n-th time increment, the times at the start and the end of the increment are t_n and t_{n+1}, respectively. Setting $\sigma_{n+1} = \sigma(t_{n+1})$, $\delta_{n+1} = \delta(t_{n+1})$ and $D_{n+1} = D(t_{n+1})$, in the framework of a non-linear, displacement-based finite-element solution scheme the problem is relative-displacement driven, whereby δ_{n+1} is assigned while σ_{n+1} and D_{n+1} are computed as follows:

$$\sigma_{n+1} = \begin{cases} (1 - D_{n+1}) \, \Sigma_{n+1} \, (\delta_{n+1}) & \text{if } \delta_{n+1} \geq 0 \\ \\ K_c \, \delta_{n+1} & \text{if } \delta_{n+1} < 0 \end{cases} \qquad (4.28)$$

where from Equation (4.26):

$$\Sigma_{n+1} \, (\delta_{n+1}) = \left[1 + \hat{\lambda} \left(\frac{t}{\mathring{N}} \right)^{-\nu} \right]^{-1} \left\{ \left[E_1 + \hat{\gamma} \left(\frac{t}{\mathring{N}} \right)^{-\nu} \right] \delta(t) + \right.$$
$$\left. + \left(\frac{t}{\mathring{N}} \right)^{-\nu} \left(\hat{\gamma} \, S_{\delta,n+1} - \hat{\lambda} \, S_{\sigma,n+1} \right) \right\} \qquad (4.29)$$

in which $S_{\delta,n+1}$ and $S_{\sigma,n+1}$ are given by:

$$S_{\sigma,n+1} = \sum_{j=1}^{\mathring{N}-1} A_{j+1} \, \sigma \left(t_{n+1} - j \frac{t_{n+1}}{\mathring{N}} \right) \qquad S_{\delta,n+1} = \sum_{j=1}^{\mathring{N}-1} A_{j+1} \, \delta \left(t_{n+1} - j \frac{t_{n+1}}{\mathring{N}} \right)$$
$$(4.30)$$

D_{n+1} is given by, see equation (4.29) :

$$D_{n+1} = \begin{cases} 0 & \text{if } \delta_{max,n+1} \leq \delta_0 \\ \\ \min \left\{ 1, \left(\frac{G_c}{G_c - G_0} \right) \left(1 - \frac{\delta_0}{\delta_{max,n+1}} \right) \right\} & \text{if } \delta_{max,n+1} \geq \delta_0 \end{cases} \qquad (4.31)$$

where the current maximum displacement $\delta_{max,n+1}$ is a history variable in the model which is initialised as $\delta_{max,0} = 0$ at the beginning of the first increment and is updated at each increment as follows:

$$\delta_{max,n+1} = \max\{\delta_{n+1}, \delta_{max,n}\} \qquad (4.32)$$

Remark 4.1.1 It is worth noting that, in general, the time increment Δt_n relevant for the Newton-Raphson scheme are chosen using an automatic incrementation procedure whereby Δt_n increases or decreases according to the rate of convergence in each increment, within user defined maximum and minimum thresholds. Instead, the time increment $t/\mathring{N}$ defining the sampling points of the Grünwald-Letnikov summation is fixed,

G_c (N mm^{-1})	δ_c (mm)	E_1 (N mm^{-3})	E_2 (N mm^{-3})	$\hat{\lambda}$ (s$^\nu$)	ν	K_c
1.55	0.75	1.81	13.25	2.5	0.3	980

Table 4.1: Input parameters used for the rubber interface.

whereby the sampling points do not in general coincide with the time increments of the analysis. This issue is circumvented by linearly interpolating the relative-displacement and stress history between Newton-Raphson time steps. ∎

Before presenting the results, it was verified that the fractional algorithm could reproduce the results presented in Chapter 3, by using a fractional exponent ν equal to 1 (yielding then back the classical SLS model rheology employed in the previous Chapter). The agreement is satisfactory and is presented in Fig.4.5.

4.2 Analysis of Experimental and Numerical Results

The fractional-calculus-based numerical model has been implemented into a user subroutine (UMAT) for the finite-element code ABAQUS, version 6.12.2, as constitutive law of interface elements. The subroutine is included in the Appendix. Material properties of the steel arms are left unaltered (Young's modulus of 200 GPa and a Poisson's ratio of 0.3) For the interface the constants reported in the Table 3.1 have been used.

The numerical algorithm requires the user-input parameter $\mathring{N}$, *i.e.* the number of terms in the Grünwald sumamtion: a value of 100 has been selected for the simulations presented.

The identification of material parameters has ultimately been performed empirically but it was possible to achieve remarkable good agreement between experimental and numerical results as shown in Fig.4.6. It is interesting to compare the value of G_c in Tables 3.1 and 4.1: the fact that G_c for the fractional CZM is lower reveals how an artificial cut-off is in a sense performed, when using an excessively narrow relaxation spectrum as was the case in Chapter 3. In other words, the G_c value used for the exponential model is higher because it has to incorporate all the viscoelastic dissipation that occurs below its slow limit, and that hence is not able to reproduce. In the fractional case this is not necessary at all.

Fig.4.7 also shows the excellent correlation between experimentally measured and numerically computed load maxima. Plotting this curve during the identification procedure has been extremely useful as it was found that the shape and the load of this curve was extremely sensitive to $\hat{\lambda}$ and to the fractional exponent ν. In particular, the slope tends to increase with increasing values of ν, the other input parameters kept fixed. The fact that the load maxima are almost perfectly aligned seems to reflect the fact that all considered load speeds were sufficiently far from both the fast and the slow limit. Once the load maxima were reasonably well captured successive iterations on the other parameters allowed to obtain a final set of values which led to the excellent correlation shown in Fig.4.6.

Differences between the model presented in the previous Chapter and the fractional CZM are highlighted in Fig.4.8, from which a further confirmation of the ability of the fractional formulation to deal with a wider range of applied test rates can be obtained; in this respect, see also Fig.4.2.c.

For future, more demanding, applications systematic approaches for material parameter identification as considered in [159, 160] could be taken into account.

One feature of the experimental response which is still not adequatey described is the initial stiffness: experimental results display less rate-dependence in this respect than the simulated response. It is conjectured that this shortcoming is caused by the lack of accuracy incurred by describing the rubber compound as a linear material as far as the elastic response is concerned (for tensile curves of the interface rubber compound see Fig.5.4, note the highly non-linear behaviour). Fracture growth is on the other hand modelled satisfactorily, in agreement with the fact that in general the dissipated energy within the process zone is far more important than the detailed shape of the traction -discontinuity jump law, see Section 2.2.2.
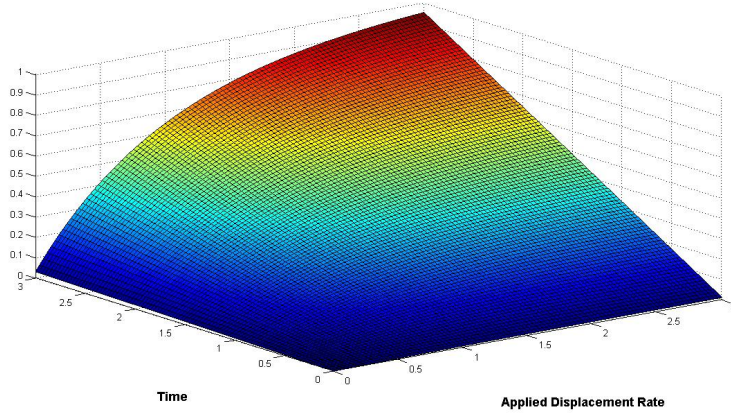
(a)
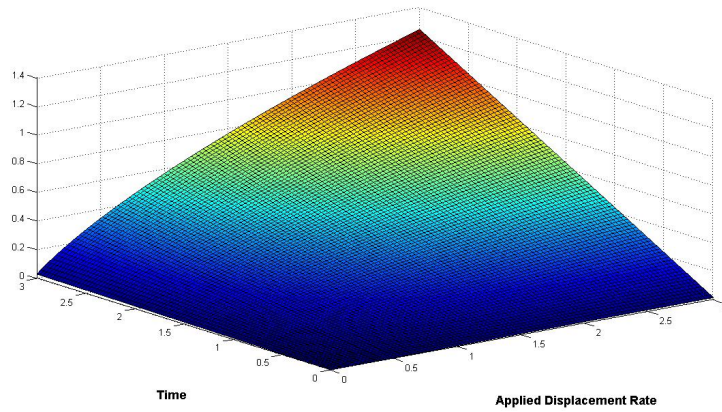
(b)
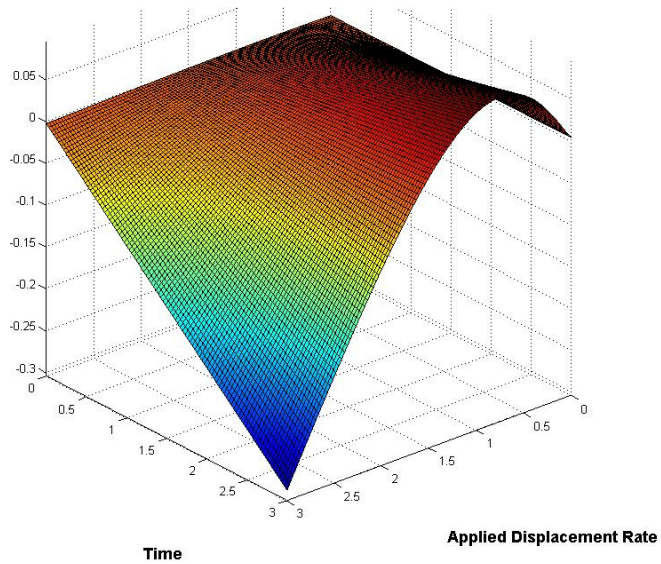
(c)

Figure 4.2: Envelope of constant strain-rate uniaxial test curves for: a) a classical Maxwell model b) a fractional Maxwell model. c) Plot of the difference between the surfaces depicted in a) and b): please note the inverted axes with respect to the charts above, in order for the surface in c) to be better visible.
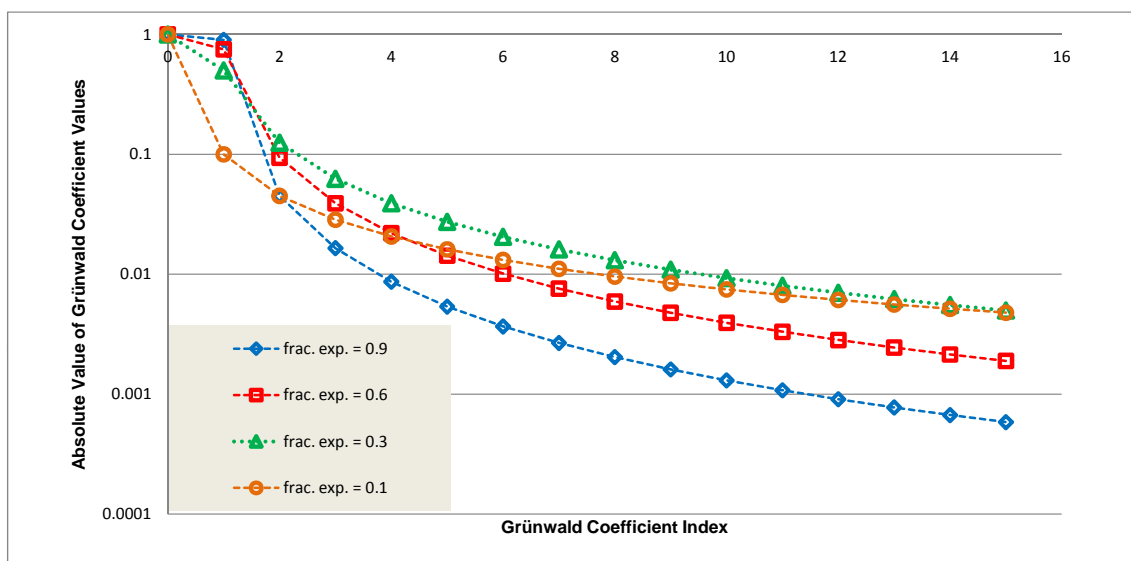
Figure 4.3: Absolute values of Grünwald-Letnikov coefficients for various fractional exponents between 0 and 1

(a)

(b)
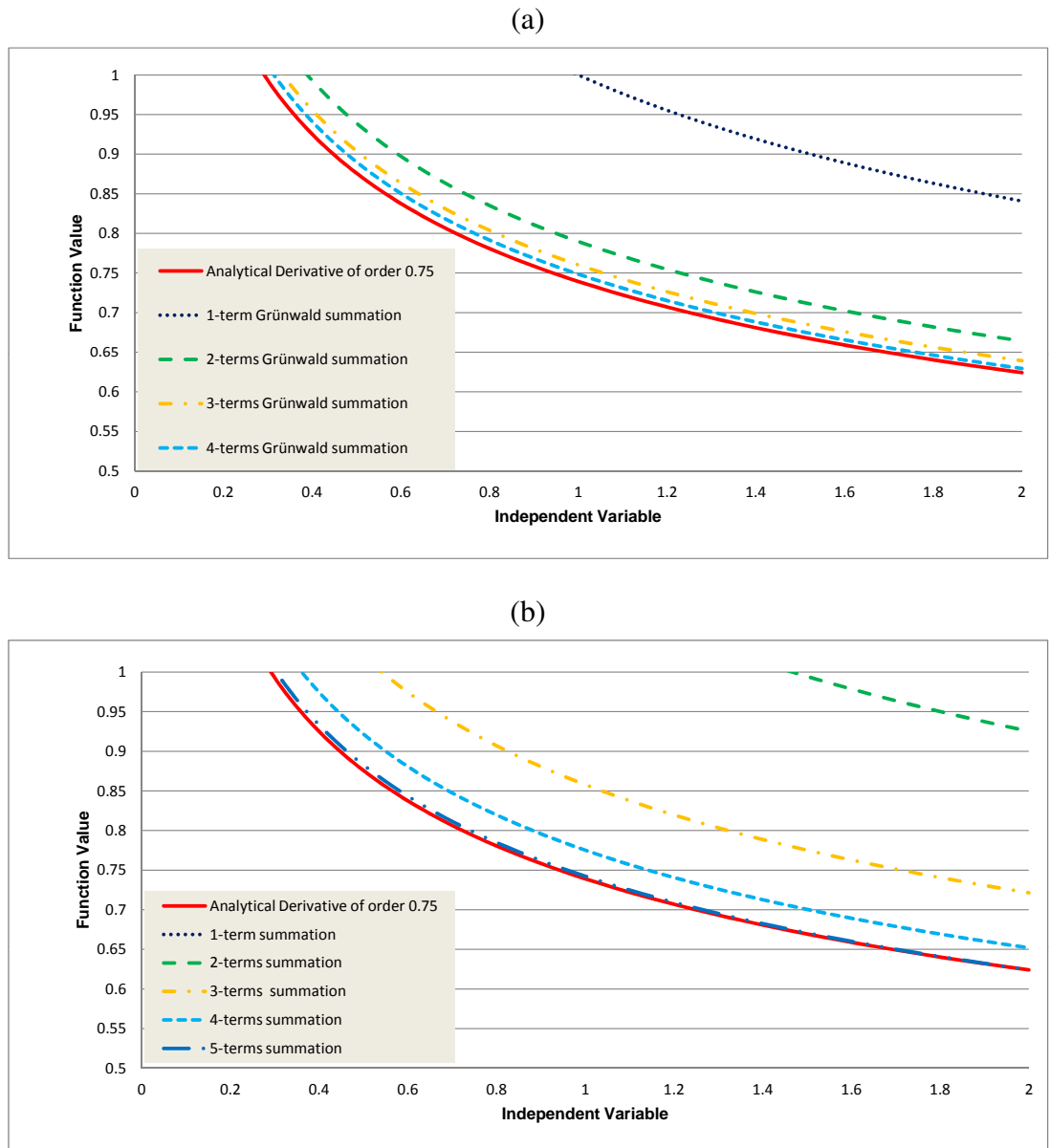
Figure 4.4: Analytical fractional derivative (continuous line) of $y(t) = \sqrt{(t)}$ with fractional exponent $\nu = 0.75$ of a power law function compared to different approximations (dashed lines) obtained by a) varying $\mathring{N}$ b) varying the number of addends in the series without varying $\mathring{N}$, hence maintaining the time step unaltered.
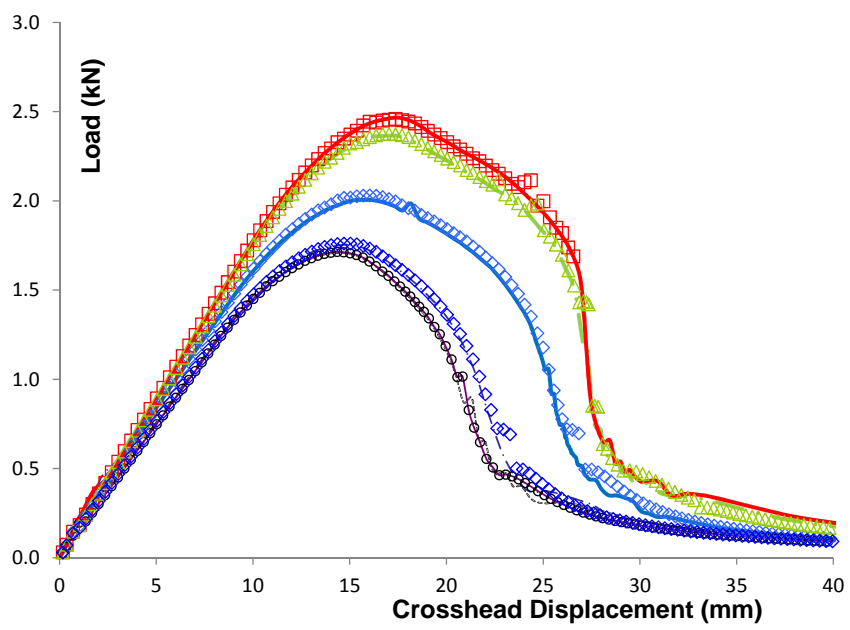
Figure 4.5: Verification of the reproducibility of the results of Chapter 3 (markers) using the fractional formulation with the fractional exponent set equal to 1 (dashed lines).
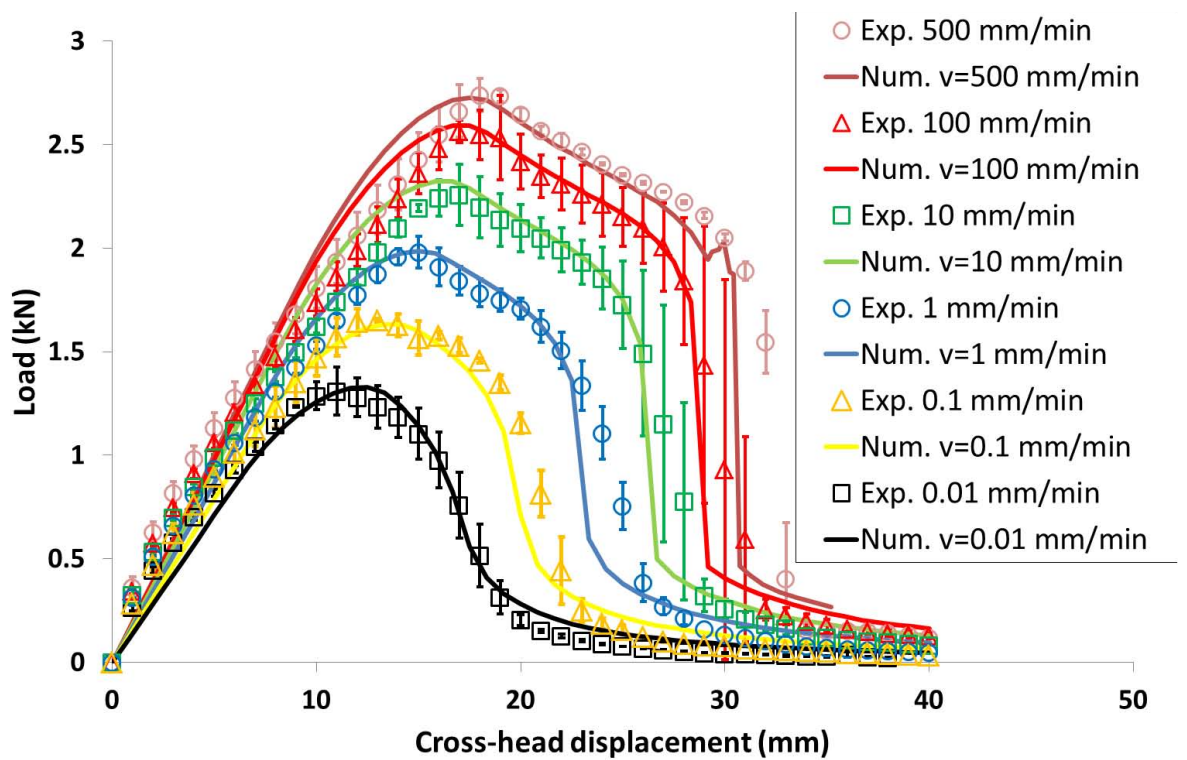
Figure 4.6: Experimental *vs* numerical load-deflection curves computed with the fractional CZM at different applied displacement rates.
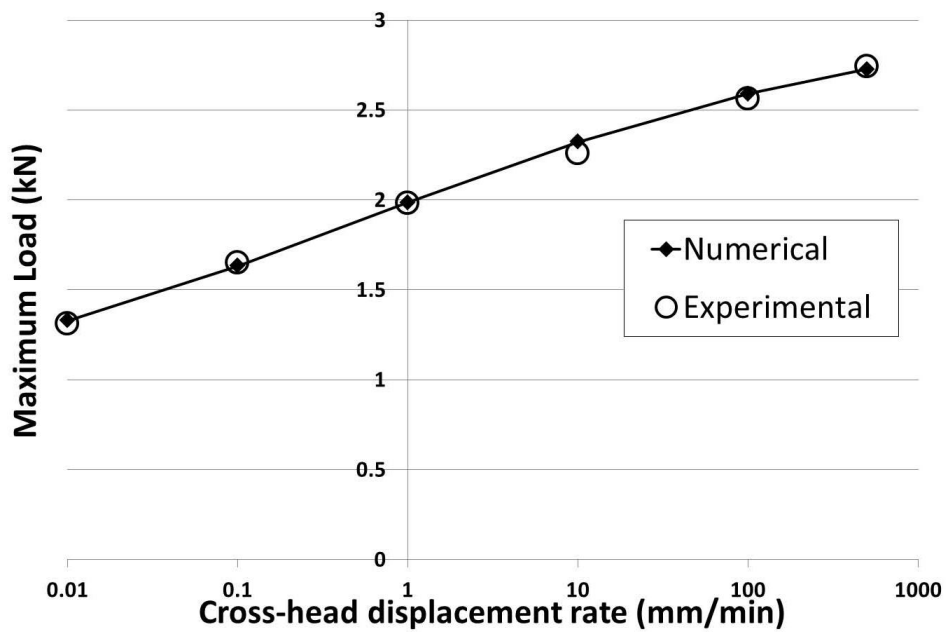
Figure 4.7: Experimental *vs* numerical load maxima at different load displacement rates: it could be noticed how the "fast limit" of the viscoelastic spectrum is approached (decreasing slope for increasing values of the displacement rate).
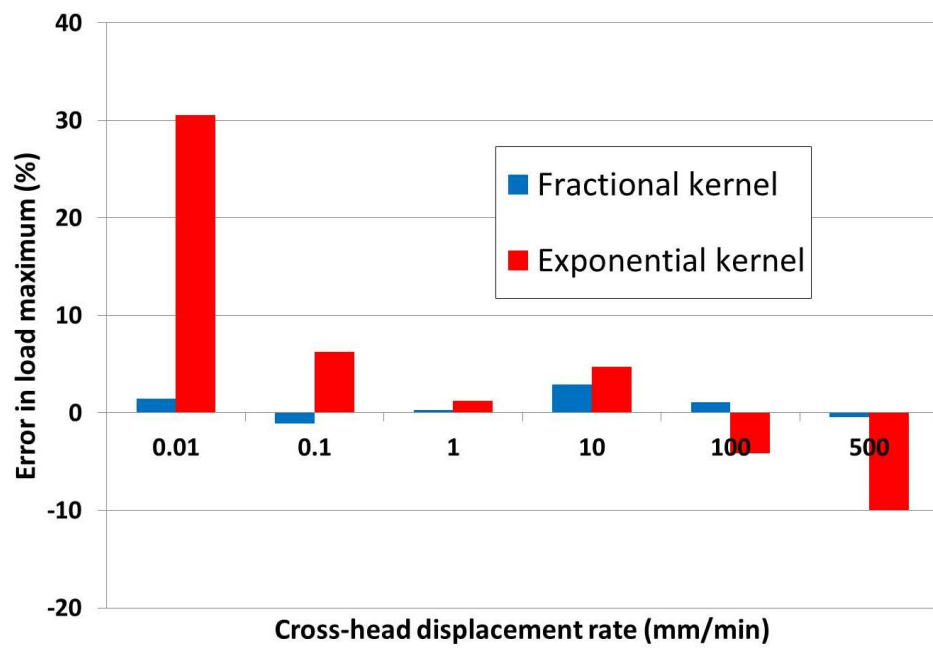
Figure 4.8: Error plot comparing the load maxima computed with the exponential kernel formulation (Chapter 3) and the fractional kernel formulation.

Chapter 5

Formulation of a Non-Local CZM

5.1 Non-monotonicity of the crack speed *vs* G_c relationship

In the case of rate-dependent crack initiation and growth, it is experimentally observed that for some materials the critical energy release rate is not monotonically increasing with the crack speed [161], also consider Fig.5.1 for test results obtained by the author on the same rubber used for the interface of the DCB specimen described in Sections 3.5 and 4.2.

Our interest in the phenomenon originates from its importance in applications. Indeed failure of polymeric structures is often characterised by the crack speed "blowing-up" once a certain crack speed range (over which the crack advances in stable fashion) is abandoned. This could be related to the critical energy release rate not being an increasing function of the crack speed: for example, the catastrophic failure of a load-controlled specimen if the imposed load increases in time is easily explained in such context. The importance of this aspect deserves a simple, yet revealing example. Let us consider a peel-test specimen of width b, the related energy release being a linear function of the applied load P and not depending on the crack length. It is assumed the fracture energy G_c of the interface depends on the crack speed *via* the function $G = G(\dot{l})$ which is assumed to be Lipschitz-continuous, everywhere positive and monotonically increasing. The function $l(t)$ describing the evolution of crack length during crack propagation is a
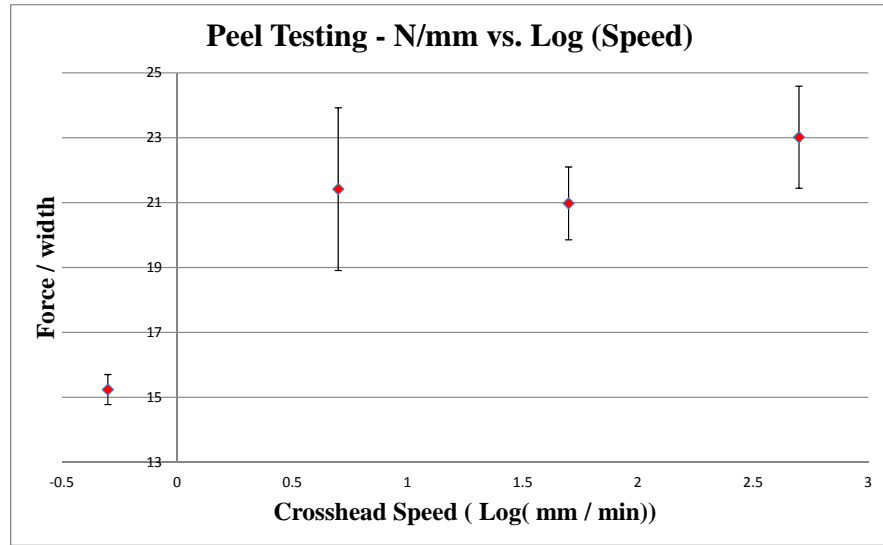
Figure 5.1: Load per unit width (twice the energy release rate) *vs* applied displacement rate for a peel test on a rubber interface

solution of the ordinary differential equation [162] in the unknown $l = l(t)$

$$\frac{2P}{b} = G_c(\dot{l}) \tag{5.1}$$

If a linearly increased load is applied, $P(t) = \alpha t$, the resulting differential equation

$$\frac{2\alpha t}{b} = G_c(\dot{l}) \qquad ; \qquad l(0) = l_0 \tag{5.2}$$

admits a unique solution, as follows directly from Picard-Lindelhof's Theorem [163] (the solution can also be shown to be monotonic by direct integration). An analysis based on CZM models of the type described in Chapters 3, 4 would reach the same conclusion because in these cases G_c is monotonic as a result of the use of linear viscoelasticity. On the other hand, if the experiment were performed it would be apparent that upon reaching a critical crack speed, corresponding to the loss of monotonicity of G_c, the crack speed would increase abruptly, and would have to be described by a discontinuity in the quasi-static approximation. The inability to predict such phenomenon, for such a simple test geometry, justifies the need for further refinement of the models.

Another consequence is possibly stick-slip propagation behaviour [102–104, 164], characterised by very fast, almost sudden propagation stages alternating with slower (if

not stationary) ones. Such a phenomenon is extremely revealing and will be considered in some detail as it could possibly furnish the basis for understanding other types of instability-related cracking processes.

Non-convex Dissipation Potentials

The following example is taken from [106] and provides a description of how stick-slip cracking could be interpreted in the framework of thermodynamics with internal variables. Considering the unwinding of an adhesive tape, a double-well dissipation potential $\mathcal{D}$, positive but not convex in α, is introduced, for which an explicit computation of the dissipated power Φ yields

$$\Phi = a \left(\frac{\dot{\alpha}^2}{\dot{\alpha}_0^2} - 1 \right) \dot{\alpha}^2 \tag{5.3}$$

Considering the thermodynamic requirement $\Phi \geq 0$ it is readily seen that the interval $(-\dot{\alpha}_0, \dot{\alpha}_0)$ is precluded to $\dot{\alpha}$ as it would entail negative dissipation, in contradiction to the Second Law. The solution consisting in convexifying $\mathcal{D}$, while mathematically legitimate, is discarded by Maugin on physical grounds as he notes that along the resulting Maxwell line [165] along the horizontal axis (see Fig.5.2) the dissipation would vanish, which is not the case of the test during which dissipation occurs at all times. The alternative then is to avoid the forbidden region by jumps in the phase plane, as in Fig.5.2. This example possibly clarifies the energetic structure causing stick-slip propagation,
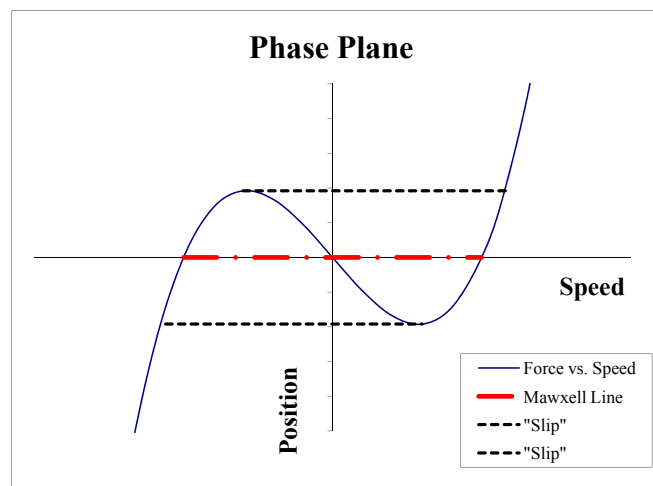
Figure 5.2: Hysteretic cycle in the $(\dot{\alpha}, \alpha)$ phase plane.

i.e. the fact that dissipative losses decrease, in a certain regime, with increased crack speed. In the next section a very similar result is presented, which was obtained by a different route. While a study of the thermodynamic reasons underlying the phenomenon is most useful, a micromechanical explanation, able to justify why dissipative losses might be non monotonically increasing with respect to crack speed, has to be attempted separately.

Introducing Dynamics

An attempt to explain the "stick-slip" behaviour commonly observed in fracture testing of polymers was provided by Webb and Aifantis [105]. They assigned an "effective" or "attached" mass to the crack tip as well as conjecturing that the critical energy release rate G_c depends additively on the extent of the crack growth Δa and crack velocity $v = \dot{a}$ and is not monotonic with respect to the latter. Such assumptions allow a differential equation to be derived from which it is seen that crack propagation is characterised by "jumps" (*relaxation oscillations*) from the stable low-velocity branch to the stable high velocity branch. Useful heuristic understanding can be gained by comparing this system with the *Van der Pol* oscillator in electrotechnics [166], which is governed by the system of first- order differential equations in the unknowns x, y

$$\begin{cases} \dot{x} = m(x - \frac{x^3}{3} - y) \\ \dot{y} = \dfrac{x}{m} \end{cases} \tag{5.4}$$

The oscillations for such a system in the case $\frac{1}{m} \gg 1$ could be understood by considering, in the phase plane (y, x), the difference $y - (x - \frac{x^3}{3})$. If the latter is of order 1, then the second equation in the system suggests that $|\dot{x}| \gg |\dot{y}|$. The motion is then characterised by high velocity in the x - direction at almost constant y values. If $y - (x - \frac{x^3}{3})$ is of order $1/m^2$ on the other hand, $|\dot{x}|$ and $|\dot{y}|$ are of the same order and (x, y) belongs to a neighbourhood of the curve $y = (x - \frac{x^3}{3})$, until the first condition applies again.

The formal similarity of Webb and Aifantis' formulation to the Van der Pol system can be shown by algebraic manipulations.

Introducing G_c Dependence on Temperature

The assumption of isothermal processes will be momentarily relaxed in this section where the possible relationship between non-convex dissipation and temperature conduction and generation is considered. The topic has been considered in [167] (see also [168] for interesting experimental measurements) by modelling a crack characterised by a rate-dependent energy-release rate running through a viscoelastic rubber body. Their aim is to enlighten the physical roots of the following empirical relationship between energy release rate G, crack speed v and temperature T,

$$G(v,T) = G_0[1 + f(v,T)] \qquad (5.5)$$

where the function f obeys $f \to 0$ as $v \to 0$. G_0 represents the intrinsic fracture energy of rubber, as it could be for example estimated by a high temperature test at very low applied velocities. For many polymeric materials the dependence upon temperature can be approximated by the inclusion of a multiplying factor, a *shift factor* a_T

$$f(v,T) = \hat{f}(a_T v) \qquad (5.6)$$

which can be satisfactorily computed through the Williams-Landel-Ferry method [169] by relying on temperature *vs* relaxation/creep data. By analytically considering the viscoelastic solution at the crack tip, heat conduction and assuming the effects of temperature on the mechanical behaviour could be captured by the Williams-Landel-Ferry approach their numerical computations show that the energy release rate ceases to be a monotonic function of crack speed (as the analysis without considering temperature effects would conclude, see for example [3]). Such non-monotonic behaviour is indicated as a possible cause for instabilities. It is worth noting that the authors attribute to thermal degradation in correspondence of the crack tip the fact that smooth fractured surface are observed for high enough crack speeds [161], also consider Fig.5.9. An alternative hypothesis will be put forward in Chapter 5.

The section is closed by an original observation according to which a crack moving at a constant speed is, in general, an abstraction. Let us consider the problem of calculating $l(t)$, given an imposed loading to which an energy release rate $\bar{G}$ corresponds (this could in general be time-dependent, but the present analysis will be limited to the constant case). It is also assumed for simplicity that $\bar{G} > \inf_{l,\hat{T}} G_c$, which forces $l(t)$ to be

strictly monotonically increasing.

Before formulating the problem in mathematical terms, let us cite [170], in which a crack moving at constant speed v is modelled as a heat source (not necessarily point-like): the conclusion is arrived at that the temperature field is constant in a reference system attached to the crack tip. This result seems very counter-intuitive and an observation of the boundary conditions they employed suggests that the conclusion originates from the fact there is no explicit mention of the time at which the crack propagation first occurred. Physical intuition suggests the picture would be different if a stationary crack is put in motion, as an interesting transient is expected.

The solution of the heat equation for a moving heat source starting its motion at time $t = 0$ is presented next. Starting by noting the solution of the problem

$$u_t - ku_{xx} = 0 \quad u(x,0) = \delta(x) \tag{5.7}$$

is given by

$$u(x,t) = \frac{1}{\sqrt{4k\pi t}} e^{-\frac{x^2}{4kt}} \tag{5.8}$$

Expression (5.8) describes the temperature field in time after the application of a "Dirac-delta" heat source at time 0. Linearity of the Heat PDE allows then to write the solution to problem (5.7) of the moving heat source as

$$u(x,t) = \int_0^t \frac{1}{\sqrt{4k\pi(t-\zeta)}} e^{-\frac{[x-l(t-\zeta)]^2}{4k(t-\zeta)}} \mathrm{d}\zeta \tag{5.9}$$

It will be shown that for a crack energy as defined in Equation (5.5) the crack tip motion is not linear in the general case. The claim is obtained by a contradiction argument. The function $l(t)$ is assumed linear, $l(t) = vt$, then

$$u(x,t) = \int_0^t \frac{1}{\sqrt{4k\pi(t-\zeta)}} e^{-\frac{[x-v(t-\zeta)]^2}{4k(t-\zeta)}} \mathrm{d}\zeta \tag{5.10}$$

Only the temperature at the crack tip is relevant for the crack propagation, so use will be made of the restriction to the crack tip of u, *i.e.* $u_{crack}(t) = u(vt, t)$, from which

$$u_{crack} = \int_0^t \frac{1}{\sqrt{4k\pi(t-\zeta)}} e^{-\frac{[v\zeta]^2}{4k(t-\zeta)}} \mathrm{d}\zeta \tag{5.11}$$

The function (5.11) is not in general constant, hence the temperature at the crack tip varies in time. As it was assumed that $\dot{l}$ was costant, the Griffith-energy balance can not

hold for the process depicted (unless for very particular functions G_c, rather uninterest-ing from the mechanical point of view). By contradiction, it is argued that l is not in general a linear function.

This line of reasoning suggests that if the critical energy release rate depends upon temperature (as it heavily does for the majority of polymers), then no steady crack propagation can be generally observed, if not in the asymptotic sense.

Phase changes

Certain amorphous elastomers (most notably, natural rubber) undergo a strain-induced phase transition to crystalline structure at sufficiently high strains. Close to the stress-free state polymeric coils are strongly entangled and the contribution to the free-energy is mainly entropic (which earned rubber the denomination of "entropic spring", or "ideal gas among solids" [1]). Upon the application of sufficiently high stretch, chains progres-sively disentagle and tend to orient themselves parallel to the load. During this process adjacent chains get closer: if chains get close enough to be mutually in each other's Van der Waals forces domain of attraction, they might eventually form a *crystallite*. This alters the mechanical behaviour as the internal energy of the inter-molecular bonds has now to be taken into account. On a macroscopic change scale the most evident manifestation of strain-crystallization is the sudden increase in stiffness after a critical stretch (usually ≈ 6), as well as the hysteresis loop observed upon unloading (possibly accompanied by the "inverse yielding phenomenon" [171]). Another consequence of paramount importance in application is the impact on crack propagation characteristics. Crystallisation occurring at the crack tip has a "reinforcing" effect, which results in re-duced crack propagation rates [22, 172] , as well as motivating why for a crystallising rubber the crack growth rate in cyclic loading conditions decreases when the minimum load level is increased (while maintaing the maximum unvaried), [173].

Strain-crystallisation is not instantaneous. Its kinetics have been studied in [174] where it was demonstrated that crystallinity during cyclic stretching is significantly lower than during quasistatic stretching, unveiling the fact that crystallisation is a time-dependent process with a characteristic time of the same order of magnitude as cycling periods typically employed in dynamic/fatigue investigations. These measurements pro-vided support for the experimental evidence showing that the crack propagation rate for crystallising rubber is much higher for a cycling load than in creep conditions, main-

taining constant the maximum energy release rate [175]. It is then natural to conjecture that the phenomenon of strain-crystallisation could explain why the dissipated energy following crack propagation could decrease once the crack speed exceeds a certain threshold. Indeed, only for a sufficienlty slowly moving crack there is sufficient time for the material around the crack tip to crystallize. Beyond a certain speed, the material around the crack tip would not have time to crystallise and the dissipated energy would then be lower. This line of thought will not be pursued further here as the non-monotonicity of the critical energy release rate vs crack speeds occurs also for non-crystallizing rubbers (as the one used in the presented experimental work), which suggests strain-crystallisation could certainly contribute, but cannot be the exclusive reason. The phenomenology just sketched will be though revisited in the last chapter in relation to another possible mechanism leading to non-monotonicity of the critical energy release rate *vs* crack speed.

Cavitation

Cavitation is an important failure mode for rubber specimens. It consists in the appearance of cavities (internal cracks of spherical shape) upon the application of negative hydrostatic pressure. It was first investigated by Gent [176] by conducting tension tests on thin rubber cylinders bonded to metal plates. The appearance of internal cracks is revealed by a sudden, irreversible, change in the stress-strain characteristics (and by a "popping sound" in Gent's words as well). Their analysis starts by the observation that for a thin cylinder the stress at the centre of the test specimen is approximately equal to a negative (volume-increasing) hydrostatic pressure equal to the applied tensile stress. Then, the conjecture is made that the specimen contains a "small" spherical cavity, in such a way that the area of interest could be modelled as an infinitely thick spherical shell. The elastic problem is then solved and a critical value σ_{crit} is found at which the cavity's radius goes to infinity.

Cavitation is evoked in [177] to explain the the non-monotonicity of energy release rates vs crack speed, as well as the differences in fracture sufaces related to "slow" and "fast" propagation, the latter being significantly smoother. Their argument relies on the fact rubber is almost incompressible at low deformation rates. As a result high hydrostatic pressures could arise, yielding cavitation. For sufficiently high crack speeds the material ceases to be incompressible, suppressing cavitation. Then two mechanisms

are described to explain rubber fracture. In the low speed region fracture originates from the nucleation, growth and coalescence of cavitation flaws. In the high speed region fracture is almost brittle, as it involves mainly primary bonds. As such bonds have to be broken anyhow, the energy dissipated in the first failing mode is higher than the one implied by the second, which could explain the observed decrease in energy release rate with increasing speed. The conceptual scheme which will be employed in the formulation of the non-local CZM in Chapter 5 is analogous.

Interestingly, cavitation occurs also as a solution of the non-linear elastostatics problem modelling a ball on which surface tractions or displacements are imposed, without the need to consider the infinitesimally small cavity (without renouncing to the *strong-ellipticity* condition [9, 122] on the energy density function, necessary for the variational problem to be well posed in general, [122]). In [178] cavitation is shown to be an instability bifurcating from the homogeneous solution at a critical stress value. Its possibility is related to the growth properties of the energy density function W for large strains. An example is made by Ball of an energy density function, describing the deformation of a body occupying a n-dimensional domain Ω, $n = 2, 3$ such that any deformation gradient corresponding to a finite energy will belong, for $p > n$, to the Sobolev space $W^{1,p}(\Omega, \Re^n)$ and hence will be described by a continuous function (due to the Sobolev Imbedding Theorem [179]): cavitation is hence excluded. These profound mathematical observations are very relevant for the practising engineer too and for this reason have been reported herein: as noted by Ball himself, the fact that only a set of homogenous deformations can be reached prior to failure during testing is not sufficient to conclude that the material is not elastic for a certain $\mathbf{F}$ outside the observable set of deformation gradients, as an instability might be preventing the specimen to reach such $\mathbf{F}$ (see [180] for a numerical analysis of an analogous "structural" failure in a concrete tensile specimen). This observation poses a serious criticism to the common engineering use of uniaxial fracture parameters such as stress at break or elongation at break as crack predictors.

De Gennes' Viscoelastic Trumpet

This review is ended by presenting the celebrated "viscoelastic trumpet" argument of De Gennes [181]. The analysis applies strictly only to weakly-crosslinked polymers characterised by a ratio $G_\infty/G_0 = \tilde{g} > 100$, although the qualitative picture preserves

its general validity even for a heavily cross-linked rubber compound as the one used for the experimental validation of the models presented in this work (see [3] for a related treatment where the assumption of weak-crosslinking is not necessary).

Considering, as an idealization of the real relaxation behaviour, the complex modulus (see Section 2.1.1) of the Standard Linear Solid [14]

$$\mu(\omega) = \mu_0 + (\mu_\infty - \mu_o)\frac{i\omega}{1 + i\omega\lambda} \tag{5.12}$$

with μ_0 and μ_∞ standing for instantaneous and long-term complex moduli (with vanishing imaginary part as the response tends to the elastic one in both the limits of slow and fast frequency, in analogy to the case of slow and fast loading rate). Three separate regimes in the frequency domain are then considered. For $\omega < 1/\lambda\tilde{g}$ the approximation $\mu \approx \mu_0$ applies. The complex modulus can be approximated as real and the material can be considered as a *soft solid*, *i.e.* the material is relaxed. For $1/\lambda\tilde{g} < \omega < 1/\lambda$ the following approximation holds

$$\mu(\omega) \approx (\mu_\infty - \mu_0)i\omega\lambda \approx i\omega\lambda \tag{5.13}$$

the last passage being motivated by the smallness of the ratio $\tilde{g}$, A purely imaginary complex modulus is recovered: the material can be considered a *liquid*. For $\omega > 1/\lambda$ the material behaves as a *strong solid*, $\mu \approx \mu_\infty$; such state is often referred to as *i.e. glassy*. Further, a simple scaling argument is put forward: the distance x from the tip of a crack moving with speed V and the frequency at a point at distance x from the crack tip are related via the scaling law

$$\omega \cong \frac{V}{x} \tag{5.14}$$

Thanks to such relation, the three regions in the frequency domain highlighted above acquire a spatial meaning, for they correspond to three different regions at increasing distance from the crack tip, see Fig.5.3.

De Gennes then continues by exploiting this relationship to find the total energy dissipated in the transition region as a function of crack speed, and to find the shape of the crack profile (which turns out to be "trumpet-like", as succesively confirmed by detailed experiments [182]). What is relevant for the present discussion is that with the crack speed growing the specimen might not be sufficiently large to accomodate all the three regions, which would cause the energy dissipated to reduce [181, 183], see also [109] for a related numerical study. The loss of monotonicity of the fracture energy
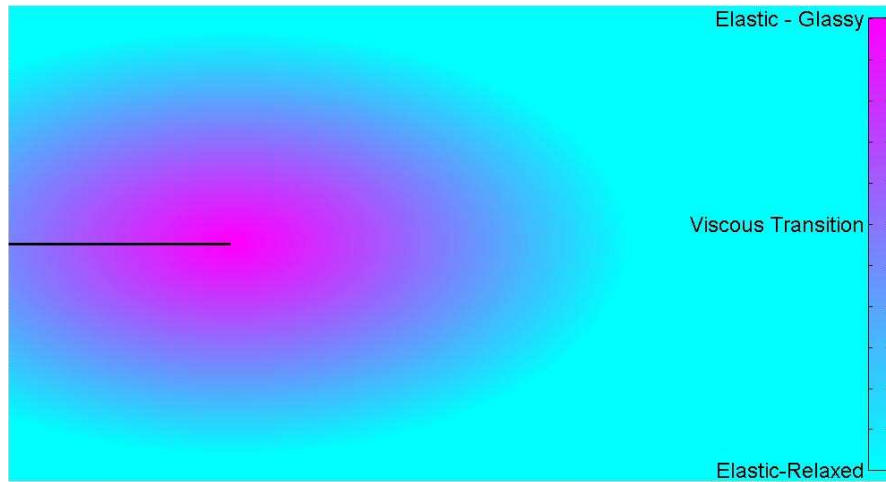
Figure 5.3: Different regions in a fracturing viscoelastic material (with a crack running from left to right) following De Gennes' analysis.

vs crack speed is then explained as a "structural" phenomenon, not intrinsically related to interface material properties.

5.2   Model Formulation and Physical Justification

Non-monotonicity of the relationship between energy-release and crack speed could be certainly captured by a phenomenological approach; an attempt to provide a simple micromechanical justification, alternative to the explanations summarised in the previous Section, is made instead. In spite of its simplicity and coarseness, the micromechanical model could possibly help in the formulation and justification of a phenomenological model more suited for practical applications. It is noted that the cohesive-zone modelling paradigm proposed in Chapters 3 and 4 cannot reproduce such behaviour for the very simple reason that such behaviour is not present at the bulk-material level. In other words, let us consider the peel specimen whose behaviour is described in Fig.5.1. Uniaxial tensile testing conducted on the same rubber would not reveal any peculiarity, in that the stress-strain curve relative to a certain testing speed would consistently fall below any stress-strain curves obtained at higher testing speed, see Fig.5.4.

The central idea of the present contribution is a novel definition of crack energy, motivated by the fact Barenblatt's description might be insufficient for materials and/or crack configurations characterised by process zones which are "long" when compared to

95
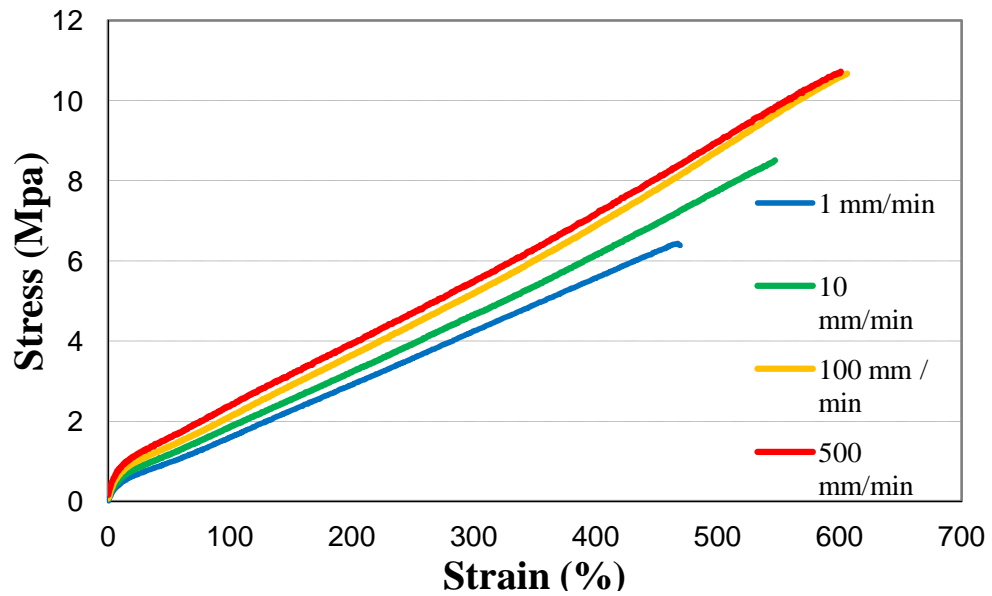
Figure 5.4: Nominal Stress-strain curves for the rubber interface material at various loading rates (strain calculated over a 25 mm long section).

a characteristic body length, see discussion in Section 2.2.1. Indeed in the case of rubber the process zone is dominated by mechanisms acting at various length and time-scales (flaws nucleation and propagation, crazing, diffuse damage, stringing, chain pull-out, fibrillation or "bridging", to mention a few). It is conjectured that certain dissipating mechanisms occur within too large an area to hope a local formulation (as in Barenblatt's case) could be sufficiently descriptive.

The formation of fibrils, see Fig.5.5, is the main phenomenon the present analysis is devoted to, but in general the approach could possibly be adapted to more complex types of micro-structural re-arrangement (for example the study of microcracking pattern studied in [184]).

The starting point is an energetic description of the formation of fibrils after agreeing on a number of assumptions, including that the crack energy does not depend only on the discontinuity jump but also on an additional internal non-local vectorial variable; the latter describes, in a simplified manner, the microstructure originating from fibrils formation. To the best of the author's knowledge this idea has not been exploited yet. Rate-dependency is introduced by postulating the (anisotropic) fracture energy evolves as a result of conformational changes occurring in the material. The evolution of the

96
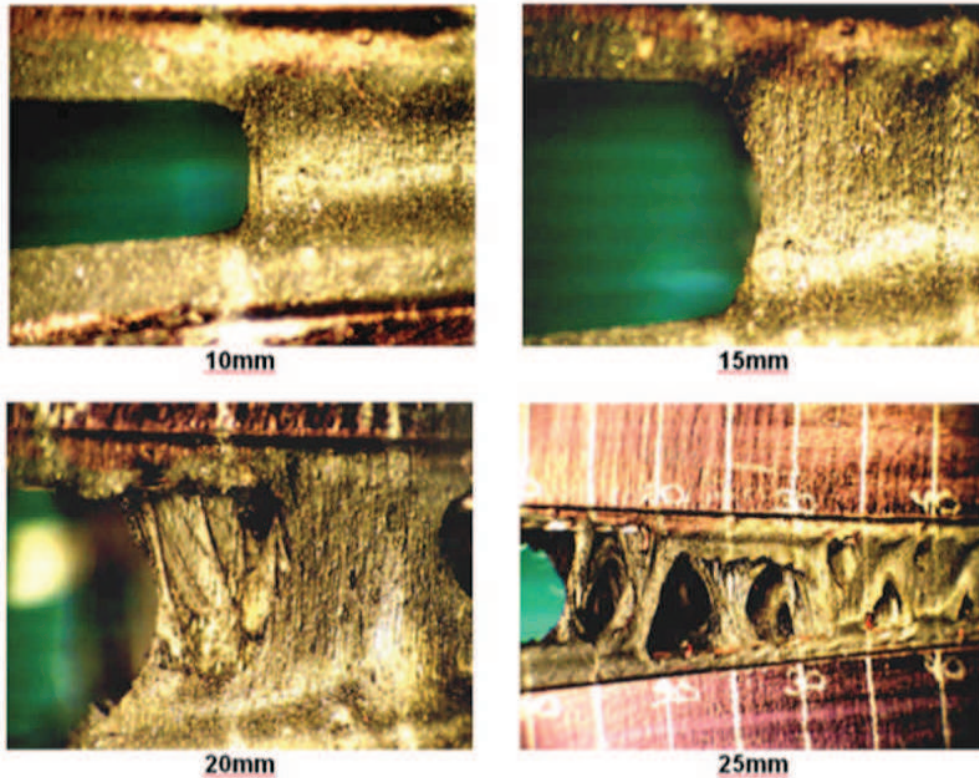
Figure 5.5: Snapshots of a "fibrillated" process zone.

internal variable is governed by the solution of a variational problem, defined at the interface level. Use will be made of some formalism characteristic to the so-called "variational theory of fracture", whose fundamentals have been reviewed in Section 2.3.

It is remarked that often material constitutive laws with non-convex potentials arise from a breach of the continuum hypothesis, *i.e.* the presence of a micro-scale structure not sufficiently separated from the macro-scale. Evidence for this observation is offered for example by polymeric foams [185], where the foam structure "buckles" at the micro-level causing overall softening. Another example particularly relevant for the present work is represented by shear-thinning in complex fluids (a phenomenon whereby the viscosity of a fluid decreases with respect to increasing shear strain rate [186, 187]), as a result of the interactions between fluid and particles at the meso-scale. A related instance is also given by phase transitions (strain-crystallization) in rubber [1], see Section 5.1. Similar physical phenomena could explain the "drawing" (localized necking) behaviour of nylon fibres, for which a gradient (hence, non-local, for not only the strain state of the material point is considered in the material constitutive law, but

97

its spatial gradient as well) formulation was proposed [188]. Last, liquid crystals are mentioned, whose peculiar behaviour originates as well from the mutual interactions of fluid-immersed particles [189].

The phenomenon of fibrillation in glassy polymers has been explained as a crack-front instability akin to the fluid meniscus Taylor instability, see Fig.5.6 [190, 191], see also [192, 193] for a similar instability occurring in a solid, incompressible, thin film.
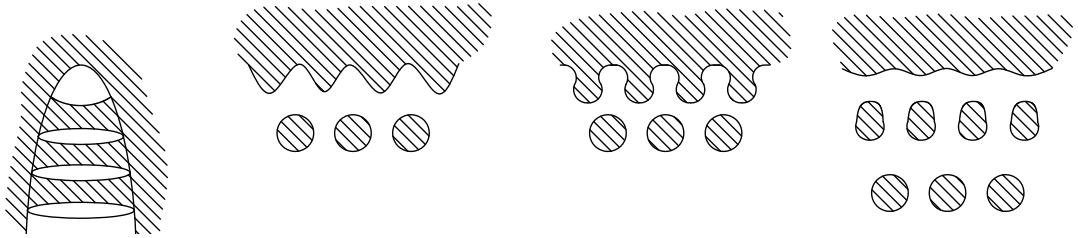
Figure 5.6: Schematic of fibrils formation by Taylor meniscus instability. Left, side view of a crack propagating upwards. Right, section through the crack (plane normal to the page): existing fibrils show as cylinders, three snapshot follow the instability of the crack front [190, 191].

The above considerations might suggest that the lack of monotonicity of the G_c *vs* crack speed relationship might arise from structural phenomena occurring at a scale lower than the one employed to view and model the material as a continuum. Following these examples, the main idea is to consider the interface in more detail and acknowledge that it might be necessary to consider additional variables other than the displacement jump between material points on its sides, see Fig.5.7.

Moreover, the simplest explanation of the loss of monotonicity of the fracture energy *w.r.t.* crack speed seems to be the presence of a dissipative mechanism which ceases to occur at a certain speed. Armed with these two observations, an examination of test samples seems to suggest that fibril formation could be such a phenomenon. Indeed, the fracture surface of the samples tested at higher than critical speed seems to be much smoother, see Fig.5.9, as mentioned in Section 5.1 and confirmed once more by the experimental work presented in Chapters 3 and 4.

It is conjectured that fibrils form as a result of cracks running perpendicularly to the crack path, within a damaged region in the neighbourhood of the crack tip, see Fig.5.8.

98
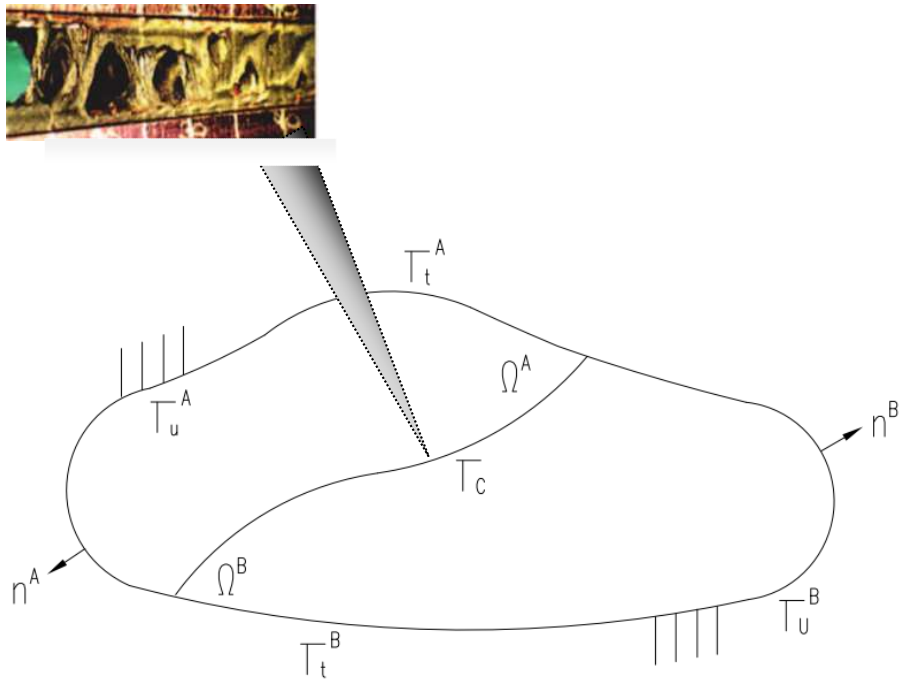
Figure 5.7: Schematic view of the proposed approach: the interface is "zoomed in" in an attempt to model additional mechanical features such as fibril formation, not dealt with in the classic cohesive-zone approach.
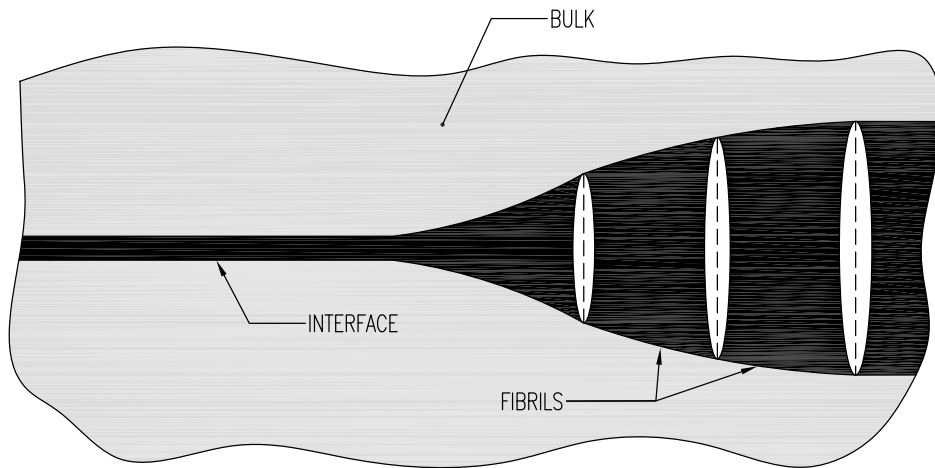
Figure 5.8: Fibrils geometry idealisation employed in the model

The associated energy release is related to the radial contraction of the fibril, modelled as a cylinder. To clarify this point, let us consider a right cylinder, made of an elastic

99

(a)

(b)
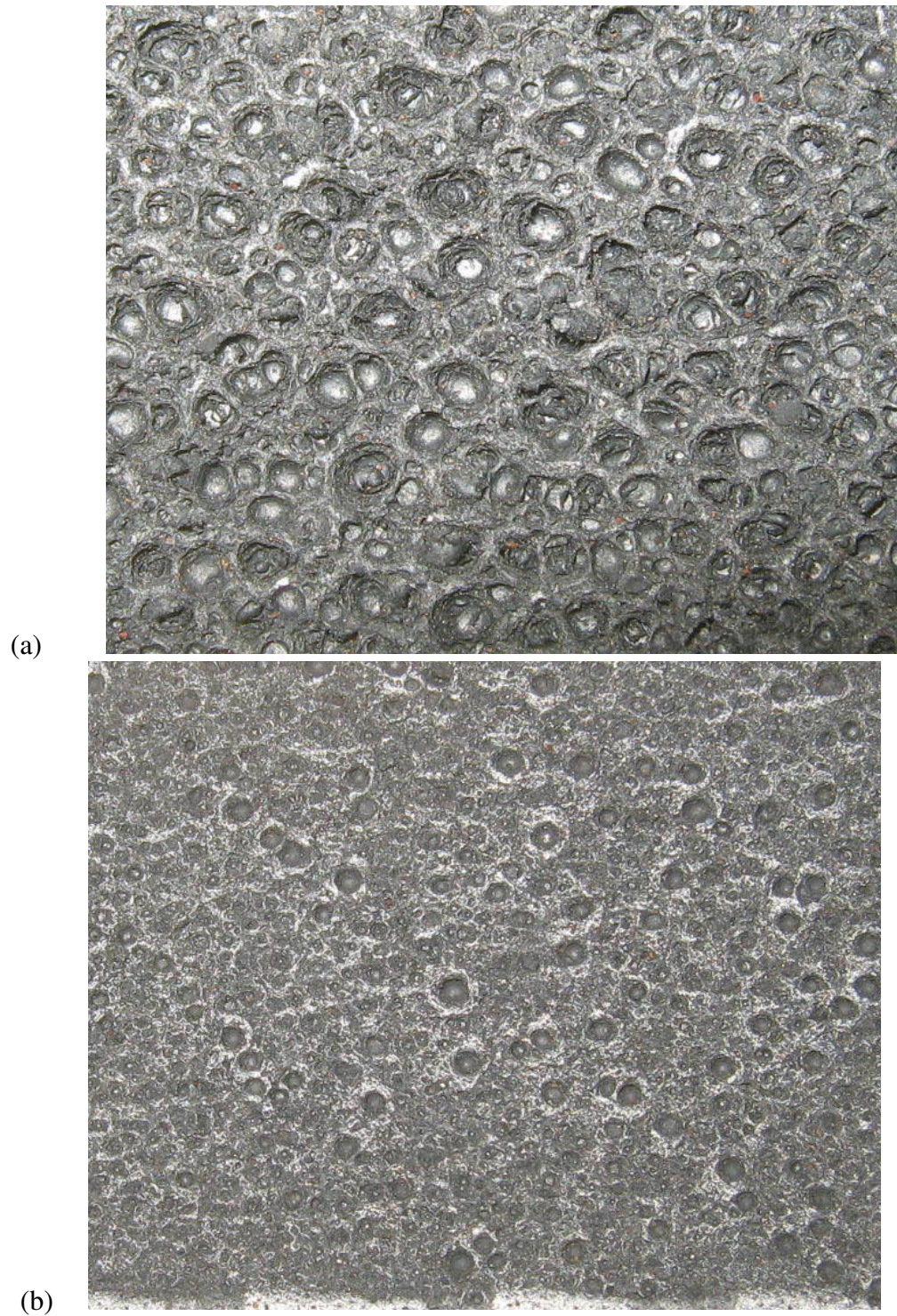
Figure 5.9: a) Fracture surface of a DCB specimen tested at 0.1 mm/min b) Fracture surface of a DCB specimen tested at 100 mm/min.

material with positive Poisson ratio. The specimen is then clamped in a hard device

and loaded such that equal in magnitude and opposite in sign displacements parallel to the axis are imposed on the two end surfaces, resulting in an increase in length. In addition, any displacement perpendicular to the lateral surface is prohibited. Let us assume now that the boundary conditions on the lateral surface are changed to a null-traction boundary condition: the elastic energy in the cylinder will reduce (this is a result of the fact the traction on the lateral surface is positive in the first configuration). One could then idealise the change in boundary conditions as originating from a fracture occurring along the lateral surface: the energetic convenice of such fracture could then be assessed.

To simplify the discussion, the two-dimensional setting is considered, in which fibrils appear as rectangles. The crack path is assumed to be of length $\hat{l}$ known in advance and is modelled as a curve Γ of the plane parametrized by its arc-length measured from an origin. The presence of the fibrils is mathematically described by introducing a partition $\mathcal{P} = \{0, x_1, ..., x_n\}$, n being yet unknown, of the crack process zone. The analysis is limited to the pure Mode-I case whereby the displacement jump is a scalar function δ representing the opening displacement at the interface.

In principle the dissipated energy could be estimated using three-dimensional elasticity, although an analytical calculation of the energy involved seems rather cumbersome even for the simplest hyper-elastic energies. To overcome this difficulty an *ad hoc* relationship is introduced by postulating that the energy of a fibril of width $l = x_m - x_{m-1}$, over which the displacement jump δ is prescribed, can be computed as

$$\mathcal{W}_e(l, \delta) = \int_{x_{m-1}}^{x_m} \vartheta(\delta(x)) \tilde{\varphi}\left(\frac{l}{h}\right) \mathrm{d}x \qquad (5.15)$$

where $\tilde{\varphi} : (0, \infty) \to (0, 1)$, is an assigned function describing the percentage of the stored energy released by allowing lateral contraction, $\vartheta : \Re^+ \to \Re^+$ is the function describing the energy associated to a displacement jump (without fibril formation) as in original Barenblatt's cohesive-zone formulation, see Section 2.2.2 and h is an internal length scale mirroring the thickness of the process zone [81], which is assumed known, or at least agreed on, *a priori*.

Remark 5.2.1 The definition above suits perfectly the case of a straight crack path and a constant displacement $\delta(x) = \bar{\delta}$. The case of non-constant $\delta(x)$ is dealt with assuming that the gradient of $\delta(x)$ does not contribute significantly to the fibril energy,

which is described in a sufficiently accurate way by the value of $\frac{l}{h}$. An alternative description could be obtained by defining a suitable variation of $\delta(x)$ across the fibrill, or by explicitly considering the gradient of δ. The extension to the curvilinear case requires further sophistication and will be considered in future work. ∎

The function ϑ is assumed continuous, convex and such that $\vartheta(0) = 0$. Physical intuition suggests that $\tilde{\varphi}$ is characterised by the conditions

$$\tilde{\varphi} \in C^2(\Re^+) \quad \tilde{\varphi}'(z) > 0 \quad \forall z \in [0, \hat{l}) \tag{5.16}$$

$$\exists \tilde{z} \in \Re^+ : \tilde{\varphi}''(z) > 0 \quad \forall z < \tilde{z} \qquad \tilde{\varphi}''(z) < 0 \quad \forall z > \tilde{z} \tag{5.17}$$

$$\lim_{z \to 0^+} \tilde{\varphi}(z) = \mathring{\varphi} > 0 \quad \lim_{z \to \infty} \tilde{\varphi}(z) = 1 \tag{5.18}$$

$$\lim_{z \to 0^+} \tilde{\varphi}'(z) = 0 \quad \lim_{z \to \infty} \tilde{\varphi}'(z) = 0 \tag{5.19}$$

$\tilde{z}$ being a costant.

The most interesting condition is expressed in equation 5.17, which characterises $\tilde{\varphi}$'s "shape" as sigmoidal. Such a requirement is actually a consequence of conditions (5.18) and (5.19), whose introduction is based on intuitive, physical grounds. Indeed, let us consider again the simple thought-experiment just performed on a cylinder, by changing boundary conditions on the lateral surface from null normal displacements to null traction. If the aspect ratio, *i.e.* the ratio of the cylinder's height and a characteristic dimension of the base, is decreased, one expects the difference between the stored energies before and after the change in boundary conditions to decrease as well (when normalised to the initial stored energy): this requirement results in conditions (5.18$_1$) and (5.19$_2$). Conditions (5.18$_a$) and (5.19$_a$) are imposed on similar grounds, at which point the sigmoidal "shape" is a consequence of the continuity and monotonicity. In the author's opinion a similar line of reasoning is implicitly used very often in Mechanics. For example, in Section 3.5 it was detailed how the plain strain assumption was used to model the DCB specimen. This is equivalent to assuming the contraction of the lateral free-surfaces of the rubber interface, as visible in Fig.3.6, is negligible as far as the global response is concerned. If the DCB specimen were much narrower (let us say, only 2 mm wide instead of 25 mm) certainly the plain stress assumption would have

been more adequate. Then, conditions (5.19) are analogous to expecting that the plain strain (respectively, plane stress) approximation "converges" to the response of the idealised body for which plane strain (respectively, plane stress) is an exact assumption, *i.e* a DCB specimen of infinite width (respectively, infinitesimally thin).

The graph of a generic function $\tilde{\varphi}$ possessing such properties is sketched in Fig.5.10. It will be assumed that such properties hold throughout the Chapter. At this stage the possibility that $\tilde{\varphi}$ could depend on $\delta(x)$ is neglected.
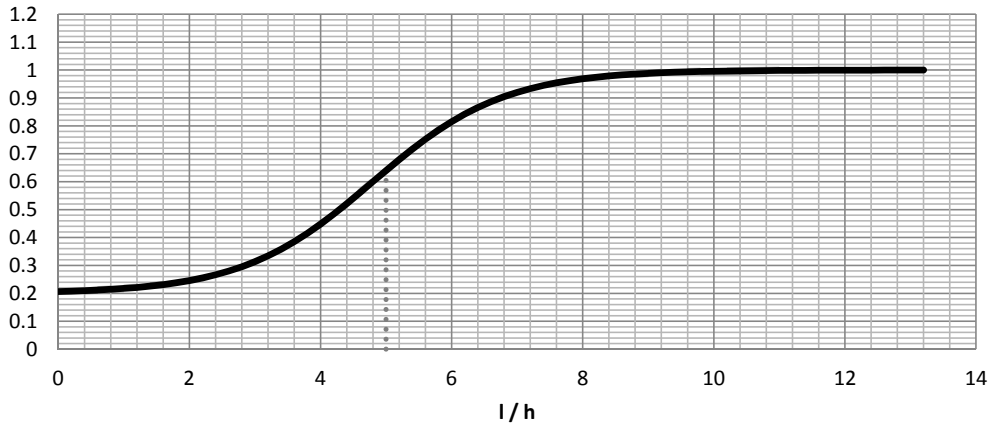
Figure 5.10: A typical function φ complying with properties (5.16), (5.17), (5.18), (5.19): $\mathring{\varphi} = 0.2$, $\tilde{z} = 5$, marked by the vertical dotted line.

The surface energy gained in the process is then described by

$$\mathcal{W}_s(\mathcal{P}) = \sum_{x \in \mathcal{P}} \tilde{\gamma}(x) h \qquad (5.20)$$

where $\tilde{\gamma}$ is a Griffith-type energy.

Intuitively it can be argued that the energy release rate associated to the transversal direction is lower than the energy release rate associated to the longitudinal direction: in other words, among all the cracks of a specified length, the maximum energy release rate is associated with the crack perpendicular to the principal strain direction. This argument was made rigorous in [72] (Proposition 4.5, pag.51). This being the case, *i.e.* as cracks in the transversal direction are characterised by lower energy release rates than cracks associated to the longitudinal direction, the doubt is raised whether fibrils are energetically convenient at all. A possible solution relies on considering an anisotropic fracture energy. It is recognised though that molecular chains in rubber-

like polymers are highly mobile and their re-orientation justifies the introduction of an anisotropic fracture energy, which in the present context is sufficiently described by a vector $\tilde{\boldsymbol{\gamma}} = [\tilde{\gamma_1} \quad \tilde{\gamma_2}]$, where 1 and 2 denote the directions parallel and perpendicular to the longitudinal (primary) crack path, respectively. Indeed fibrillation is likely to be observed in lightly-reinforced and low crosslink-density rubbers, and is promoted in uncured ("green", in the industry jargon) rubbers, as the absence of cross-sulphur bonds and reinforcing particles in green rubbers greatly facilitates chain re-orientation possibilities.

The exact measurement of the anisotropic, possibly rate-dependent fracture energy is a formidable task, yet in the author's opinion there is experimental qualitative evidence justifying its introduction [194,195], see also [196] for an analogous example of fracture energy anisotropy for cold-drawn steel wire (interestingly structural re-orientation is not exclusive to polymers). Indeed it seems tempting to justify crack paths such as the ones depicted in Fig.5.11 allowing for an anisotropic fracture energy. In other words, it seems reasonable to assume the fracture energy in the transversal direction is lower than the one in the longitudinal direction for the transversal crack (parallel to the tensile dumbell length direction) to be more energetically favourable than a crack in the longitudinal direction (across the tensile dumbell, see Fig.5.11) .

Time-dependency will be later introduced in the description by simply stating $\tilde{\gamma}$ follows an assigned evolution law. In the global solution scheme at a certain time step the time-dependent parameters will be known (as well as the tentative imposed displacement jump function $\delta(x)$), and the fibrils formation pattern is given by the minima, should they exist at all, of the energy described as a mapping $\mathcal{W} : \mathcal{P} \mapsto \mathcal{R} \cup \{+\infty\}$, given by the sum of elastic and surface energy terms such as represented in Equations (5.15) and (5.20), yielding the following expression:

$$\mathcal{W}(\mathcal{P}) = \sum_n \int_{x_n}^{x_{n+1}} \vartheta(\delta(x)) \tilde{\varphi}(\frac{x_{n+1} - x_n}{h}) \mathrm{d}x + \sum_{x \in \mathcal{P}} \tilde{\gamma_1}(x) h \qquad (5.21)$$

Fibrils formation could interact with other dissipating mechanism in the process zone, as the viscoelastic dissipation described in Chapter 3, possibly yielding complicated behaviour. Let us consider the total observed fracture energy as function of the crack speed $G_c(\dot{l})$. G_c can be viewed as the sum of the dissipation associated with the longitudinal crack propagation and related viscoelastic mechanisms $G_{visco}(\dot{l})$ and the energy lost in the formation of fibrils $G_{fibrill}(\dot{l})$:

(a)

(b)

Figure 5.11: Typical fracture path for a low-crosslink-density rubber tested at a low applied strain rate ($\approx$ 5%/min): a) general b) close up of the fracture surface, please note the "hairy" appearance.

$$G_c(\dot{l}) = G_{visco}(\dot{l}) + G_{fibrill}(\dot{l}) \tag{5.22}$$

It is clear that for the function G_c not to be monotonically increasing it is necessary for

its first derivative

$$\frac{\mathrm{d}G_c}{\mathrm{d}\dot{l}} = \frac{\mathrm{d}G_{visco}}{\mathrm{d}\dot{l}} + \frac{\mathrm{d}G_{fibrill}}{\mathrm{d}\dot{l}} \tag{5.23}$$

to be locally negative: indeed $\mathrm{d}G_{visco}/\mathrm{d}\dot{l} \to 0$ as the crack speed approaches the upper side of the viscous spectrum, hence if $\mathrm{d}G_{fibrill}/\mathrm{d}\dot{l} \leq 0$ the loss of monotonicity might eventually occur. This is a result of the fact that $\mathrm{d}G_{fibrill}/\mathrm{d}\dot{l} = 0$ for speeds at which fibrils do not form. The term $G_{visco}(\dot{l})$ has been discussed, and a suitable model presented, in Chapter 4: the reminder of the present Chapter is devoted to illustrate, for the simplest loading condition, the behaviour of a model whose aim is to qualitatively model the term $G_{fibrill}(\dot{l})$. Although unnecessary as far as the understanding of the physical mechanism herein described is concerned, having in mind more complex applications it is relevant to note that the problem of minimising the total (elastic + fracture) energy described by equation (5.21) can be recast as a variational problem, consisting in the minimisation of the following functional defined on the space PC of piecewise constant functions:

$$\mathcal{F}(u) = \begin{cases} \int_\Gamma \vartheta(\delta)\varphi\left(u(x)\right)\mathrm{d}x + \sum_{x \in J(u)} \gamma_1(x) & \text{if} \quad u \in SPC \\ \\ \infty & \text{if} \quad u \notin SPC \end{cases} \tag{5.24}$$

where for notational simplicity the notation

$$\varphi\left(u(x)\right) = \tilde{\varphi}\left(\frac{u(x)}{\hat{l}}\right) \qquad \gamma_1 = \tilde{\gamma}_1 h \tag{5.25}$$

is used. The set $SPC \subset PC$ is defined in the Appendix: loosely speaking, it consists of piecewise constant functions such that the length of the interval over which the function is constant equals the value of the function over that interval. It can be appreciated that the argument of ϑ in equation (5.24) is the value of the function, while in equation (5.21) the argument is the interval's length. The definition of the set SPC tantamounts to a "trick", employed in order for the functional $\mathcal{F}$ in equation (5.24) to penalise any function $\notin SPC$, for which the functional is not physically meaniful (if the function $\notin SPC$, the connection to equation (5.21) is lost).

The existence of a minimising partition can then proven using the Direct Method of Calculus of Variations: the interested reader is directed to the Appendix for more mathematical details. It is necessary to address the existence of a solution. Indeed, physical intuition alone suggests situations in which the energy minimisation process could be badly posed: for example, given a configuration with one transversal crack at a

location $\bar{l}$, the case could occur that any competing configuration with the crack placed by a "small" amount towards one end of the interface is energetically favourable. Then the minimisation process would force the fibril to be placed closer and closer to the end of the interface: keeping in mind that the configuration with no cracks might not in general be minimising, it could be appreciated the problem would not have a solution. The Direct Method of Calculus of Variations allows to determine the conditions under which such instances are eliminated (see end of Section 2.3 and Appendix).

5.3 The Rate-Independent Case

The behaviour of the proposed cohesive-zone model will now be elucidated in a simple case. As stated in the previous section the cohesive-zone behaviour is obtained as a minimization of the energy $\mathcal{W}$, equation (5.21) or equivalently $\mathcal{F}$, equation (5.24). The partition $\mathcal{P}$, or analogously the function u, encodes physical variables represented by the number of transversal cracks and their location. In a realistic situation the displacement-jump along the interface would not be prescribed: boundary conditions would usually apply to the boundary of the body containing the interface. In this case the minimization process could in principle be achieved in two stages (analogously to the stepwise minimization procedure proposed in [81], [197]). Firstly, at imposed δ the optimum fibril pattern could be determined; then, total minimization could be achieved by comparing configurations with different imposed displacement-jump δ. Restricting the attention to the case of imposed interface displacement-jump, as done in the sequel, eliminates the need for the second stage: only the interface behaviour will hence be investigated. Furthermore, the displacement-jump will be assumed to be uniform along the length $\hat{l}$ of the interface. This is a further drastic semplification which allows a straightforward solution to be determined. It is in essence analogous to presenting the cohesive traction-separation law for a point only of the interface. The main feature of the model's response, as far as monotonicity of the fracture energy *w.r.t.* crack speed is concerned, can anyhow be appreciated.

   Firstly, the analysis will be limited to the case where transversal cracks only form. Let us assume that the evolution starts from the uncracked, undeformed state and the interface is loaded in displacement-control by a device imposing a monotonically increasing displacement $\delta(t)$, with $\delta(0) = 0$. The interface energy in the absence of

transversal cracks is characterised by the function $\breve{\mathcal{F}}$, with $\breve{\mathcal{F}}(0, N)|_{N=0} = 0$,

$$\breve{\mathcal{F}}(t, N)|_{N=0} = \hat{l}\vartheta\left(\delta(t)\right) \tag{5.26}$$

which is continuous in the first argument and convex. Due to the convexity of $\breve{\mathcal{F}}$ there exist times t_0 and t_1 such that

$$\breve{\mathcal{F}}(t_0, 0) = \gamma \qquad \breve{\mathcal{F}}(t_1, 0) = 2\gamma \tag{5.27}$$

Evidently fracture is not energetically favourable for $t \leq t_0$ (as the total energy is less than the minimum energy required for a transversal crack), while the appearance of one single transversal crack can not be excluded for $t_0 \leq t \leq t_1$. For times t belonging to the interval (t_1, t_2) the energy minimization reduces to the one-dimensional problem

$$\min U(z) \qquad z \in (0, \hat{l}) \tag{5.28}$$

where

$$U(z) = \begin{cases} \vartheta(\delta(t)) \left[z\varphi(z) + (\hat{l} - z)\varphi(\hat{l} - z) \right] + \gamma_1 & \text{if} \quad z \in]0, \hat{l}[\\ \hat{l}\vartheta\left(\delta(t)\right) & \text{if} \quad z \in \{0, \hat{l}\} \end{cases} \tag{5.29}$$

where dependence on t is omitted for notational simplicity. Equation (5.29) is the specialisation of the functional (5.24) to the case of uniform imposed displacement along the interface: the first term in square brackets refers to the fibril whose base rests on the interval $(0, z)$ ($(z, \hat{l}$ for the second term respectively). It is apparent U is continuous except for $x \in \{0, \hat{l}\}$, points in which it is lower semicontinuous (which can be verified by directly applying the definition of lower semicontinuity, see the Appendix, and the fact γ_1 is strictly positive). U being also bounded away from zero, it admits a global minimum by Weierstrass's extreme value theorem, in its generalisation for semi-continuous functions [56, 198].

The existence of local minimizers can now be addressed. The stationarity condition

$$\frac{\mathrm{d}U}{\mathrm{d}z} = 0 \tag{5.30}$$

yields

$$\vartheta(\delta) \left[\varphi(z) + z\varphi'(z) - \varphi(\hat{l} - z) - (\hat{l} - z)\varphi'(\hat{l} - z) \right] = 0 \tag{5.31}$$

108

The minimum condition

$$\frac{\mathrm{d}^2 U}{\mathrm{d}z^2} > 0 \qquad (5.32)$$

yields

$$\vartheta(\delta) \left[2\varphi'(z) + 2\varphi'(\hat{l} - z) + z\varphi''(z) + (\hat{l} - z)\varphi''(\hat{l} - z) \right] > 0 \qquad (5.33)$$

The value $\tilde{z}$ separating the convex from the concave domain of φ introduces an internal length scale in the model.

The focus will be from now on put exclusively on the case of a "short" interface, *i.e.* an interface such that $\hat{l} \leq \tilde{z}$, as this suffices to exhibit the physical behaviour the model is meant to reproduce. In such case $\mathrm{d}^2 U/\mathrm{d}z^2 \geq 0$ everywhere in $(0, \hat{l})$ because $\varphi'(z)$, $\varphi'(\hat{l} - z)$, $\varphi''(z)$ and $\varphi''(\hat{l} - z)$ are all positive for $z \in (0, \hat{l})$ and in the case $N = 1$ a unique global minimum exists, equal to $U(\frac{\hat{l}}{2})$ because U is symmetric about $\frac{\hat{l}}{2}$.

In the case of N transversal cracks it can be shown (see Proposition 5.5.1 in the Appendix) that a countable infinity of local minima exist, and they are characterised by the fibrils being equidistant, in a periodic pattern. It is also worth noting that in the case of a "short" interface, the uncracked configuration can only evolve to a single-cracked configuration: a proof of this statement is also included in the Appendix, see Proposition 5.5.1. Then, the interface will evolve as follows: starting from the configuration with no transversal cracks, its elastic energy will grow during loading until the point when it is energetically convenient to form a transversal crack, by paying the energetic cost represented by the transversal surface energy term but gaining in terms of elastic energy release.

The energy landscape resulting from the proposed model is illustrated in Fig.5.12. The restriction of the surface to the set $x = \{x : \text{applied displacement} = 0\}$ is a stepwise constant function, as a result of the surface energy term in equation (5.21), *i.e.* γ_1 multiplied by the number of transversal cracks. The restrictions of the surface to any set $x = \{x : \text{number of transversal cracks} = N\}$, N being an integer constant, are convex curves characterised by the function ϑ (see equation (5.15)). Any evolution along such curves is elastic only, and is in general interrupted by "switching" to another elastic evolution characterised though by an increased number of transversal cracks. The black continuous line exemplifies the equilibrium path in the [*applied displacement*] $\times$ [*number of fibrils*] configuration space, made by alternating elastic evolution paths

and jumps to configurations characterised by an increased number of transversal cracks. Such path could be visualised by considering a material point whose coordinate [*applied displacement*] is prescribed as a function of time, while the coordinate [*number of transversal cracks*] is selected as the argument for which the height of the surface is minimum along the same coordinate.
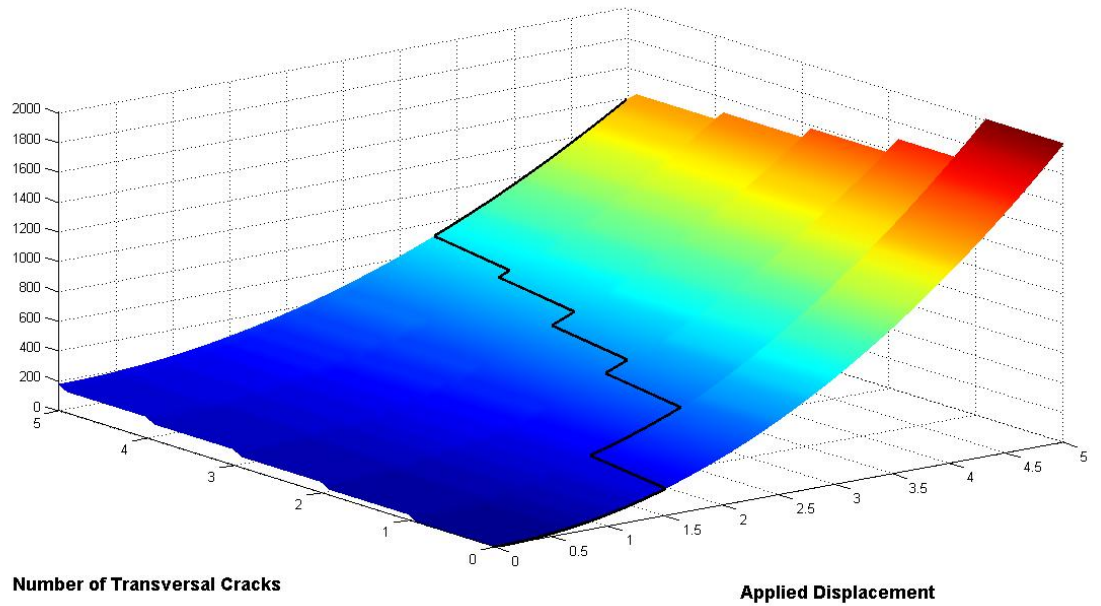
Figure 5.12: Energy Landscape of a "short", rate-independent interface under (uniform) imposed displacement. It can be noticed how the restriction of the surface to the set $x = \{x : \text{applied displacement} = 0\}$ is a stepwise constant function, as a result of the presence of the surface energy term in equation (5.21), *i.e.* the transversal fracture energy γ_1 multiplied by the number of transversal cracks.

It can be appreciated from Fig.5.12 how an important physical feature is missing, *i.e.* irreversibility. Indeed once the uncracked configuration evolves to the configuration with one transversal crack, further evolution to a configuration with two transversal cracks entails crack healing by necessity. It was mentioned that transversal cracks have to be equidistant (see Proposition 5.5.1 in the Appendix) , and this is incompatibe with the previously attained configuration, unless cracks were allowed to heal. This option is discarded and an irreversibility constraint transversal cracks have to be subject to is hence introduced. More specifically, if at time $\tilde{t}$ the fibrils structure is characterized by

a function $u_{\tilde{t}} \in SPC(0, \hat{l})$, then the following condition can be imposed:

$$\forall t > \tilde{t} \qquad J(u_{\tilde{t}}) \subseteq J(u_t) \qquad\qquad (5.34)$$

This criterion, based on the physical assumption of not allowing cracks to heal, defines an admissible class of energetic competitors based on the actual globally minimizing configuration. After a crack appeared, the irreversibility condition would allow to consider separately the intervals separated by the cracks. As Proposition 5.5.1 applies (upon substituing $\hat{l}$ with Δz, future cracks interior to the fibril will be necessarily equispaced and their number will evolve according to the sequence $2^j - 1$, $j = 0, 1, 2, ...$), in period-halving fashion.

Considering again Fig.5.12, it is seen that the "jump" between the configuration with one and two cracks is prohibited by irreversibility: the transition then is delayed until the applied displacement reaches the value at which the transition from two to three cracks appears, at which point the transition from one to three transversal cracks will occur.

The results presented so far allow to define for each time t the globally minimizing configuration among all the admissible competitors with transversal cracks.

5.3.1 Longitudinal Crack and Global Minimization

So far attention was only given to the formation of transversal cracks. A mechanism to justify the formation of the primary, longitudinal, crack needs to be introduced. This is to be achieved in the simplest possible way, postulating that a surface energy of Griffith's type [72] is assigned to the primary crack. Physically this means that the surface energy is independent of the crack opening and equals a constant γ_2 for any positive displacement jump. It is also to be noticed that the formation of a primary crack releases all the elastic energy stored in the fibrils. Referring again to Fig.5.12, this means that the achievable energy is bounded above by $\hat{l}\gamma_2$: upon reaching this value the longitudinal cracks appears and no further evolution in terms of transversal cracks is possible.

The solution then can be found by computing the global minimum, as a function of time t, among configurations with transversal cracks (whose energy has been characteried in the previous Section) and a longitudinal crack, to which an energy $\hat{l}\gamma_2$ is assigned as detailed above.

Remark 5.3.1 The fact that minimisers are characterised by equi-spaced fibrils if their width belongs to an interval over which φ is convex is a feature which echoes other models defined using convex functionals, [184, 199] (where also references to experimental evidence are made). This is not surprising at all and it is echoed even in the elastic one-dimensional setting (*e.g.* a rod under tension), where the convexity of the free energy forces the strain to be equal on each material region [200] (the property of *quasiconvexity* [122] guarantees analogous results in higher dimensions). It is then interesting to remark that the functional $\mathcal{F}$ is not defined over a linear space, as the sum of two functions $u_1, u_2 \in SPC$ needs not belong to SPC. As a result, the usual definition of convexity, see Section 2.3.1, can not be applied. On the other hand, suitable definitions have been developed for a metric space setting [201]: for example, the notion of *convexity along curves* [201] is applicable. ∎

It is noted that the minimization is to be performed globally, to prevent the cohesive zone from remaining locked in a locally minimizing configuration such as the uncracked configuration. Heuristically it is immediate to verify that process-zone configurations with a different number of equispaced cracks are separated by an energy barrier. Indeed, immediately after the sudden, "brutal", formation of a transversal crack the bulk energy will be the same, loosely speaking, while the surface energy will have increased.

Discussion

In the field of variational fracture there is a vivid debate about the merits and shortcomings of global *vs* local minimization, for which the reader is referred to [72, 127, 202]. It will just briefly be mentioned that the global solution might be deemed physically unacceptable as "jumping" over configurations separated by an energy barrier might be considered unphysical in the lack of an external power input (see also [62] for the quasistatic evolution case and the ability of global minimization to "see into the future", in the authors' own words). It is conjectured that the micromechanics mechanism used herein to describe fibrillation is just an idealisation of a fibrils formation mechanism possibly involving defects, by which transversal cracks grow smoothly, providing a viable path between local minimizers. The fact that the latter is possibly the correct physical description is supported by experimental observations, see Fig.5.13, in which a micro-crack nucleating in a relatively long time compared to the almost instantaneous

112

propagation across the interface is shown (pictures taken at 1 minute intervals).

The concept of energy barrier between two local minima is an essential ingredient of kinetic theories (the most relevant and successful from the mechanical point of view being Zhurkov's kinetic theory on the strength of solids, [203], see also [137, 204–206] for more recent approaches): within such theories the additional energy needed to jump over the barrier is given by random thermal fluctuations, which are then seen to play a role analogous to the defects invoked in the preceding paragraph to justify the use of global minimization. The reader is referred to [207] for a variational model for plasticity exploiting global minimization upon justifying overcoming energetic barriers via the use of physical arguments, and for the related discussion about global vs local minimization.

5.4   The Rate-Dependent Case

So far both γ_1 and γ_2 have been considered given material properties. Now the case of history-dependent γ_1 is considered. In general, the time evolution of $\boldsymbol{\gamma} = [\gamma_1\,\gamma_2]$ could be described by micro-mechanical models, yielding an evolution law

$$\dot{\boldsymbol{\gamma}} = f(\delta, \alpha, \boldsymbol{\gamma}) \tag{5.35}$$

It can be argued that physically it might be difficult to justify the fact the surface energy varies without any macroscopic effect on the strain energy. If it is assumed that the surface energy varies in relation to structural re-arrangements at the micro-scale, it seems plausible to assume such re-arrangements require a power input: hence it is plausible to employ a history-dependent material formulation for the interface elasticity as well.

Assuming a satisfactory evolution law is found, approximated solutions could be sought using an incremental variational scheme. Let us consider a loading path, $t \mapsto \delta(t), t \in [0, T]$, assumed continuous. The loading path can be discretised by introducing a sequence $\{t_i\}_{i \in \mathcal{N}}$, Δt_i being defined as $(t_{i+1} - t_i)$.

Let us consider a loading path, $t \mapsto \delta(t)$, $t \in [0, T]$, assumed continuous. The loading path can be discretized by introducing a sequence $\{t_i\}_{i \in \mathcal{N}}$, Δt_i being defined as $(t_{i+1} - t_i)$.

The incremental procedure is then formalised as follows: for $i \in \mathcal{N}$ and $\delta_0 = \delta(0), \gamma_0 = \gamma_1(0) = \tilde{\gamma}, u_0 = u(0)$, find $u_{t_i} \in SPC_{t_i}$, such that

$$\mathcal{F}_{t_i}(u_{t_i}) \leq \mathcal{F}_{t_i}(u) \qquad \forall u \in SPC_{t_i} \tag{5.36}$$

$$\delta_{t_i} = \delta_{t_{i-1}} + \Delta t_i \tag{5.37}$$

$$\gamma_{t_i} = f(\delta_{t_{i-1}}, \alpha_{t_{i-1}}, \vec{\gamma}_{t_i-1})\Delta t_i + \gamma_{t_{i-1}} \tag{5.38}$$

where

$$SPC_{t_i} = \{p \in SPC(\Omega) : J(p_{t_{i-1}}) \subseteq J(p)\} \tag{5.39}$$

For the purposes of the present, qualitative discussion, no effort will be spent in identifying a plausible evolution law for the anisotropic surface energy $\boldsymbol{\gamma}$. It will suffice instead to require that the following conditions hold. Given a displacement jump history $\delta^1(t)$ let us assume that the corresponding surface energy evolution is given by a function $\gamma_1^1(\delta)$, γ_2 being on the other hand constant. It is then required that, given a parameter $\lambda > 1$, the following holds:

$$\gamma_1^\lambda(\delta) < \gamma_1^1(\delta) \tag{5.40}$$

where γ_1^λ is the evolution of γ_1 associated to the accelerated displacement jump history $\delta^\lambda(t) = \delta^1(\lambda t)$. The condition expresses the physically reasonable requirement that the fracture energy for transversal cracks (fibrils) at any given displacement-jump is a decreasing function of the applied deformation rate. This is a result of the fact any re-orientation occurring within the molecular structure will be characterised by its own characteristic time: analogously to the case of viscoelasticity, one then expect that in the limit of slow deformation rate (respectively, fast deformation rate) the transversal fracture energy γ_1 reaches its minimum (respectively, maximum). Also, it is required that $\lim_{\lambda \to \infty} \gamma_1^\lambda(\delta) = \breve{\gamma}_1$, $\breve{\gamma}_1$ being a positive constant. If $\breve{\gamma}_1$ is sufficiently smaller than γ_2 then these conditions alone are sufficient to provide a mechanical mechanism by which the energy required to fracture at a sufficiently low applied displacement rate is higher than the energy needed at faster applied displacement rates, contrary to the models presented in Chapters 3 and 4. Attention is still restricted to a "short" interface in the sense of Section 5.3: also, only the first transition to a fibrillated configuration is considered.

Fig.5.14.a refers to a "fast" displacement history: the energy for a crackless configuration is plotted together with the energetic threshold at which the primary, longitudinal crack will appear. For the given displacement jump history the evolution of γ_1 is plotted as well: the energy pertaining to three different values of γ_1, relative to three successive times (and hence displacements) highlighted by the markers, is plotted. The chart shows that for fast enough displacement jump histories the energy of the cracked configurations is higher than the uncracked one: the uncracked configuration then evolves to the longitudinally cracked one without the appearance of fibrils.

Decelerating the displacement jump history, the situation depicted in Fig.5.14.b could occur. At the moment of time highlighted by the second marker γ_1 is approaching a value such that the energy of the configuration with one transversal crack is lower than the energy of the uncracked configuration: the transition from uncracked to fibrillated configuration is incipient (see Fig.5.15, where both the total energy, elastic plus surface components, and elastic energy only are plotted). As elastic energy is the only available for the transition to completely ruptured (longitudinally cracked) configuration, it appears that in order to reach fracture an additional energy of $\gamma_1(\delta(t^*))$ is needed, where t^* denotes the time at which the transition from uncracked to fibrillated configuration occurs: it is then confirmed that the total energy needed to fracture the interface increases as the applied displacement rate is lowered.

It can be seen how the interface "resists", in a sense, to fracture by dissipating elastic energy (the driving force for longitudinal cracking) in the formation of transversal cracks. As a result, the elastic energy is lowered (as the surface energy is always positive, in any direction) and an increased applied displacement is needed to reach the energy threshold required for longitudinal fracture. Nevertheless, at a sufficiently high applied test rate, the conformational changes responsible for fracture anisotropy cannot occur fast enough, and the energy threshold needed for longitudinal cracking is reached prior to the formation of fibrils. This is a consequence of the fact that fibrils formation is intrinsically less energetically convenient than longitudinal cracking, as detailed in Section 5.2): in other words, if the anisotropicity of the fracture energy is not developed enough (and sufficiently slow rates are needed for this to occur), longitudinal cracking will occur first, as it is more favourable in itself (*i.e.* unless transversal cracking is favoured by the anisotropic fracture energy). Total failure is then reached at a reduced energetic cost compared to the case of fibrils formation; the fracture energy hence drops

upon reaching the applied rate threshold, possibly leading to an instability as discussed in Section 5.1. Similar dissipating mechanisms are present in many structures designed to achieve optimum energy-absorption resistance, *e.g* epoxy-reinforced rubbers [22], see also [208] for a numerical study of a one-dimensional, rate-independent, chain-like structure exhibiting analogous behaviour in dynamic conditions.
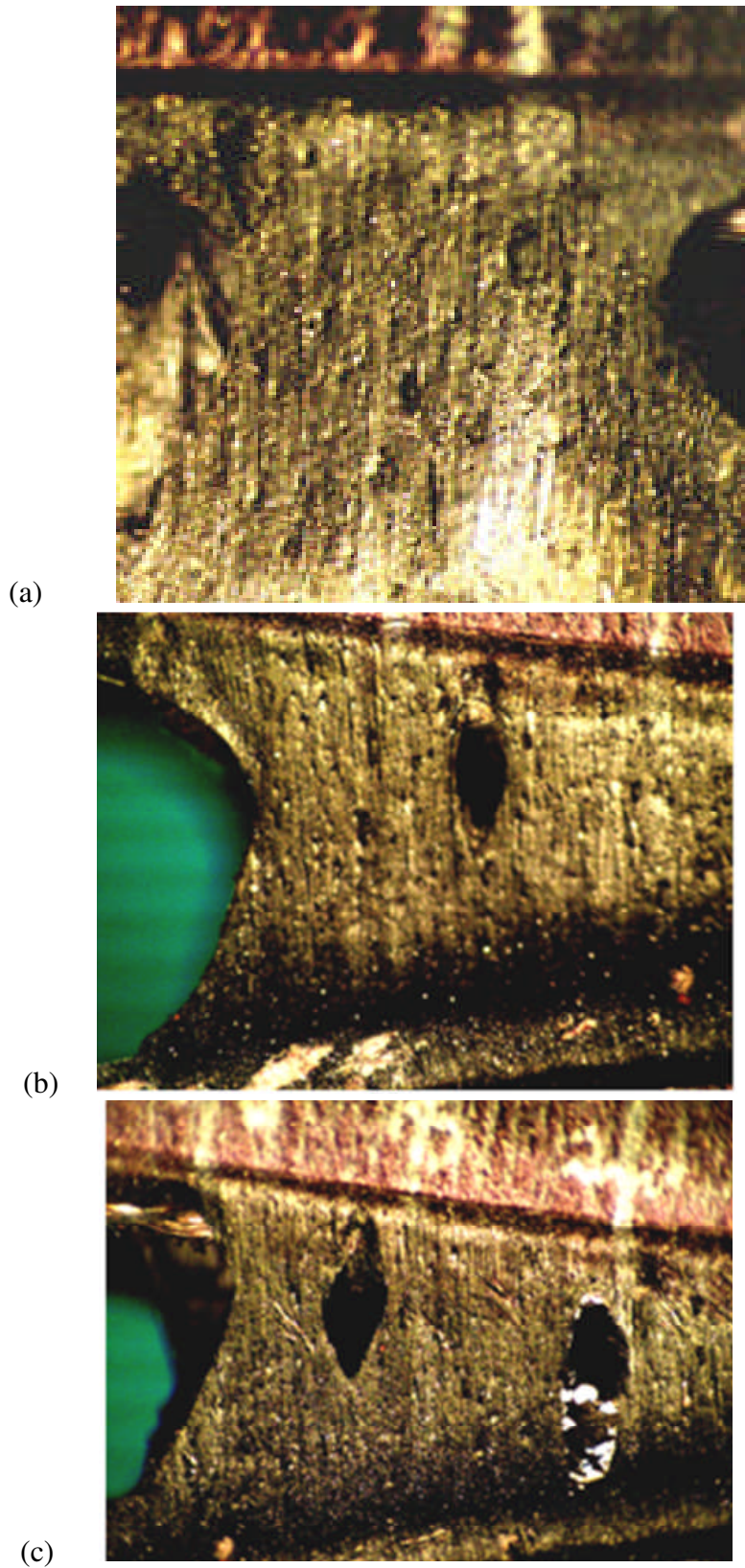
Figure 5.13: (a) Close up of the process zone for a DCB under a displacement rate of 1 mm/min: a micro-crack is just visible. (b) The evolution of the vertical cracks from b) can be appreciated. (c) The evolution of the vertical cracks continues.
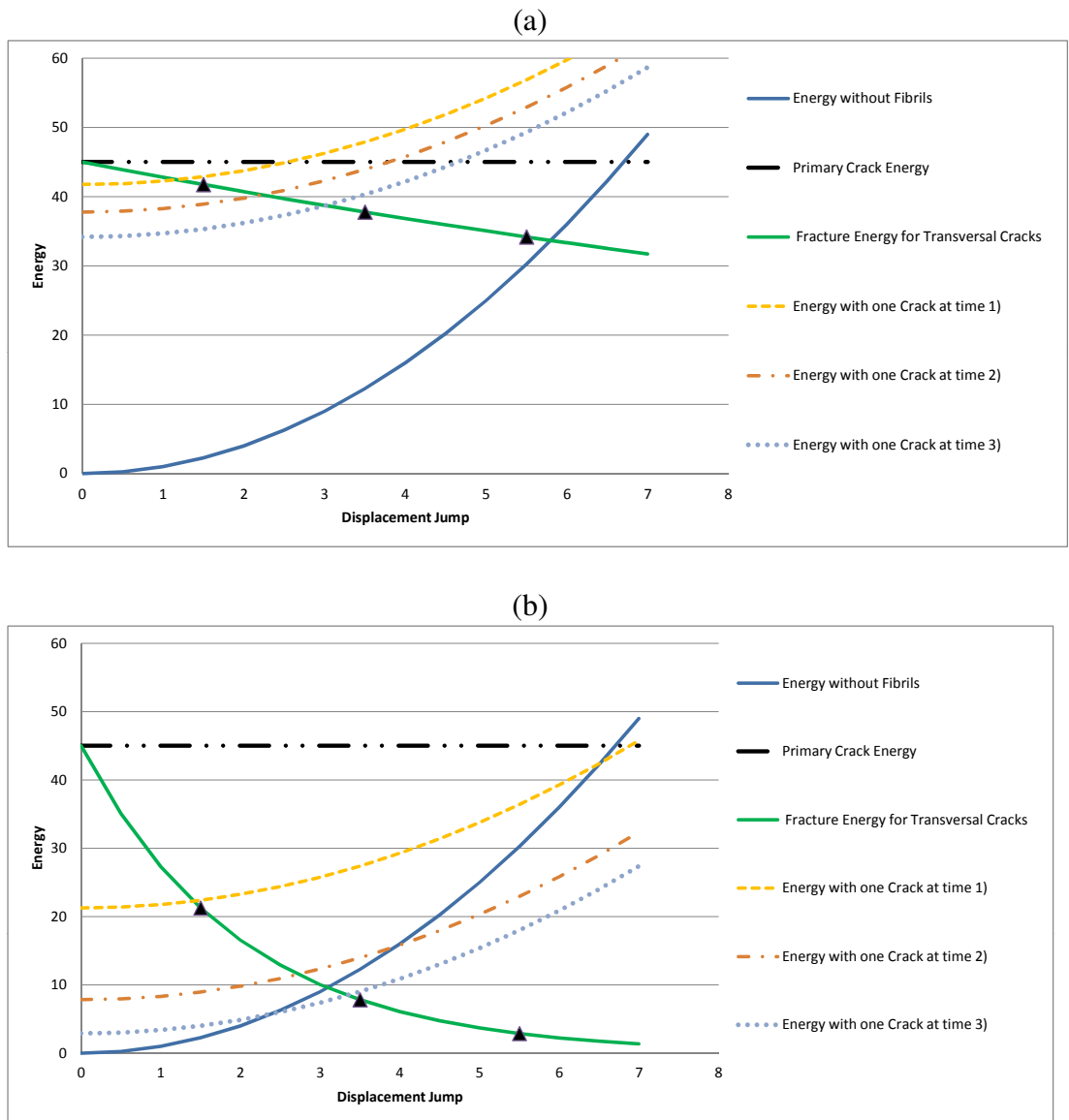
Figure 5.14: Energy for different cracked configurations at different applied displacement rates (essentially a lateral view of Fig.5.12): (a) "fast" displacement jump history: the fibrillated configuration is never energetically favourable. (b) "slow" displacement jump history: the fibrillated configuration becomes energetically favourable shortly after the instant marked by the second marker.
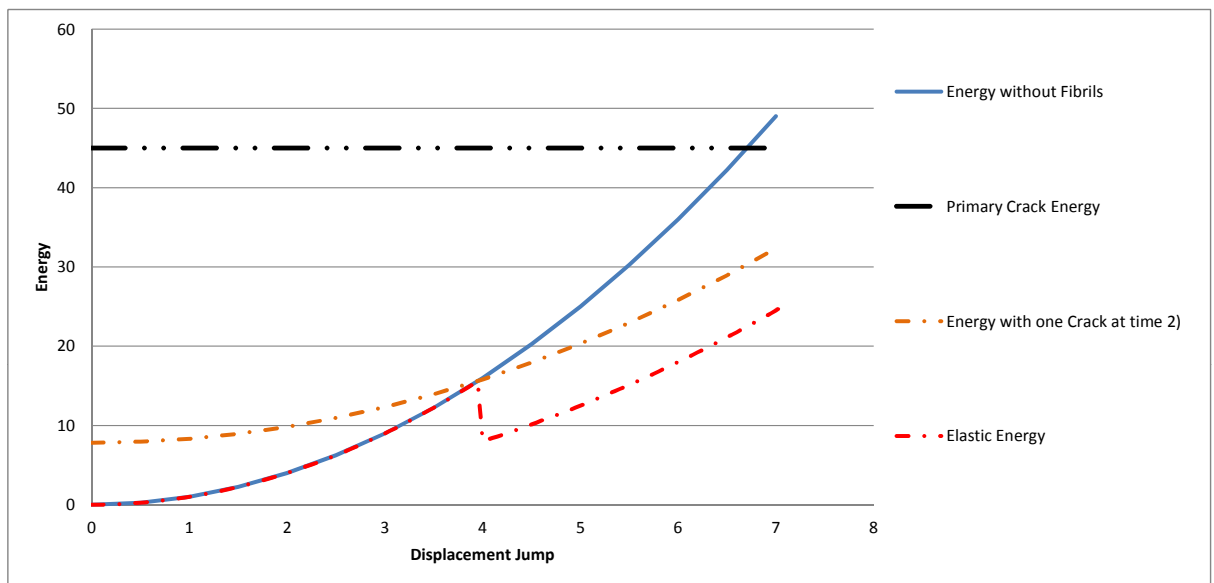
Figure 5.15: Plot of the total (elastic plus surface) energy for the uncracked configuration, a configuration with one single transversal crack and the elastic energy of the solution.

Conclusions

The research work presented in this Thesis generally achieved its objectives as stated in the Introduction. In more detail:

- *to develop a general cohesive-zone model "template" able to reproduce rate-dependence and in general, history dependence, for a vast range of inelastic material behaviours*: this has been been achieved to a good extent in Chapter 3. The key assumption on the existence of an intrinsic fracture energy, on top of which further dissipated energy is accounted for by considering the same dissipative properties pertinent to the continuum, bulk material, has been formalised in the context of thermodynamics with internal variables and shown to be a viable, practical approach in the case of a viscoelastic interface. Further research is though required in practice to assess the ability to deal with material behaviours other than viscoelasticity. Work on an application of the approach proposed in this thesis to the case of a viscoplastic cohesive-zone model in the context of dynamic fracture is currently under preparation.

- *to specialise the cohesive-zone model to the case of an interface made of a thin elastomeric layer*: this has been achieved in Chapters 3 and 4 by successive refinements. In Chapter 3 a coarse viscoelastic description was assumed: it was noted that while the predicted traction-deflection curves showed a satisfactory qualitative behaviour in relation to the empiric data, the rate-dependency was accurately predicted only over a limited range of applied displacement rates. This observation suggested it was necessary to improve the rate-dependency description of the model rather than focus on an accurate elastic description of rubber's behaviour. As a result the choice was made to maintain the rheological structure employed in Chapter 3 unaltered, while improving only on the Newtonian damper's viscous behaviour characterisation. This was achieved in Chapter 4 by

resorting to a fractional calculus formalism. The model so obtained is more effective in faithfully reproducing the materal behaviour over an extended range of applied displacement rates but on the other hand is computationally burdensome in that a significant portion of the previous history has to be stored. A completely positive judgement is though subject to performing additional tests, possibly involving long-term creep conditions as well as variable loading, in order to truly assess the merits of the fractional formulation in a more demanding setting.

- *to design and execute a testing plan suitable for a validation of numerical results*: DCB samples have been designed (as well as the mould needed for their manufacture), built and tested, providing a very useful set of experimental data.

The formulation of Chapter 5 was not planned at the beginning of the programme: it was instead the studying itself that made the problem of somehow understanding the mechanical origins of possible crack instabilities progressively interesting. The formulation introduces rather unusual, yet physically well motivated, ingredients (such as the rate-dependent, "conformational", anisotropic fracture energy) and has a simple yet effective micromechanical foundation allowing it to explain the phenomenon under observation without resorting to additional physical complexity, as done by the models reviewed in Section 5.1. While it is acknowledged that the formulation has at the moment only an academic value, if any, it might still be valuable in that it could provide a paradigm for more realistic and detailed descriptions of the cracking process.

5.5 Outline of future work

First and foremost, the formulation will be enriched to include mode-mixity, which is necessary to approach real-world problems. Such improvement is not foreseen to present, in principle, conceptual difficulties: the adaptation to the scheme presented in [209], physically rather appropriate for an elastomeric interface, seems almost immediate. The experimental determination of the response under combined fracture modes is on the other hand expected to be more challenging. Related to the last comment it is worth mentioning the importance of studying the relationship between interface and bulk properties of a given material, with a view on making the experimental characterisation of the interface properties easier and clearer. Results presented in this thesis are

encouraging in this respect: let us remark that the fractional coefficient $\nu = 0.3$, see Table 4.1, is in the range of the values expected for a cross-linked rubber [38]. Further experimental work is needed though as the vast majority of data available in published literature refers to thermoplastics.

The formulation of Chapter 5 has to be put to the test in a more realistic and challenging setting. At the moment the presented non-local cohesive-zone model seems difficult to implement directly in a standard finite-element algorithm due to its non-locality. The study of a dedicated solution algorithm for the general case could be the subject of future work: on the other hand, the best approach might instead be the formulation of a phenomenological law physically founded on the micromechanical model. In this sense it could be interesting to investigate the possibility to replace the discrete internal variable, detailing the number of transversal cracks, by a continuous *fracture density* variable, as mentioned in a similar context in [199].

The next line of research the author intends to pursue is an investigation on the performance of the cohesive-zone model of Chapter 4 under low-load, cyclic conditions, *i.e.* fatigue. Fatigue has already been modeled using a cohesive-zone model in [120] using a particular definition of surface energy, see equation (2.69), which accounts for the previous loading history. It seems to the author that the cohesive-zone model presented in this thesis could reproduce a qualitatively similar behaviour as it stands, without any further assumption or modification. This future attempt justifies the care that has been put in this thesis to incorporate one of the most faithful class of models of viscoelasticity available, as well as the related increased computational burden. Indeed, if a realistic fatigue prediction is to be attempted it seems necessary to have the most reliable long-term prediction of the material stiffness. This could mitigate the issues highlighted in [135] while attempting to simulate the long-term response by employing an excessively narrow relaxation spectrum. The intriguing (and industrially very desirable) possibility that fatigue behaviour of polymers could be deduced, with an engineering approximation, by their relaxation spectrum might be within reach.

Finally, an idea of a more speculative nature is mentioned as well, which will certainly be investigated in future. It was noted in Section 2.1.3 how the "springpot", governed by the constitutive law $\sigma(t) = c \cdot {_0}D_t{^\nu}\epsilon$ interpolates between a fluid and a hookean solid as the fractional exponent ν is varied between 0 and 1. The choice of the appropriate fractional exponent is performed as part of the material's characterisation

and does not change during the analysis. It seems then to the author that there might be scope to introduce a novel type of fractional differential equation, whereby the order of differentiation is prescribed by a function, and possibly varies in time with the solution itself: in other words, could a sound mathematical meaning be appended to a differential equation of the type

$$\prescript{*}{0}{D}_t^{\zeta(u(t))}u(t) + u(t) = 0 \quad t \geq 0 \quad , \quad u(0^+) = u_0 \tag{5.41}$$

where $\zeta(s)$ is a given function, and under what technical conditions? This approach seems interesting in that one could rather naturally model the deformation of a material undergoing structural changes during its deformation process (for example, viscoelastic creep at low stretch, secondary liquid-type creep at higher stretch). It was noted during the final correction stage that no originality for this idea could though be claimed, as the concept of variable-order fractional differential equations had already been introduced (see for example [210] and references therein).

APPENDIX

ABAQUS^{TM} UMAT subroutines

Exponential Kernel Viscoelastic Model

This computer code is property of Dunlop Oil and Marine, Division ContiTech of Continental AG. Licenses for its use might be granted by Dunlop Oil and Marine. Inquiries concerning license rights should be forwarded to the attention of the Technical Manager, Dunlop Oil and Marine, Moody Lane, Pyewipe, Grimsby, North East Lincolnshire, DN31 2SY, England (website: www.dunlop-oil-marine.co.uk).

```
      SUBROUTINE UMAT
     A(   STRESS     ,STATEV     ,DDSDDE     ,SSE        ,SPD        ,
     B    SCD        ,RPL        ,DDSDDT     ,DRPLDE     ,DRPLDT     ,
     C    STRAN      ,DSTRAN     ,TIME       ,DTIME      ,TEMP       ,
     D    DTEMP      ,PREDEF     ,DPRED      ,CMNAME     ,NDI        ,
     E    NSHR       ,NTENS      ,NSTATV     ,PROPS      ,NPROPS     ,
     F    COORDS     ,DROT       ,PNEWDT     ,CELENT     ,DFCRD0     ,
     G    DFGRD1     ,NOEL       ,NPT        ,LAYER      ,KSPT       ,
     H    KSTEP      ,KINC       )
C
      IMPLICIT DOUBLE PRECISION(A-H,O-Z)
c     INCLUDE 'ABA_PARAM.INC'
C
      CHARACTER*80 CMNAME
      DIMENSION
     A    STRESS(NTENS)      ,STATEV(NSTATV)      ,DDSDDE(NTENS,NTENS),
     B    DDSDDT(NTENS)      ,DRPLDE(NTENS)       ,STRAN(NTENS)       ,
     C    DSTRAN(NTENS)      ,TIME(2)             ,PREDEF(1)          ,
     D    DPRED(1)           ,PROPS(NPROPS)       ,COORDS(3)          ,
```

```fortran
      E    DROT(3,3)          ,DFGRD0(3,3)          ,DFGRD1(3,3)
        LOGICAL
      A    DEBUG
C-----------------------------------------------------------------------
C     Get the update relative dispalcements
      SS=STRAN(1)+DSTRAN(1)
C     Initialise
      DDSDDE(2,2)=0.0D0
      DDSDDE(1,2)=0.0D0
      DDSDDE(2,1)=0.0D0
STRESS(2)=0.0D0
        CALL CZMVEL
      #(   NPROPS        ,PROPS          ,SS            ,DSTRAN(1)       ,
      #    STATEV(1)     ,STATEV(2)      ,STATEV(3)     ,STATEV(4)       ,
      #    STRESS(1)     ,DDSDDE(1,1)    ,DTIME         )
        END




        SUBROUTINE CZMVEL
      #(   NMPRPS        ,DMPRPS         ,SS            ,DS              ,
      #    SMAX          ,HCUR           ,DAM           ,HPREV           ,
      #    SIG           ,TANG           ,DT            )
        IMPLICIT NONE
C-----------------------------------------------------------------------
        INTEGER
      #    NMPRPS
        REAL*8
      #    SS            ,DS             ,SMAX          ,HCUR            ,
      #    DAM           ,HPREV          ,SIG           ,TANG            ,
      #    DT            ,XX             ,DMPRPS(NMPRPS)
C-----------------------------------------------------------------------
        INTEGER
      #    I
        REAL*8
      #    GF            ,SIGMX          ,BETA          ,MU0             ,
      #    TAU           ,SC             ,S0            ,E0              ,
      #    DDAMDS        ,MU1            ,SSPREV        ,DELTAH          ,
      #    DAMNEW        ,KCOMP
C------------------Get input parameters
      GF=DMPRPS(1)
```

126

```fortran
      SIGMX=DMPRPS(2)
      BETA=DMPRPS(3)
      TAU=DMPRPS(4)
      MU0=DMPRPS(5)
      KCOMP=DMPRPS(6)
C------------------Initialise values
SC=2.0D0*GF/SIGMX
      S0=(1.0D0-BETA)*SC
      E0 =(SIGMX / S0)
MU1 = 1-MU0
      SSPREV=SS-DS
      DDAMDS=0.0D0
C------------------Update damage
      SMAX=MAX(SMAX,SS)
      IF(SMAX.LT.0.0D0) THEN
        DAMNEW=DAM
C         Mode-I compression
      ELSEIF(SMAX.LE.S0)THEN
C         Mode-I tension but elastic
        DAMNEW=0.0D0
      ELSEIF(SMAX.GT.SC)THEN
C         Complete damage
        DAMNEW=1.0D0
C         Loading beyond SMAX
      ELSEIF(SS.EQ.SMAX)THEN
        DAMNEW= (1/(1 - (S0 / SC)))*(1 - S0/(SS))
        DDAMDS=(1/(1 - (S0 / SC)))*(S0/(SS*SS))
      ENDIF
      IF(DAMNEW.GT.DAM)THEN
        DAM=DAMNEW
      ENDIF
C-----------RECURSIVE VISCOELASTIC TERM COMPUTATION
      DELTAH = (TAU/DT)*(1-DEXP(-DT/TAU))*(SS-SSPREV)
HCUR =DEXP (-DT/TAU)*HCUR+DELTAH
C------------------Compute stress
      IF(SS.LT.0.0D0)THEN
        SIG=KCOMP*SS
      ELSE
        SIG=(1.0D0-DAM)*(E0*(MU0*SS+MU1*HCUR))
      ENDIF
```

```
C------------------Update tangent
      IF(DAM.EQ.1.0D0)THEN
        TANG=0.0D0
      ELSEIF(SS.GT.0.0D0)THEN
        TANG=(1.0D0-DAM)*E0*MU0+
     #       (1.0D0-DAM)*E0*MU1*(TAU/DT)*(1-DEXP(-DT/TAU))-
     #       DDAMDS*E0*(MU0*SS+MU1*HCUR)
ELSEIF(SS.LT.0.0D0)THEN
  TANG=KCOMP
      ENDIF
C------------------Slightly reduce SMAX to ensure tangent predictor
C                  in the next increment
      IF(SS.EQ.SMAX) THEN
        SMAX=SMAX*(1-1.0D-12)
ENDIF
C
      END
```

Fractional Kernel Viscoelastic Model

```
      SUBROUTINE UMAT
     A(   STRESS     ,STATEV     ,DDSDDE     ,SSE        ,SPD        ,
     B   SCD         ,RPL        ,DDSDDT     ,DRPLDE     ,DRPLDT     ,
     C   STRAN       ,DSTRAN     ,TIME       ,DTIME      ,TEMP       ,
     D   DTEMP       ,PREDEF     ,DPRED      ,CMNAME     ,NDI        ,
     E   NSHR        ,NTENS      ,NSTATV     ,PROPS      ,NPROPS     ,
     F   COORDS      ,DROT       ,PNEWDT     ,CELENT     ,DFCRD0     ,
     G   DFGRD1      ,NOEL       ,NPT        ,LAYER      ,KSPT       ,
```

128

```
      H    KSTEP        ,KINC          )
C
       IMPLICIT DOUBLE PRECISION(A-H,O-Z)
c      INCLUDE 'ABA_PARAM.INC'
C
       CHARACTER*80 CMNAME
       DIMENSION
      A    STRESS(NTENS)      ,STATEV(NSTATV)     ,DDSDDE(NTENS,NTENS),
      B    DDSDDT(NTENS)      ,DRPLDE(NTENS)      ,STRAN(NTENS)       ,
      C    DSTRAN(NTENS)      ,TIME(2)            ,PREDEF(1)          ,
      D    DPRED(1)           ,PROPS(NPROPS)      ,COORDS(3)          ,
      E    DROT(3,3)          ,DFGRD0(3,3)        ,DFGRD1(3,3)
C    My variables
       LOGICAL
      A    DEBUG
C-----------------------------------------------------------------
C       Common block for fractional algorithm
       INTEGER   NXMINC   ,NHISFR
       PARAMETER (NXMINC =100)
       PARAMETER (NHISFR =NXMINC)
       REAL*8 TTT,DTF,AAG,NU
       COMMON / FRCALG / TTT(NXMINC),DTF,AAG(NHISFR) ! Real variable
C-----------------------------------------------------------------
C    Get the updated relative dispalcements
       SS=STRAN(1)+DSTRAN(1)
C    Initialise
       DDSDDE(2,2)=0.0D0
       DDSDDE(1,2)=0.0D0
       DDSDDE(2,1)=0.0D0
STRESS(2)=0.0D0
DTALGN=DTIME
       CALL INTFRC
      #(   NPROPS          ,PROPS          ,DTALGN          ,SS              ,
      #    STATEV(1)       ,STATEV(2)      ,STATEV(3)       ,STATEV(3+NHISFR),
      #    STRESS(1)       ,DDSDDE(1,1)    ,DTIME           ,NPT             ,
      #    KINC            ,DSTRAN(1)      ,NOEL            )
       END


       SUBROUTINE INTFRC
```

129

```fortran
#(    NMPRPS          ,DMPRPS          ,DTALGN          ,SS             ,
#     SMAX            ,DAM             ,HSPAST          ,SGPAST         ,
#     SIG             ,TANG            ,DT              ,NG             ,
#     INC             ,DS              ,NEL             )
      IMPLICIT NONE
C------------------------------------------------------------------------
C       Common block for fractional algorithm
      INTEGER   NXMINC   ,NHISFR
      PARAMETER (NXMINC =100)
      PARAMETER (NHISFR =NXMINC)
      REAL*8 TTT,DTF,AAG,NU
      COMMON / FRCALG / TTT(NXMINC),DTF,AAG(NHISFR) ! Real variable
C------------------------------------------------------------------------
      INTEGER
#     NMPRPS          ,NG              ,INC             ,NEL
      REAL*8
#     DMPRPS(NMPRPS),DTALGN            ,SS              ,SMAX           ,
#     DAM             ,HSPAST(NHISFR),SGPAST(NHISFR),SIG              ,
#     TANG            ,DT              ,DS
      REAL*8
#    HSPALG(NHISFR)        ,SGALG(NHISFR)          ,ETA              ,
#    GF                    ,SIGMX                  ,BETA             ,
#    KT                    ,E1                     ,E2               ,
#    SUMSS                 ,SUMSIG                 ,NXMINCR
      REAL*8
#    TJ     ,TJM    ,TJP    ,SJM    ,SJP    ,SIGJM ,SIGJP ,TINCM
      INTEGER
#    J      ,M      ,INTCOUN          ,I      ,JR
REAL*8
#    SC        ,S0        ,DDAMDS          ,DAMNEW           ,DBG     ,
#    LAMBDA1   ,DELTAHPREV    ,DELTAH               ,MU0     ,
#    MU1       ,HCUR      ,GC              ,Y                ,DDHDS   ,
#    TEST1     ,TEST2     ,KCOMP           ,DAMNEW2          ,DDAMDS2,
#    SIGSLS    ,SSM             ,SIGM                 ,LAMBDA ,GAMMA   ,
#    FACT
C------------------------------------------------------------------------
      GF=DMPRPS(1)
      SIGMX=DMPRPS(2)
      BETA=DMPRPS(3)
      LAMBDA=DMPRPS(4)
```

```
      MU0=DMPRPS(5)
      KCOMP=DMPRPS(6)
      NU=DMPRPS(7)
C     Grunwald coefficients
      IF(INC.EQ.1.AND.NG.EQ.1)THEN
        AAG(1) = 1.0D0
        DO J=1,NXMINC-1
       JR=DBLE(J)
          AAG(J+1)=(JR-1.0D0-NU)/JR*AAG(J)
        END DO
      ENDIF
C-------------------------------------------------------------------
C     Store current relative displacement and traction values in the past history
      HSPAST(INC)=SS
C-----Determine other parameters
SC=2.0D0*GF/SIGMX
      S0=(1.0D0-BETA)*SC
      E1=SIGMX/S0
      E2=(1.0D0-MU0)/MU0*E1
GAMMA=LAMBDA*(E1+E2)
      FACT=(1.0D0/(1.0D0+LAMBDA*DTALGN**(-NU)))
KT=FACT*(E1+GAMMA*DTALGN**(-NU))
C     Initialise
      DDAMDS=0.0D0
C-----Interpolate Displacements and stresses
HSPALG(1)=HSPAST(INC)
      DO J=1,NXMINC
C     Get time where SSj is to be computed
         TJ=TTT(INC)-J*DTALGN
         IF(TJ.LT.0.0D0)THEN
           HSPALG(J)=0.0D0
           SGALG(J)=0.0D0
         ENDIF
C     Determine increment times before and after, TJM and TJP,
C     and related relative displacement values SJM and SJP
         DO I=INC,1,-1
           IF(I.GT.1)THEN
             TINCM=TTT(I-1)
           ELSE
             TINCM=0.0D0
```

131

```
              ENDIF
C        Inpterpolate
              IF(TJ.LT.TTT(I).AND.TJ.GE.TINCM)THEN
                 TJM=TINCM
                 TJP=TTT(I)
C        Determine adjacent previous values of stress and rel.dsp
                 IF(I.GT.1)THEN
                    SJM=HSPAST(I-1)
                    SIGJM=SGPAST(I-1)
                 ELSE
                    SJM=0.0D0
                    SIGJM=0.0D0
                 ENDIF
C        Determine adjacent next values of rel.dsp
                 SJP=HSPAST(I)
C        Determine/estimate adjacent next values of strain
                 IF(I.LT.INC)THEN
                    SIGJP=SGPAST(I)
                 ELSE
C        Estimate
C                    SIGJP=SIGJM+KT2*DS
                    SIGJP=SIGJM+KT*DS
                 ENDIF
                 HSPALG(J)=SJM+(SJP-SJM)/(TJP-TJM)*(TJ-TJM)
                 SGALG(J)=SIGJM+(SIGJP-SIGJM)/(TJP-TJM)*(TJ-TJM)
              ENDIF
           END DO
        END DO
C----------------------------------------------------------------------
C        Compute DAMAGE
        SMAX=MAX(SMAX,SS)
        IF(SS.LT.0.0D0) THEN
         DAMNEW=DAM
C          Mode-I compression
        ELSEIF(SMAX.LE.S0)THEN
C           Mode-I tension but elastic
          DAMNEW=0.0D0
        ELSEIF(SMAX.GT.SC)THEN
C           Complete damage
          DAMNEW=1.0D0
```

132

```
C        Loading beyond SMAX
      ELSEIF(SS.EQ.SMAX)THEN
        DAMNEW=(1.0D0/(1.0D0-(S0/SC)))*(1.0D0-S0/(SS))
        DDAMDS=(1.0D0/(1.0D0-(S0/SC)))*(S0/(SS*SS))
      ENDIF
C------------------Update damage
      IF(DAMNEW.GT.DAM)THEN
        DAM=DAMNEW
      ENDIF
C----------------------------------------------------------------------
C     Compute sums and SLS stress
      SUMSS = 0.0D0
      SUMSIG = 0.0D0
      DO J=1,NXMINC-1
        SUMSS=SUMSS +AAG(J+1)*HSPALG(J)
      END DO
      DO J=1,NXMINC-1
        SUMSIG=SUMSIG +AAG(J+1)*SGALG(J)
      END DO
SIGSLS=KT*SS+FACT*DTALGN**(-NU)*(GAMMA*SUMSS-LAMBDA*SUMSIG)
C-----Compute stress
      IF(SS.LT.0.0D0)THEN
  SIG=KCOMP*SS
      ELSE
C       Calculate stress
        SIG =(1.0D0-DAM)*SIGSLS
      ENDIF
C-----Slightly reduce SMAX to ensure tangent predictor
C                 in the next increment
      IF(SS.EQ.SMAX) THEN
  SMAX=SMAX*(1-1.0D-12)
ENDIF
C------------------Update tangent
      IF(DAM.EQ.1.0D0)THEN
        TANG=0.0D0
      ELSEIF(SS.GT.0.0D0)THEN
        TANG = (1.0D0-DAM)*KT-DDAMDS*SIGSLS
ELSEIF(SS.LT.0.0D0)THEN
  TANG=KCOMP
      ENDIF
```

133

```
C------Store stress value
SGPAST(INC)=SIGSLS
      END
```

The non-local CZM as a variational problem

Firstly the space PC of piecewise constant functions is introduced. The following definition is taken from [82].

Definition 1 *A function* $u : (a,b) \rightarrow \Re$ *is* piecewise constant on *(a,b) if there exist points $a = x_0 < x_1 < x_n < x_{n+1} = b$ such that u(x) is constant almost everywhere on (x_{i-1}, x_i) for all i = 1,..., n+1. The subspace of L^∞ of all such functions u is denoted by $PC(a, b)$. If $u \in PC(a, b)$ then $J(u)$ is the (minimal) set $\{x_1, ..., x_n\} \subset$ (a,b) such that the definition holds. Elements of $J(u)$ are denoted $J(u)_k$, $k = 1, ..., n$. The notation $\sharp J(u)$ is used to indicate the cardinality of $J(u)$.*

For completeness it is remarked that at all points $x \in (a, b)$ the values $u(t+)$ and $u(t-)$ can be defined as the values taken a.e. by u on $(x, x+\epsilon)$ and $(x, x-\epsilon)$ respectively for ϵ small enough.

A subset of $PC(a, b)$, whose elements will be indicated as "square piecewise constant" is introduced next. This set will be named $SPC(a, b)$ and is defined as follows (see Fig.5.16)

Definition 2 *A function* $u : (a, b) \rightarrow \Re$ *belongs to* $SPC(a, b)$ *if* $u \in PC(a, b)$ *and* $\forall x \in (x_{i-1}, x_i)$ *u(x) = x_i-x_{i-1} a.e.*

It can be confirmed that there is a one-to-one correspondence between interval partitions $\mathcal{P}$ and SPC functions: given a partition the corresponding SPC function is built by assigning to each interval a value equal to the interval width. The opposite procedure links each partition to one SPC function only.

With these definitions in mind, the energy $\mathcal{W}$ defined as a function of a partition $\mathcal{P}$, see equation (5.21), can be expressed as a functional $\mathcal{F}$ defined on functions $u \in PC(0, \hat{l})$
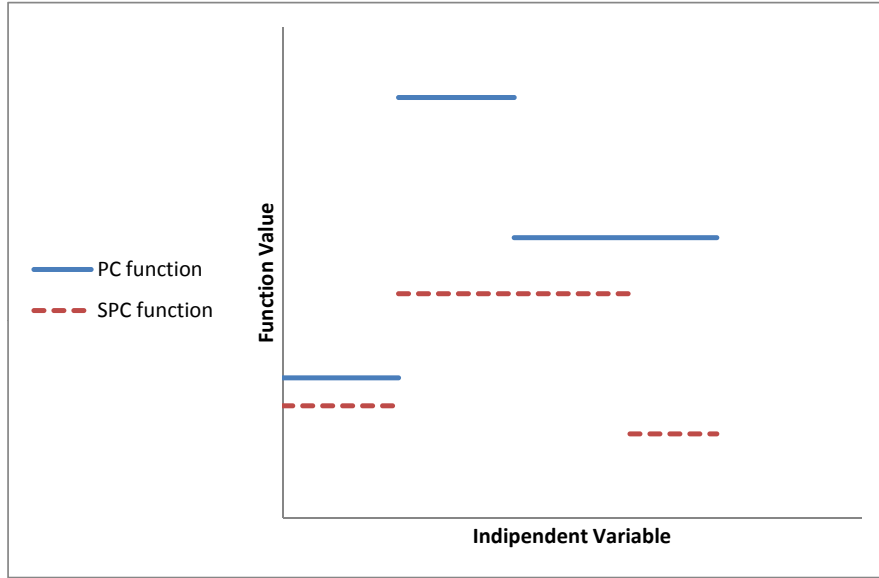
Figure 5.16: Graphs of a PC and a SPC function: in addition to constancy over connected open intervals, the SPC function is also characterised by having the same value over an open interval as the width of the interval itself.

$$\mathcal{F}(u) = \begin{cases} \int_\Gamma \vartheta(\delta)\varphi\left(u(x)\right)\mathrm{d}x + \sum_{x\in J(u)}\gamma_1(x) & \text{if} \quad u \in SPC \\ \\ \infty & \text{if} \quad u \notin SPC \end{cases} \tag{5.42}$$

where for notational simplicity the notation

$$\varphi\left(u(x)\right) = \tilde{\varphi}\left(\frac{u(x)}{\hat{l}}\right) \qquad \gamma_1 = \tilde{\gamma}_1 h \tag{5.43}$$

is used.

It might be worth remarking that $SPC(a, b)$ is not a subspace of PC under the common multiplication-by-scalar and addition operations. It can though be given a metric space structure. Among various possible choices the L^1 distance will be employed, *i.e.*

$$d(u, v) = \int_a^b |u(x) - v(x)|\mathrm{d}x \tag{5.44}$$

This definition of distance will be referred to later when discussing local minima. The chosen definition does not necessarily attribute a distance $d > \bar{d} > 0$, $\bar{d} \in \Re^{++}$

to functions such that $\sharp J(u) \neq \sharp J(v)$, which is physically interesting as it means the nucleation of a new crack does not necessarily imply a finite distance from the previous configuration.

We will now address the issue of existence of minimizers for the functional $\mathcal{F}$.

The Direct Method of the Calculus of Variations, [198, 211], is to be employed. The initial step consists usually in proving the functional is bounded from below, *i.e.* $\inf\{\mathcal{F}(y) : y \in X\}$ is finite: this guarantess the existence of an infimum. The second step is to prove that from one sequence u_j for which $\lim_{j\to\infty} \mathcal{F}(y_j) = \inf\{\mathcal{F}(y) : y \in X\}$, X being the class of admissible competitors of interest, a converging subsequence can be extracted (the notion of convergence to be employed being problem-specific). As third an last step, if it can be shown that the sequence converges to $\bar{u} \in X$ such that $\mathcal{F}(\bar{u}) = \inf\{\mathcal{F}(y); y \in X\}$, then the existence of a minimizer is proven.

The first step is in the present case straightforward to complete, as will be shown shortly. The second step is in general often achieved by requiring the stronger property that a converging subsequence can be extracted from any arbitrary minimizing sequence, namely requiring that any arbitrary minimizing sequence lies in a compact subset of the class of admissible competitors (PC in the present case).

The third step requested by the described approach could be verified by ensuring that for the candidate minimizing sequence u_j tending to u the following lower semicontinuity requirement holds

$$\mathcal{F}(u) \leq \liminf_{j\to\infty} \mathcal{F}(u_j) \tag{5.45}$$

A stronger requirement can and will be considered in the present case, namely the fact that the lower semicontinuity inequality holds for all sequences.

The whole procedure results in the following set of inequalities

$$\inf\{\mathcal{F}(u) : u \in X\} \leq \mathcal{F}(\bar{u}) \leq \liminf_{j\to\infty} \mathcal{F}(u_j) \leq \inf\{\mathcal{F}(y) : y \in X\} \tag{5.46}$$

from which the conclusion $\mathcal{F}(\bar{u}) = \inf\{\mathcal{F}(y) : y \in X\}$ follows.

Let us then follow the described procedure by noting that in the present case $\inf\{\mathcal{F}(u) : u \in PC(0, \hat{l})\}$ exists because the codomain of the functional $\mathcal{F}$ is bounded below by 0. The compactness of $SPC(a, b)$, in relation to the second step, is addressed next. It is noted that in the present case if $u \in \mathcal{C}_k$ then $u \in SPC(0, \hat{l})$: this stems from the definition of the functional $\mathcal{F}$ which penalises competitors not belonging to

SPC . Then, following the described approach, it is sufficient to prove that the set $SPC(0, \hat{l})$ is compact. Actually, for the present purposes it suffices to prove that the set $\mathcal{C}_\sharp = \{u \in SPC(0, \hat{l}) : \sharp J(u) < +\infty\}$ is compact, again as a result of the fact competitors that do not belong to SPC are penalised by the functional definition.

Proposition 1 *Let (u_j) be a sequence in $SPC(a, b)$ such that $\sup_j \sharp(J(u_j)) < +\infty$. Then u_j converges to $u \in SPC(a, b)$*

Proof: Let us define $\bar{J} = \max_j \{J(u_j)\}$. The set of $SPC(a, b)$ functions with n discontinuity points is isomorphic to the set of partitions $\{u\} = \{x_0, x_1, ...x_n, x_{n+1}\}$. Also let us note that any $SPC(a, b)$ function with n discontinuity points coincides pointwise with an $SPC(a, b)$ function with $n+1$ discontinuity points, $u = \{x_0, x_1, ...x_n, x_{n+1}, x_{n+2}\}$, $x_k = x_{k+1}$ for a certain k. Then, any partition u can be considered as a SPC function with $\bar{S}$ points of discontinuity. Let us consider the sequence of partitions $\{u_j\}$, from which the sequence $\{u_{k_j}\}$, obtained by selecting the k-th discontinuity point of u_j. Let us then consider $\{u_{1_j}\}$. This sequence is bounded, hence a convergent subsequence could be extracted, converging to $\bar{x}_1$. The sequence made of the corresponding elements u_j is denoted $\{u_{j_1}\}$. Iterating the same argument, *i.e* considering the sequence obtained by selecting the second element from the sequence $\{u_{j_1}\}$, this is again bounded and a convergent subsequence could be extracted from it, determining a corresponding sequence $\{u_{j_2}\}$. The procedure can be re-iterated as many times as the number of discontinuity points, yielding a chain of subsequences

$$\{u_{j_1}\} \supseteq \{u_{j_2}\} \supseteq \ldots \tag{5.47}$$

The last subsequence is then convergent by construction to $u = \{x_0, x_1, ..., x_{\bar{S}-1}, t_{\bar{S}}\}$, from which $u \in SPC(a, b)$ follows. ∎

Remark 5.5.1 The above proposition is an immediate consequence of Helly's Theorem [179], as any $SPC(a, b)$ function with a finite number of discontinuities belongs to the space $BV(a, b)$ of functions of bounded variation on (a, b). An elementary proof is preferred only for clarity. ∎

In reference to the third step, the lower semicontinuity of the functional will be proved by considering the two terms in $\mathcal{F}$, for $u \in SPC(0, \hat{l})$, separately. The re-

sult will follow by noting that a functional defined as a sum of lower semicontinuous functionals is lower semicontinuous.

Let us recall that by Fatou's lemma [179] any non-negative and measurable function f defined pointwise (the Lemma still holds considering convergence in measure) using a sequence f_n as

$$f(x) = \liminf_{n \to \infty} f_n(x) \tag{5.48}$$

satisfies

$$\liminf_{n \to \infty} \int_a^b f_n \mathrm{d}x \geq \int_a^b f \mathrm{d}x \tag{5.49}$$

As a result the first term in $\mathcal{F}$ for $u \in SPC(0, \hat{l})$, namely $\int_\Gamma \vartheta(\delta) \varphi\left(u(x)\right) \mathrm{d}x$ is lower semicontinuous (non-negativeness and measurability being guaranteed by the conditions imposed on φ).

The lower semicontinuity of the second term in equation 5.42, *i.e.* $\sum_{x \in J(u)} \gamma_1$, is addressed in the next proposition. Use is made of Theorem 5.8 from [82], whose statement is reported below for the reader's convenience.

Proposition 2 *Let $F : PC(a, b) \to [0, +\infty]$ be given by $F(u) = \sum_{x \in S(u)} \theta(u(t-), u(t+))$, where $\theta : \Re^2 \to [0, +\infty]$. The the following conditions are equivalent:*
(i) F is lower semicontinuous on $PC(a, b)$ with respect to a.e. convergence (also convergence in measure and $L^1(a, b)$-convergence)
(ii) θ is lower semicontinuous and sub-additive

The lower semicontinuity of the term $\sum_{x \in J(u)} \gamma_1$ is a corollary of this Theorem, specialising θ to the constant function of value γ_1 and noting that any constant function is lower semicontinuous and sub-additive (see equation (2.92) for the definition of sub-additivity).

The whole argument proves the existence of minimizers for the functional $\mathcal{F}$.

Proposition 3 *Given a function $\varphi : (0, \infty) \to (\mathring{\varphi}, 1)$, $\mathring{\varphi} \in \Re^{++}$, satisfying conditions (5.16, 5.17, 5.18, 5.19), a continuous and convex function $\vartheta : \Re^+ \to \Re^+$ such that $\vartheta(0) = 0$, a constant $\gamma_1 \in \Re^{++}$, there exists at least one function $u \in SPC \subset PC$ solution to the minimisation problem*

138

$$\min \begin{cases} \int_\Gamma \vartheta(\delta)\varphi\left(u(x)\right) \mathrm{d}x + \sum_{x \in J(u)} \gamma_1(x) & \text{if} \quad u \in SPC \\ \\ \infty & \text{if} \quad u \notin SPC \end{cases}$$

Then following two propositions characterise local minima and have been mentioned in Section 5.3.

Proposition 4 *Let us assume $\varphi \in C^2(\Re)$ and is convex. Then any equidistant partition $\mathcal{P}_N = \{0, \frac{1}{N+1}\hat{l}, \frac{2}{N+1}\hat{l}, ..., \frac{n}{N+1}\hat{l}, \frac{n+1}{N+1}\hat{l}\}$, $\forall N$, is a local minimizer of $\int_\Omega \vartheta(\delta)\varphi(u)\mathrm{d}x + N\gamma_1$ with respect to the L^1 distance. Conversely, any local minimizer is an equidistant partition $\mathcal{P}_N = \{0, \frac{1}{N+1}\hat{l}, \frac{2}{N+1}\hat{l}, ..., \frac{n}{N+1}\hat{l}, \frac{n+1}{N+1}\hat{l}\}$*

Proof: The one-to-one correspondence from $u \in SPC$ and partitions $\mathcal{P}$ will be exploited for notational simplicity. A variation $\mathcal{P}_N^\epsilon$ of $\mathcal{P}_N$ can be expressed in general as

$$\mathcal{P}_N^\epsilon = \{0, \left(\frac{1}{N+1} + \epsilon_1\right)\hat{l}, \left(\frac{2}{N+1} + \epsilon_2\right)\hat{l}, ..., \left(\frac{N}{N+1} + \epsilon_n\right)\hat{l}, \left(\frac{N+1}{N+1} + \epsilon_{n+1}\right)\hat{l}\}$$
(5.50)

subject to

$$\sum_n \epsilon_n = 0, \qquad -\frac{1}{N+1} < \epsilon_i < \frac{N}{N+1} \tag{5.51}$$

It is sufficient though to consider the case

$$\mathcal{P}_N^\epsilon = \{0, \left(\frac{1}{N+1} + \epsilon\right)\hat{l}, \left(\frac{2}{N+1} - \epsilon\right)\hat{l}, ..., \left(\frac{N}{N+1}\right)\hat{l}, \left(\frac{N+1}{N+1}\right)\hat{l}\} \tag{5.52}$$

as the line of reasoning can be iterated for any variation by considering suitably defined intervals separately and successively their union. The proof of the if-part of the proposition then follows by observing that (after introducing the notation $\Theta(x) = \varphi(\frac{1}{N+1} + x)(\frac{1}{N+1} + x)$

$\mathcal{F}(P_N^\epsilon) = \vartheta(\delta)(N-2)\varphi(\frac{1}{N+1})(\frac{1}{N+1})\hat{l} + \vartheta(\delta)\varphi(\frac{1}{N+1} + \epsilon)(\frac{1}{N+1} + \epsilon)\hat{l} + \vartheta(\delta)\varphi(\frac{1}{N+1} - \epsilon)\frac{1}{N+1} - \epsilon)\hat{l} + N\gamma_1 =$
$= \vartheta(\delta)\hat{l}[(N-2)\Theta(0) + \Theta(\epsilon) + \Theta(-\epsilon)] + N\gamma_1 \geq \vartheta(\delta)\hat{l}[(N-2)\Theta(0) + 2\Theta(0) + 2\Theta''(\epsilon)\epsilon^2] + N\gamma_1 \geq \vartheta(\delta)N\Theta(0) + N\gamma_1 = \mathcal{F}(P_N)$

To prove the only-if-part of the proposition it will be shown that if a partition is not equidistant then it is not a local minimizer. A partition $\mathcal{P}_{ineq} = \{0, x_1, x_2, x_3, ...x_n\}$ is considered for which

$$\exists i \in \{2, 3, ..., n\} : x_i - x_{i-1} \neq x_{i-1} - x_{i-2} \tag{5.53}$$

Let us select one i for which the above inequality holds. The proof follows by considering the convexity of the function U over the interval (x_{i-2}, x_i). ■

Proposition 5 *In a "short" interface, $\hat{l} < \tilde{z}$, the uncracked configuration can only evolve to a single-cracked configuration.*

Proof: Let us determine the displacements δ at which the energy of a configuration with j cracks equals the energy of a configuration with $j + 1$ cracks, for $j = 0, 1, 2$. Such displacements, which are denoted δ_0 and δ_1 are roots of the following equations

$$\vartheta(\delta)[\varphi(1) - \varphi(\tfrac{1}{2})] = \gamma_1 \qquad \vartheta(\delta)[\varphi(\tfrac{1}{2}) - \varphi(\tfrac{1}{3})] = 2\gamma_1 \tag{5.54}$$

which yield

$$\vartheta(\delta_k) = \frac{k\gamma_1}{\varphi(\tfrac{1}{k}) - \varphi(\tfrac{1}{k+1})} \qquad k = 1, 2 \tag{5.55}$$

ϑ is monotonic and can be inverted. As a result of the convexity (following from the restriction to a "short" interface) of φ, $\varphi(\tfrac{1}{N}) - \varphi(\tfrac{1}{N+1}) > \varphi(\tfrac{1}{N+1}) - \varphi(\tfrac{1}{N+2})$ for any N. Then, $\delta_1 > \delta_0$ which concludes the proof. ■

Papers published or in preparation

Published journal papers

- M. Musto and G. Alfano, A novel rate-dependent cohesive-zone model combining damage and visco-elasticity, *Computers & Structures* 118 (2013), 126-133.

Journal papers in preparation

- M. Musto and G. Alfano, A fractional calculus based rate-dependent cohesive-zone model, to be submitted to *International Journal for Numerical Methods in Engineering*.

- M. Musto and G. Alfano, A non-local cohesive-zone model yielding a surface energy non-convex *w.r.t.* crack speed, in preparation.

Conference papers

- M. Musto and G. Alfano, A damage-mechanis-based rate-dependent cohesive-zone-model, presented by the first author at the 19th UK Conference of the Association of Computational Mechanics, 5-6 April 2010, Herriott-Watt University, Edinburgh.

- M. Musto and G. Alfano, A novel viscoelastic cohesive-zone-model: formulation, validation and enrichment through process-zone micromechanics, presented by the first author at the 8th European Solid Mechanics Conference, 9-13 July 2012.

Bibliography

[1] I. Muller and P. Strehlow. *Rubber and Rubber Baloons: Paradigms of Thermodynamics*. Springer, I edition, 2004.

[2] G.J. Lake and A.G. Thomas. The strength of highly elastic materials. *Proceedings of the Royal Society London. Series A*, 300:108–119, 1967.

[3] B.N.J. Persson and E.A. Brener. Crack propagation in viscoelastic solids. *Physical Review E*, 71(3), 2006.

[4] S. Keten, Z. Xu, B. Ihle, and M.J. Buehler. Nanoconfinement controls stiffness, strength and mechanical toughness of β-sheet crystals in silk. *Nature Materials*, 9:359–367, 2010.

[5] P.-G. de Gennes and K. Okumura. On the toughness of biocomposites. *Comptes Rendus Académie des Sciences, Paris*, t.1, Série IV:257–261, 2000.

[6] E. Bouchbinder and E.A. Brener. Viscoelastic fracture of biological composites. *Journal of the Mechanics and Physics of Solids*, 59:2279–2293, 2011.

[7] A.A. Griffith. The phenomena of rupture and flow in solids. *Phil. Trans. Roy. Soc.*, A221:163–198, 1920.

[8] G.I. Barenblatt. The mathematical theory of equilibrium cracks in brittle fracture. *Advances in Applied Mechanics*, 7:55–129, 1962.

[9] R.W. Ogden. *Non-Linear Elastic Deformations*. Dover Publications, 1997.

[10] C. Truesdell and W. Noll. The non-linear field theories of mechanics. In S. Flugge, editor, *Handbuch der Physik. Vol III/3*, Berlin, 1965. Springer.

[11] M. Fabrizio and A. Morro. *Mathematical Problems in Linear Viscoelasticity*. SIAM, 1987.

[12] G. Fichera. Avere una memoria tenace crea gravi problemi. *Archive for Rational Mechanics and Analysis*, 70:101–112, 1979.

[13] M.E. Gurtin and E. Sternberg. On the linear theory of viscoelasticity. *Archive for Rational Mechanics and Analysis*, 11:291–356, 1962.

[14] R. M. Christensen. *Theory of Viscoelasticity*. Courier Dover Publications, 1982.

[15] B.D. Coleman. Thermodynamics of materials with memory. *Archive for Rational Mechanics and Analysis*, 17:1–46, 1964.

[16] L. Boltzmann. Zur theorie der elastichen nachwirkung. *Sitzber. Kaiserl. Akad. Wiss. Wien, Math-Naturw.*, 70:275–300, 1874.

[17] A.N. Beris and B.J. Edwards. On the admissibility criteria for linear viscoelastic kernels. *Rheologica Acta*, 32:505–510, 1993.

[18] R.S.J. Akyildiz and K. Walters. On the spring-dashpot representation of linear viscoelastic behaviour. *Rheologica Acta*, 29:482–484, 1990.

[19] S. Hazanov. Back to the thermodynamic admissibility of creep-relaxation functions. *Rheologica Acta*, 33:468–472, 1994.

[20] S. Hazanov. New class of creep-relaxation functions. *International Journal of Solids and Structures*, 32:165–172, 1993.

[21] W.A. Day. *The thermodynamics of simple materials with fading memory*. Springer-Verlag, 1972.

[22] R.J. Kinloch, A.J.and Young. *Fracture Behaviours of Polymers*. Elsevier Applied Science, Barking, England, 1999.

[23] B.D. Coleman and W. Noll. An approximation theorem for functionals, with application in continuum mechanics. *Archive for Rational Mechanics and Analysis*, 6:355–370, 1960.

[24] G. Del Piero and L. Deseri. On the concepts of state and free energy in linear viscoelasticity. *Archive for Rational Mechanics and Analysis*, 138:1–35, 1997.

[25] M.E. Gurtin and I. Herrera. On dissipation inequalities and linear viscoelasticity. *Quarterly of Applied Mathematics*, 23:235–245, 1965.

[26] S. Breuer and E.T. Onat. On uniqueness in linear viscoelasticity. *Quarterly of Applied Mathematics*, 19:355–359, 1962.

[27] D. Graffi. *The thermodynamics of materials with memory*. ed. Liguori, Naples, 1979.

[28] D. Graffi and M. Fabrizio. Sulla nozione di stato per materiali viscoelastici di tipo "rate". *Atti Accad. Naz. Lincei Rend. C1 Sci. Fi. Mat. Natur.*, 8:201–208, 1989.

[29] G.W. Leibniz. *Mathematische Schiften*. Georg Olms Verlagsbuchhandlung, Hildesheim, 1962.

[30] I. N. Rabotnov. *Theory of Viscoelasticity*. MIR, 1980.

[31] F. Mainardi. *Fractional Calculus and Waves in Linear Viscoelasticity*. Imperial College Press, 2010.

[32] N. Heysmans and I. Podlubny. Physical interpretation of initial conditions for fractional differential equations with Riemann-Liouville fractional derivative. *Rheologica Acta*, 45:765–772, 2006.

[33] I. Podlubny. *Fractional Differential Equations*. Academic Press, 1999.

[34] I. Podlubny. Geometric and physical interpretation of fractional integration and fractional differentiation. *Frac.Calc.Appl.Anal.*, 5:367–386, 2002.

[35] P.G. Nutting. A new general law of deformation. *J. Frankline Inst.*, 191:679–685, 1921.

[36] G.W. Scott Blair. The role of psychophysics in rheology. *Journal of Colloid Sciences*, 2:21–32, 1947.

[37] A. Jaishankar and G.H. McKinley. Power-law rheology in the bulk and at the interface: quasi-properties and fractional constituitive equations. *Proceedings of the Royal Society London. Series A*, 469:20120284, 2012.

[38] A.D. Drozdov. Fractional differential models in finite viscoelasticity. *Acta Mechanica*, 124:155–180, 1997.

[39] Hannah Rebecca Whittle Gruffudd. Relaxation spectrum recovery using fourier transforms. *PhD Thesis, Pryfisgol Aberystwyth University*, 2012.

[40] G. Bellettini, M. Novaga, and E. Paolini. Global solutions to the gradient flow equation of a nonconvex functional. *SIAM Journal of Mathematical Analysis*, 37:1657–1687, 2006.

[41] Metzler R. Blumen A. Schiessel, H. and T.F. Nonnenmacher. Generalized viscoelastic models: their fractional equations with solutions. *J.Phys.A: Math. Gen.*, 28:6567–6584, 1995.

[42] R.L. Bagley and J. Torvik. A theoretical basis for the application of fractional calculus to viscoelasticity. *Rheologica Acta*, 27:201–210, 1983.

[43] P.E. Rouse. A theory of the linear viscoelastic properties of diluite solutions of colling polymers. *Journal of Chemical Physics*, 21, 1953.

[44] J.-C. Bauwens. A deformation model of polycarbonate extended to the loss curve in the α transition range. *Plastics, rubber and composites processing and applications*, 18:149–153, 1992.

[45] A. Lion. On the thermodynamics of fractional damping elements. *Continuum Mechanics and Thermodynamics*, 9:83 – 96, 1999.

[46] H. Schiessel and A. Blumen. Hyerarchical analogues to fractional relaxation equations. *Journal of Physics A: Math. Gen*, 26:5057 – 5069, 1993.

[47] N. Heysmans and J.-C. Bauwens. Fractal rheological models and fractional differential equations for viscoelastic behaviour. *Rheologica Acta*, 33:210–219, 1994.

[48] S. Sakakibara. Continued fractions and fractional derivative viscoelasticity. *Departmental Bullettin Paper, Tokyo Denki University*, 1381:21–41, 2004.

[49] J.L. Le, Z.P. Bažant, and M.Z. Bazant. Unified nano-mechanics based probabilistic theory of quasibrittle and brittle structures: I. strength, static crack growthm lifetime and scaling. *Statistical Science*, 10:354–363, 1995.

[50] T.P. Hill. A statistical derivation of the significant-digit law. *Statistical Science*, 10:354–363, 1995.

[51] A. Lesne and M. Laguës. *Scale Invariance:From Phase Transitions to Turbulence*. Springer, 2012.

[52] P. Bak, C. Tang, and K. Wiesenfeld. Self-organized criticality: An explanation of $1/f$ noise. *Physical Review Letters*, 59:381–384, 1987.

[53] P. Bak. *How Nature Works: The Science of Self-Organised Criticality*. Copernicus Press, Ney York, 1996.

[54] S. W. Wheatcraft and M. M. Meerschaert. Fractional conservation of mass. *Advances in Water Research*, 31:1377–1381, 2008.

[55] H.J. Schellnhuber and A. Seyler. Fractional differentiation of devil's starcases. *Physica A*, 191:491–500, 1992.

[56] R. Kannan and C.K. Krueger. *Advanced Analysis on the Real Line*. Universitext, Springer-Verlag, 1996.

[57] A. Carpinteri, B. Chiaia, and P. Cornetti. A fractional calculus approach to the mechanics of fractal media. *Rendiconti Seminario Matematica Universita' Politecnico di Torino*, 58:57–67, 2000.

[58] T.L. Anderson. *Fracture Mechanics: Fundamentals and Applications*. Taylor and Francis, 2005.

[59] G. Galileo. *Discorsi e dimostrazioni matematiche intorno a due nove scienze*. 1638.

[60] C.E. Inglis. Stresses in a plate due to the presence of cracks and sharp corners. *Transactions of the Institute of Naval Architects*, 55:219–241, 1913.

[61] J.R. Rice. Thermodynamics of the quasi-static growth of Griffith cracks. *Journal of the Mechanics and Physics of Solids*, 26:61–78, 1978.

[62] M. Negri and C. Ortner. Quasi-static crack propagation by Griffith's criterion. *Math. Models Methods Appl. Sci.*, 18(11):1895–1925, 2008.

[63] G.A. Francfort and J.-J. Marigo. Revisiting brittle fracture as an energy minimization problem. *Journal of the Mechanics and Physics of Solids*, 46:1319–1342, 1998.

[64] M.L. Williams. On the stress distribution at the base of a stationary crack. *Journal of Applied Mechanics*, 24:109–114, 1957.

[65] N.I. Mushelivshili. *Some Basic Problems of the Mathematical Theory of Elasticity*. Wolters-Noordhoff, Groningen, 1963.

[66] A.H. England. *Complex Variable Methods in Elasticity*. Wiley-Interscience, 1971.

[67] R.M. Christensen. Yield functions/failure criteria for isotropic materials. *Proceedings of the Royal Society London. Series A*, A453:1473–1491, 1997.

[68] R.M. Christensen. Yield functions, damage states and intrinsic strength. *Mathematics and Mechanics of Solids*, 5:285–300, 2000.

[69] J.-J. Marigo and L. Truskinovsky. Initiation and propagation of fracture in the models of Griffith and Barenblatt. *Continuum Mechanics and Thermodynamics*, 16:391–409, 2004.

[70] A.P. Kfouri. Continuous crack growth or quantized growth steps? *International Journal of Fracture*, 15:23–29, 1979.

[71] N.M. Pugno and R.S. Ruoff. Quantized fracture mechanics. *Philosophical Magazine*, 21:2829–2845, 2004.

[72] B. Bourdin, G. Francfort, and J.-J. Marigo. The variational approach to fracture. *Journal of Elasticity*, 1-3:5–148, 2008.

[73] Z.P. Bažant. Scaling laws in mechanics of failure. *Journal of Engineering Mechanics*, 119:1828–1844, 1993.

[74] G.I. Barenblatt. *Scaling*. Cambridge Texts in Applied Mathematics, 2003.

[75] R.M. Christensen. A rate-dependent criterion for crack growth. *International Journal of Fracture*, 15:3–21, 1979.

[76] H.-K. Mueller. Stable crack propagation in a viscoelastic strip. *PhD thesis, Caligornia Institute of Technology*, 1969.

[77] W.G. Knauss and H. Dietmann. Crack propagation under variable load histories in linearly viscoelastic solids. *International Journal of Engineering Science*, 8:643–656, 1970.

[78] R.A. Schapery. A theory of crack initiation and growth in viscoelastic media: I. theoretical developments. *International Journal of Fracture*, 11:141–159, 1975.

[79] B.V. Kostrov and L.V. Nikitin. Some general problems of mechanics of brittle fracture. *Archiwum Mechaniki Stosowanej*, 1:749–776, 1965.

[80] P.A. Rebinder. Physico-chemical study of deformation processes in solids. *Yubileinyi Sbornik, Posviashchennyi XXX-letiu Velikoi Oktyabr'skoi , izd. AN SSSR*, pages 53–561, 1947.

[81] L. Truskinovsky and G. Zanzotto. Ericksen's bar revisited: Energy wiggles. *Journal of the Mechanics and Physics of Solids*, 44(8):1371–1408, 1996.

[82] A. Braides. *Γ-convergence for Beginners*. Oxford University Press, i edition, 2002.

[83] J.L. Chaboche, F. Feyel, and Y. Monerie. Interface debonding models: a viscous regulatization with a limited rate dependency. *International Journal of Solids and Structures*, 38:3127–3160, 2001.

[84] P. Suquet. *Discontinuities and Plasticity*. In: Moreau, J.J., Panagiotopoulus, P.D. (Eds.), Nonsmooth Mechanics and Applications. Springer Berlin, pp 280-340, 1987.

[85] M.E. Gurtin and A.I. Murdoch. A continuum theory of elastic material surfaces. *Archive for Rational Mechanics and Analysis*, 5:291–323, 1975.

[86] M.E. Gurtin and A.I. Murdoch. Surface stress in solids. *International Journal of Solids and Structures*, 14:431–440, 1978.

[87] Z.P. Huang and J. Wang. A theory of hyperelasticity of multi-phase media with surface/interface energy effect. *Acta Mechanica*, 182:195–210, 2006.

[88] Z.P. Huang and J. Wang. Erratum to: A theory of hyperelasticity of multi-phase media with surface/interface energy effect. *Acta Mechanica*, 215:365–366, 2010.

[89] A. Klarbring. Derivation of a model of adhesively bonded joints by the asymptotic expansion method. *International Journal of Engineering Science*, 29:493–512, 1991.

[90] G. Geymonat, F. Krasucki, and S. Lenci. Mathematical analysis of a bonded joint with a soft thin adhesive. *Mathematics and Mechanics of Solids*, 4:201–225, 1999.

[91] G. Alfano. On the influence of the shape of the interface law on the application of cohesive-zone models. *Composites Science and Technology*, 66(6):723–730, 2006.

[92] G.T. Camacho and M. Ortiz. Computational modelling of impact damage in brittle materials. 33:2899–2938, 1996.

[93] G. Alfano and M.A. Crisfield. Solution strategies for the delamination analysis based on a combination of local-control arc length and line searches. *International Journal for Numerical Methods in Engineering*, 58(7):999–1048, 2003.

[94] G. Alfano and E. Sacco. Combining interface damage and friction in a cohesive-zone model. *International Journal for Numerical Methods in Engineering*, 2006. Early view on-line. DOI: 10.1002/nme.1728.

[95] M.E. Gurtin. Thermodynamics and the cohesive-zone in fracture. *Zeitschrift für Angewandte Mathematik unt Physik*, 30:991–1003, 1979.

[96] A. Braides. *Approximation of Free-Discontinuity Problems*. Lecture Notes in Mathematics 1694, Springer Verlag, Berlin, 1998.

150

[97] R. Frassine, M. Rink, and A. Pavan. Viscoelastic effects on the interlaminar fracture toughness of epoxy/carbon fibre. *International Journal of Composite Materials*, 27:921–933, 1993.

[98] R. Frassine and A. Pavan. Viscoelastic effects on the interlaminar fracture behaviour of thermoplastic matrix composites: I. Rate and temperature dependence in unidirectional pei / carbon-fibre laminates. *Journal of Composite Science Technology*, 54:193–200, 1995.

[99] R. Frassine, M. Rink, and A. Pavan. Viscoelastic effects on the interlaminar fracture behaviour of thermoplastic matrix composites: II. Rate and temperature dependence in unidirectional peek / carbon-fibre laminates. *Journal of Composite Science Technology*, 56:1253–1260, 1996.

[100] J. Du, M.D. Thouless, and A.F. YEE. Effects of rate on crack growth in a rubber modified epoxy. *Acta Materialia*, 48:3581–3592, 2000.

[101] C. Xu, T. Siegmund, and K. Ramani. Rate-dependent crack growth in adhesives II. experiments and analysis. *International Journal of Adhesion and Adhesives*, 23:15–22, 2003.

[102] J.-C. Gu, J.R. Rice, A.C. Ruina, and S.T. Tsu. Slip motion and stability of a single degree of freedom elastic system with rate and state dependent friction. *Journal of the Mechanics and Physics of Solids*, 32:167–196, 1984.

[103] T. Yamaguchi, S. Ohmata, and M. Doi. Regular to chaotic transition of stick-slip motion in sliding friction of an adhesive gel-sheet. *Journal of Physics: Condensed Matter*, 21:1–7, 2009.

[104] J.M. Carlson and J.S. Langer. Properties of earthquakes generated by fault dynamics. *Physical Review Letters*, 62.

[105] T.W. Webb and E.C. Aifantis. Crack growth resistance curves and stick-slip fracture. *Mechanical Research Communications*, 246.

[106] G.A. Maugin. *The thermomechanics of nonlinear irreversible behaviors*. World Scientific, Singapore, 1999.

[107] D. Maugis. Subcritical crack growth, surface energy, fracture toughness, stick-slip and embrittlement. *Journal of Materials Science*, 20:3041–3073, 1985.

[108] M.J. Van Der Bosch, P.J.G Schreurs, and M.G.D. Geers. On the development of a 3D cohesive zone element in the presence of large deformations. *Computational Mechanics*, 42:171–180, 2006.

[109] T. D. Nguyen and S. Govindjee. Numerical study of geometric constraint and cohesive parameters in steady-state viscoelastic crack growth. *International Journal of Fracture*, 141(1-2):255–268, 2006.

[110] C. Xu, T. Siegmund, and K. Ramani. Rate-dependent crack growth in adhesives I. modelling approach. *International Journal of Adhesion and Adhesives*, 23:9–13, 2003.

[111] A. Corigliano and M. Ricci. Rate-dependent interface models: formulation and numerical applications. *International Journal of Solids and Structures*, 38(4):547–576, 2001.

[112] D.H. Allen and C.R. Searcy. A micromechanical model for a viscoelastic cohesive zone. *International Journal of Fracture*, 107:159–176, 2001.

[113] K.M. Liechti and J.D. Wu. Mixed-mode, time-dependent rubber/metal debonding. *Journal of the Mechanics and Physics of Solids*, 49:1039–1072, 2001.

[114] C.M. Landis, Pardoen, and J.W T., Hutchinson. Crack velocity dependent toughness in rate dependent materials. *Mechanics of Materials*, 32:663–678, 2000.

[115] D.B. Xu, C.Y. Hui, and E.J. Kramer. Interface fracture and viscoelastic deformation in finite size specimens. *Journal of Applied Physics*, 72(8):3305–3316, 1992.

[116] R.M. Christensen and E.M. Wu. A theory of crack growth in viscoelastic materials. *Engineering Fracture Mechanics*, 14:215–225, 1981.

[117] J.A. Hauch and M.P. Marder. Energy balance in dynamic fracture, investigated by a potential drop tecnique. *International Journal of Fracture*, 90:133–151, 1998.

[118] G. Del Piero and L. Truskinovsky. Macro- and micro-cracking in one dimensional elasticity. *International Journal of Solids and Structures*, 38:1135–1148, 2001.

[119] V. Berdichevsky. *Variational Principles in Continuum Mechanics*. Springer-Verlag, 2010.

[120] A. Jaubert and J.-J. Marigo. Justification of Paris-type laws from cohesive-forces model via a variational approach. *Continuum Mechanics and Thermodynamics*, 18.

[121] E. De Giorgi and L. Ambrosio. Un nuovo tipo di funzionale del calcolo delle variazioni. *Atti Accad. Naz. Lincei Rend. Cl Sci. Fi. Mat. Natur.*, 82:199–210, 1988.

[122] J.E. Marsden and T.J.R. Hughes. *The Mathematical Foundations of Elasticity*. Dover Publications, 1994.

[123] P. Ciarlet. *Mathematical Elasticity*. Springer-Verlag, 1998.

[124] G. Dal Maso and G. Lazzaroni. Quasistatic crack growth in finite elasticity with non-interpenetration. *Annales de l' Institut Henri Poincare (C): Non Linear Analysis*, 27:257–290, 2010.

[125] C. Miehe, F. Welschinger, and M. Hofacker. Thermodynamically consistent phase-field models of fracture: Variational principles and multi-field FE implementations. *International Journal for Numerical Methods in Engineering*, 83:1273–1311, 2010.

[126] C.V. Verhoosel and R. de Borst. A phase-field model for cohesive-fracture. *International Journal for Numerical Methods in Engineering*, 96:43–62, 2013.

[127] G. Del Piero. A variational approach to fracture and other inelastic phenomena. *Journal of Elasticity*, 112:3–77, 2013.

[128] A. Giacomini. Size effects on quasi-static growth of cracks. *SIAM Journal of Mathematical Analysis*, 36(6):1887–1928, 2005.

[129] A. Chambolle, A. Giacomini, and M. Ponsiglione. Crack initiation in brittle materials. *Archive for Rational Mechanics and Analysis*, 188:309–349, 2008.

[130] G.J. Lake, C.C. Lawrence, and A.G. Thomas. High-speed fracture of elastomers: part I. *Rubber Chemistry and Technology*, 73:801–817, 2000.

[131] K. Kendall. Control of cracks by interfaces in composites. *Proceedings of the Royal Society London. Series A*, 341:409–428, 1975.

[132] K. Kendall. The dynamics of slow peeling. *International Journal of Fracture*, 11:3–12, 1975.

[133] R. Frassine, M. Rink, A. Leggio, and A. Pavan. Experimental analysis of viscoelastic criteria for crack initiation and growth in polymers. *International Journal of Fracture*, 81:55–75, 1996.

[134] A.N. Gent. Adhesion and strength of viscoelastic solids. Is there a relationship between adhesion and bulk properties? *Langmuir*, 12:4492–4496, 1996.

[135] P. Rahulkumar, A. Jagota, S.J. Bennison, and S. Saigal. Cohesive element modeling of viscoelastic fracture: application to peel testing of polymers. 37:1873–1897, 2000.

[136] A.J. Kinloch, C.C. Lau, and J.G. Williams. The peeling of flexible laminates. *International Journal of Fracture*, 66:45–70, 1994.

[137] M.K. Chaudhury. Rate-dependent fracture at adhesive interface. *Journal of Physical Chemistry B*, 103:6562–6566, 1999.

[138] L.M Kachanov. On the Time to Failure under Creep Conditions. *Izv.Akad.Nauk.SSR*, 8:26–31, 1958.

[139] C. Zener. *Elasticity and Anelasticity of Metals*. University of Chicago Press, Chicago, 1948.

[140] M. Destrade, M.D. Gilchrist, J.A. Motherway, and J.G. Murphy. Bimodular rubber buckles early in bending. *Mechanics of Materials*.

[141] B.D. Coleman and W. Noll. The thermodynamics of elastic materials with heat conduction and viscosity. *Archive for Rational Mechanics and Analysis*, 13.

[142] B.D. Coleman and M.E. Gurtin. Thermodynamics with internal variables. *Journal of Chemical Physics*, 47:597–613, 1967.

[143] G. Alfano and M.A. Crisfield. Finite element interface models for the delamination analysis of laminated composites: mechanical and computational issues. *International Journal for Numerical Methods in Engineering*, 50(7):1701–1736, 2001.

[144] R.T. Rockfeller. *Convex Analysis*. Princeton University Press, 1997.

[145] J.S. Bergstrom and M.C Boyce. Large strain time-dependent behavior of filled elastomers. *Mechanics of Materials*, 32:627, 644, 2000.

[146] R.L. Taylor, K.S. Pister, and G.L. Goudeau. Thermomechanical analysis of viscoelastic solids. *International Journal for Numerical Methods in Engineering*, 2:45–59, 1970.

[147] J.C. Simo and T.J.R. Hughes. *Computational Inelasticity*. Springer, Berlin, 1998.

[148] Y. Mi, M.A. Crisfield, G.A.O. Davies, and H.B. Hellweg. Progressive delamination using interface elements. *Journal of Composite Materials*, 32(14):1246–1272, 1998.

[149] L.I. Slepyan. *Models and Phenomena in Fracture Mechanics*. Springer Verlag Berlin-Heideberg, 2002.

[150] L.I. Slepyan. Principle of maximum energy dissipation rate in crack dynamics. *Journal of the Mechanics and Physics of Solids*, 41:1019–1033, 1993.

[151] T.F. Nonnenmacher and W.G. Glöckle. A fractional model for mechanical stress relaxation. *Philosophical Magazine Letters*, 64.

[152] M. Ortiz and E.A. Repetto. Nonconvex energy minimization and dislocation structures in ductile single crystals. *Journal of the Mechanics and Physics of Solids*, 47:397 – 462, 1999.

[153] C. Miehe. Homogenization of inelastic solid materials at finite strains based on incremental minimization principles. application to the texture of polycristals. *Journal of the Mechanics and Physics of Solids*, 50:2123 – 2167, 2002.

[154] K.B. Oldham and J. Spanier. *The Fractional Calculus*. Academic Press, London, 1974.

[155] A.K Grünwald. Über 'begrentze' derivationen und deren auwendung. *Zeitschrift für Angewandte Mathematik unt Physik*, 12:441 – 480, 1867.

[156] M. Riesz. L' integral de Riemann-Liouville et le probléme de Cauchy. *Acta Math.*, 81, 1949.

[157] A. Schmidt and L. Gaul. Application of fractional calculus to viscoelastically damped structures in the finite elements method. *Nonlinear Dynamics*, 29:37–55, 2002.

[158] J. Padovan. Computational algorithms for FE formulations involving fractional operators. *Computational Mechanics*, 2:271–287, 1987.

[159] A. Corigliano. Formulation, identification and use of interface models in the numerical analysis of composite delamination. *International Journal of Solids and Structures*, 30(20):2779–2811, 1993.

[160] A. Corigliano and S. Mariani. Parameter identification of a time-dependent elastic-damage interface model for the simulation of debonding in composites. *Composite Science and Technology*, 61:191–203, 2003.

[161] K. Tsunoda, J.J.C. Busfield, K.L. Davies, and A.G. Thomas. Effects of materials variables on the tear behaviour of a non-crystallising elastomer. *J. Mat. Science*, 35:5187–5198, 2000.

[162] M. Negri. From rate-dependent to rate-independent brittle crack propagation. *Journal of Elasticity*, 98:159–178, 2010.

[163] G. Shilov. *Elementary Functional Analysis*. Dover Publications, 1995.

[164] Schubel P.M. Gdoutos, E.E. and I.M. Daniel. Determination of critical tearing energy of tyre rubber. *Strain*, 40:119–125, 2004.

[165] R.H. Swendsen. *An introduction to Statisitcal Mechanics and Thermodynamics*. Oxford Graduate Texts, 2012.

[166] B. Van der Pol. On relaxation-oscillations. *The London, Edinburgh and Dublin Philosophical Magazine and Journal of Science*, 2(7):978–992, 1927.

[167] G. Carbone and B.N.J. Persson. Crack motion in viscoelastic solids: The role of flash temperature. *Eur. Phys. J. E*, 17:261–281, 2005.

[168] F. D'Amico, G. Carbone, M.M. Foglia, and U. Galietti. Moving cracks in viscoelastic materials: Temperature and energy-release rate measurements. *Engineering Fracture Mechanics*, 98:315–325, 2013.

[169] M.L. Williams, R.F. Landel, and J.D. Ferry. The temperature dependence of relaxation mechanisms in amorphous polymers and other glass-forming liquids. *Journal of the American Chemical Society*, 77:3701–3707, 1955.

[170] R. Weichert and W. Schönert. Temperature distribution produced by a moving heat source. *Journal of the Mechanics and Physics of Solids*, 26:151–161, 1978.

[171] J. Albouy, P.A.and Marchal and J. Rault. Chain orientation in natural rubber, part I: The inverse yielding effect. *Eur. Phys. J. E*, 17:247–259, 2005.

[172] P.G. Santangelo and M. Roland. Role of strain-crystallization in the fatigue resistance of double nteworks elastomers. *Rubber Chemistry and Technology*, 76:892–898, 2003.

[173] W.V. Mars and A. Fatemi. A phenomenological model for the effect of the r-ratio on fatigue of strain-crystallizing rubbers. *Rubber Chemistry and Technology*, 76:1241–1258, 2003.

[174] K. Brüning, K. Schneider, S.V. Roth, and G. Heinrich. Kinetics of strain-induced crystallization in natural rubber studied by WAXD: Dynamic and impact tensile experiments. *Macromolecules*, 45:7914–7919, 2012.

[175] C.J. Derham and A.G. Thomas. Creep of rubber under repeated stressing. *Rubber Chemistry and Technology*, 50:397–402, 1977.

[176] A.N. Gent and P.B. Lindley. Internal rupture of bonded rubber cylinders in tension. *Phil. Trans. Roy. Soc.*, 249:195–205, 1959.

[177] T. Horst and G. Heinrich. Crack propagation behavior in rubber materials. *Polymer Science, Ser. A*, 50:583–590, 2008.

[178] J.M. Ball. Discontinuous equilibrium solutions and cavitation in nonlinear elasticity. *Phil. Trans. Roy. Soc.*, 306:557–611, 1982.

[179] H. Attouch, G. Buttazzo, and G. Michaille. *Variational Analysis in Sobolev and SBV Spaces*. MPS-SIAM Series on Optimization, SIAM, 2006.

[180] J.G. Rots and R. de Borst. Analysis of concrete fracture in "direct" tension. *International Journal of Solids and Structures*, 25:1381–1394, 1989.

[181] P.-G. de Gennes. *Soft Interfaces: The Dirac Memorial Lecture*. Cambridge University Press, 1997.

[182] F. Saulnier, T. Ondar¸cuhu, A. Aradian, and E. Raphaël. Adhesion between a viscoelastic material and a solid surface. *Macromolecules*, 37:1067–1075, 2004.

[183] B.N.J. Persson, O. Albohr, G. Heinrich, and H. Ueba. Crack propagation in rubber-like materials. *Journal of Physics: Condensed Matter*, 17:R1071–R1142, 2005.

[184] K.C. Le and L. Truskinovsky. Periodic debonding of an adhesive film. *C.R. Mecanique*, 336:170–175, 2008.

[185] G. Del Piero and G. Pampolini. The influence of viscosity on the response of open-cell polymeric foams in uniaxial compression: experiments and theoretical model. *Continuum Mechanics and Thermodynamics*, 24(3):181–199, 2012.

[186] H.A. Barnes. Thixotropy - a review. *Journal of Non-Newtonian Fluid Mechanics*, 70:1–33, 1997.

[187] J. Petera, K. Kaminski, and M. Kotynia. A generalized viscoelastic maxwell model for semi-solid thixotropic alloys. *International Journal of Material Forming*, 3:775–778, 2010.

[188] B.D. Coleman. Necking and drawing in polymeric fibers under tension. *Archive for Rational Mechanics and Analysis*, 83(2):115–137, 1983.

[189] P.-G. de Gennes and J. Prost. *The Physics of Liquid Crystals*. Oxford University Press, 2 edition, 1995.

[190] A.S. Argon and M. Salama. The mechanism of fracture in glassy materials capable of some inelastic deformation. *Materials Science and Engineering*, 23:219–230, 1976.

[191] A.S. Argon and M. Salama. Growth of crazes in glassy polymers. *Philosophical Magazine*, 36:1217–1234, 1977.

[192] A. Ghatak, M.K. Chaudhury, V. Shenoy, and A. Sharma. Meniscus instability in a thin elastic film. *Physical Review Letters*, 85:4329–4332, 2000.

[193] J. S. Biggins, B. Saintyves, Z. Wei, E. Bouchard, and L. Mahadevan. Digital instability of a confined elastic meniscus. *Proceedings of the National Academy of Science (USA)*, 110:12545–12548, 2013.

[194] C. Marano, R. Calabro', and M. Rink. Effect of molecular orientation on the fracture behavior of carbon black-filled natural rubber compounds. *Journal of Polymer Science B*, 48:1509–1515, 2010.

[195] J.J.M. Baltussen and M.G. Northolt. The Eyring reduced time model for viscoelastic and yield deformation of polymer fibres. *Polymer*, 45:1717–1728, 2004.

[196] J. Toribio and A. Valiente. Failure analysis of cold drawn eutectoid steel wires for prestressed concrete. *Engineering Failure Analysis*, 13:301–311, 2006.

[197] G. Del Piero and L. Truskinovsky. Elastic bars with cohesive energy. *Continuum Mechanics and Thermodynamics*, 21:141–171, 2009.

[198] G. Buttazzo, M. Giaquinta, and S. Hildebrandt. *One Dimensional Variational Problems*. Oxford University Press, i edition, 1998.

[199] J.-J. Marigo. Fracture and debonding of a thin film on a stiff substrate: analytical model and numerical solutions of a one dimensional variational model. *Continuum Mechanics and Thermodynamics*, 1-3:5–148, 2008.

[200] J.L. Ericksen. Equilibrium of bars. *Journal of Elasticity*, 5.

[201] L. Ambrosio, N. Gigli, and G. Savare'. *Gradient Flows: In Metric Spaces and Spaces of Probability Measures*. Birkhäuser, ETH Lecture Notes in Mathematics, 2005.

[202] J.-J. Marigo. Initiation of cracks in griffith's theory: an argument of continuity in favor of global minimization. *Journal of Nonlinear Science*, 20:831–868, 2010.

[203] S.N. Zhurkov. Kinetic concept of the strength of solids. *International Journal of Fracture*, 1(4):295–307, 1965.

[204] Y. Pomeau. Fundamental problems in brittle fracture: unstable cracks and delayed breaking. *C.R. Mecanique*, 330:249–257, 2002.

[205] S. Santucci, L. Vanel, and S. Ciliberto. Slow crack growth: Models and experiments. *Eur. Phys. J. Special Topics*, 146:341–356, 2007.

[206] D. Vella and L. Mahadevan. A simple macroscopic model for the dynamics of adhesive failure. *Langmuir*, 22:163–168, 2006.

[207] L. Ambrosio, A. Lemenant, and G. Royer-Carfagni. A variational model for plastic slip and its regularization via Γ-convergence. *Journal of Elasticity*, 1(1):1–2, 2010.

[208] A. Cherkaev, E. Cherkaev, and L. Slepyan. Transition waves in bistable structures. I delocalization of damage. *Journal of the Mechanics and Physics of Solids*, 53:383–405, 2005.

[209] M.J. Van Der Bosch, P.J.G Schreurs, and M.G.D. Geers. Identification and characterization of delamination in polymer coated metal sheet. *Journal of the Mechanics and Physics of Solids*, 56:3259–3276, 2008.

[210] T.M. Atackanovič and S. Pilipovič. Hamilton's principle with variable order fractional derivatives. *Fractional Calculus and Applied Analysis*, 14:94–109, 2011.

[211] L. Tonelli. Sur une méthode directe du calcul des variations. *Comptes Rendus Académie des Sciences, Paris*, 158:1776–1778, 1983–1985, 1914.